R. & M. No. 2908

MINISTRY OF SUPPLY

AERONAUTICAL RESEARCH COUNCIL
REPORTS AND MEMORANDA

The Subsonic Flow Past Swept Wings at Zero Lift Without and With Body

By

D. KÜCHEMANN, Dr.rer.nat.

and

J. WEBER, Dr.rer.nat.

LONDON: HER MAJESTY'S STATIONERY OFFICE

1956

PRICE 17*s* 6*d* NET

The Subsonic Flow Past Swept Wings at Zero Lift Without and With Body

By

D. Küchemann, Dr.rer.nat., and J. Weber, Dr.rer.nat.

Communicated by the Principal Director of Scientific Research (Air), Ministry of Supply

Reports and Memoranda No. 2908

March, 1953

(*Note.*—This memorandum is a summary of the material contained in a number of earlier Royal Aircraft Establishment Reports by the authors and was prepared at the request of the Aeronautical Research Council for publication as an R. & M.)

Summary.—A review is given of the effects associated with the subsonic inviscid flow past swept wings at zero lift with the aim of providing the information needed for an understanding of the flow phenomena. Methods of obtaining the full benefit of sweep are described.

Detailed solutions for incompressible flow are given for three basic cases :

(*a*) the sheared wing of infinite span

(*b*) the centre-section of a swept wing of infinite span

(*c*) the flow in the curved intersection line between wing and body.

These solutions are used to find approximate solutions for any given wing of finite aspect ratio. The Prandtl-Glauert procedure is extended and applied to derive approximations for the compressible flow in the subcritical region. The special cases treated in detail are: the flow in the tip regions of wings; tapered wings; wing-fuselage interference for symmetrical arrangements; and modifications to the wing or to the body shape, for instance to restore sheared-wing conditions.

1. *Introduction.*—The reasons for the use of swept wings in the design of aircraft for high subsonic speeds are now well-established. A swept wing has a greater critical Mach number—above which the drag may rise sharply—than a corresponding unswept wing. Briefly the effects of sweepback on the flow over the wing are:

(i) At low Mach numbers the perturbation velocities are smaller than on the unswept wing with the same aerofoil section along wind

(ii) The rate of change of the pressure coefficient with Mach number is smaller

(iii) The critical value of the pressure coefficient is reached at a higher free-stream Mach number. Thus there is a gain in critical free-stream Mach number from point P_1 to point P_2 in Fig. 1.

To obtain precisely this gain in critical Mach number, the flow must be ' two-dimensional ' with the isobars as straight lines inclined at an angle (other then 90 deg) to the main flow. Thus, in theory, the precise effect of a given angle of sweep can be achieved only with an ideal sheared wing of infinite span.

The flow round a sheared wing of infinite span at zero incidence is associated with a particular pattern of the streamlines, as seen from Fig. 2. These streamlines are curved in plan view. Any obstructions to this curved flow will alter the ' sweep effects '. For example, two sheared wings of opposite sweep joined to form a A-wing of infinite span must have a straight streamline at the centre-section, for reasons of continuity and symmetry, and the gradual straightening of the streamlines as the centre is approached alters the characteristic pattern of the two-dimensional flow and reduces the sweep effects. Similar effects occur at the tips of a wing of finite aspect ratio where the streamlines are again straightened as the tip is approached, although they are likely to be entirely straight only at some distance from the tip, as indicated in Fig. 2. Finally, bodies mounted on the wing, such as a fuselage or engine nacelles, again disturb the curved flow of the ideal sheared wing.

One purpose of this paper is to investigate the distortions of the flow at the centre of the wing, the wing tips, and at a junction with fuselage or engine nacelle, and to provide practical methods of calculating them. At the same time, an attempt will be made to understand the physics of the flow. Another purpose is to find ways of counteracting these distortions and restoring, for example, two-dimensional conditions as far as possible. The approach adopted is to find detailed solutions for three basic cases: (*a*) the sheared wing of infinite span; (*b*) the centre-section of a swept wing of infinite span; (*c*) the flow in the curved intersection line between a wing and a body. These solutions can be combined to obtain approximate solutions to the general case of a tapered swept wing of finite aspect ratio, and to calculate the pressure distribution over the surface of a given wing with symmetrical aerofoil sections of non-zero thickness, at zero incidence without or with a body. The methods are derived for inviscid incompressible flow and subsequently extended to compressible flow at subcritical Mach numbers.

2. *The Sheared Wing of Infinite Span.*—Although the concept of a sheared wing of infinite span is somewhat academic, it is helpful to an understanding of the flow past swept wings; it may also serve as a guide to perfection. We shall find that the sheared wing of infinite span is one of the few cases where a simple solution of the equations of motion can be found, with a speed and accuracy sufficient for practical purposes. As a basis, the two-dimensional unswept aerofoil is discussed first, in section 2.1, and the results obtained are then applied to the sheared wing in section 2.2. The subsequent sections deal with the compressible flow past the sheared wing in the subcritical range, the extent of which is first defined in section 2.3.

2.1. *Incompressible Flow past a Two-dimensional Aerofoil.*—Because of later applications to three-dimensional flow problems, we use the method of singularities rather than conformal transformations in treating the two-dimensional aerofoil. The aerofoil is replaced by a distribution of straight source filaments of strength $q(x)\,dx$ along the chord $c(=1)$ from $x=0$ (leading edge) to $x=1$ (trailing edge), the x-axis being in the direction of the main stream. The source lines are of infinite length in the y-direction, *i.e.*, normal to the free stream. The source distribution induces the velocity components v_x and v_z in the directions of the x- and z-axes, *i.e.*, parallel and vertically to the main stream. The source distribution is determined by the condition that the induced velocities together with that of the main stream, V_0, make the given aerofoil $z(x)$ into a streamline :—

$$\frac{dz(x)}{dx} = \frac{v_z(x,z)}{V_0 + v_x(x,z)} \qquad (2.1)$$

This relation is usually simplified in two ways :—In the first place, the velocity increment v_x is assumed to be small compared with the velocity V_0 of the main stream. This is justifiable only for thin aerofoils, and even then only outside their stagnation regions, since $v_x = -V_0$ at a stagnation point. Secondly, the value of v_z is determined on the chord-line $z=0$ instead of on the surface $z(x)$ of the aerofoil. Again this is justifiable only for thin aerofoils. With these simplifications,

$$v_z(x,0) = \pm\, q(x)/2\,, \qquad (2.2)$$

and the streamline condition reads:—

$$\frac{dz(x)}{dx} = \frac{v_z(x,0)}{V_0} = \pm\frac{q(x)}{2V_0} \text{ or } q(x) = 2V_0\frac{dz(x)}{dx}. \quad .. \quad .. \quad .. \quad (2.3)$$

By integration,

$$z(x) = \frac{1}{2V_0}\int_0^x q(x')\,dx',$$

and in particular,

$$z(0) = z(1) = \frac{1}{2V_0}\int_0^1 q(x')\,dx' = 0,$$

i.e., the overall strengths of the sources and sinks must be equal in order to obtain a practical aerofoil section which forms a closed contour. The validity of the two main assumptions above must be checked in the later applications.

With the source distribution being known, the streamwise velocity increment v_x can be determined. On the chord-line of the aerofoil, the increment due to a single source filament is

$$dv_x(x,0) = \frac{1}{2\pi}\frac{q(x')\,dx}{x - x'},$$

so that, by integration,

$$\frac{v_x(x,0)}{V_0} = \frac{1}{2\pi V_0}\int_0^1 q(x')\,\frac{dx'}{x - x'} = \frac{1}{\pi}\int_0^1 \frac{dz(x')}{dx'}\,\frac{dx'}{x - x'} \quad .. \quad .. \quad .. \quad (2.4)$$

which expresses the velocity increment as a function of the aerofoil shape.

The approximation $V(x,z) = V_x(x,0) = V_0 + v_x(x,0)$ for the velocity along the surface of the aerofoil is not adequate in most practical cases and a more accurate solution is needed. For this purpose, consider the circulation around the aerofoil (the line integral of the velocity along the contour) and the circulation around the sources on the chord-line. Both of these must be zero:

$$\oint V(x,z)\,ds = \oint V(x,z)\sqrt{\{dx^2 + dz(x)^2\}} = 0; \text{ and } \oint V_x(x,0)\,dx = 0.$$

If the assumption is now made that over any elemental part of the section

$$V(x,z)\,ds = V_x(x,0)\,dx,$$

we have

$$V(x,z) = V_x(x,0)\frac{1}{ds/dx} = V_x(x,0)\frac{1}{\sqrt{\left\{1 + \left(\frac{dz(x)}{dx}\right)^2\right\}}}. \quad .. \quad .. \quad (2.5)$$

Hence, by equation (2.4),

$$\frac{V(x,z)}{V_0} = \frac{1}{\sqrt{\left\{1 + \left(\frac{dz(x)}{dx}\right)^2\right\}}}\left(1 + \frac{1}{\pi}\int_0^1 \frac{dz(x')}{dx'}\,\frac{dx'}{x - x'}\right). \quad .. \quad .. \quad (2.6)$$

It can be shown (R. & M. 2918), by means of the method of conformal transformations, that equation (2.6) is strictly correct for aerofoils with elliptic cross sections of any thickness/chord ratio; and that the numerical results obtained for the Joukowsky aerofoil and also for the R.A.E.

sections 100 to 104 (*see* R. C. Pankhurst, H. B. Squire[1], 1950) in the normal range of thickness/chord ratio, up to about 20 per cent, agree well with the exact solutions and with the results of S. Goldstein's method[2] (1942).

The numerical evaluation can be simplified considerably by replacing the integral and the function dz/dx in equation (2.6) by summations,

$$\frac{1}{\pi}\int_0^1 \frac{dz(x')}{dx'}\frac{dx'}{x_\nu - x'} = \frac{v_x(x_\nu,0)}{V_0} = \sum_{\mu=1}^{N-1} s_{\mu\nu}{}^{(1)} z_\mu = S_\nu{}^{(1)}, \quad \ldots \quad (2.7)$$

$$\frac{dz(x_\nu)}{dx} = \sum_{\mu=1}^{N-1} s_{\mu\nu}{}^{(2)} z_\mu = S_\nu{}^{(2)}, \quad \ldots \quad (2.8)$$

following the methods of H. Multhopp[3] (1938) and F. Riegels and H. Wittich[4] (1942). The functions $S^{(1)}(x)$ and $S^{(2)}(x)$ represent approximate expressions for the two terms at certain discrete points

$$x_\nu = \frac{1 + \cos\frac{\nu\pi}{N}}{2} \quad \ldots \quad (2.9)$$

along the chord. The accuracy will, of course, increase with the number, N, of points taken. $N = 16$ is usually sufficient for practical purposes. The sums involve only the given ordinates z of the aerofoil at the pivotal points x_ν. The values of the coefficients $s_{\mu\nu}{}^{(1)}$ and $s_{\mu\nu}{}^{(2)}$ can be determined once and for all for any given aerofoil. Numerical values are given in Tables 1 and 2. The complete calculation of a pressure distribution takes about 2 or 3 computor hours.

The velocity on the surface of the aerofoil now becomes

$$\frac{V(x,z)}{V_0} = \frac{1 + S^{(1)}(x)}{\sqrt{\{1 + S^{(2)}(x)^2\}}}, \quad \ldots \quad (2.10)$$

by equations (2.6), (2.7), (2.8); and the pressure coefficient

$$C_p(x,z) = 1 - \left(\frac{V(x,z)}{V_0}\right)^2 = 1 - \frac{(1 + S^{(1)}(x))^2}{1 + S^{(2)}(x)^2} = \frac{-2S^{(1)}(x) - S^{(1)}(x)^2 + S^{(2)}(x)^2}{1 + S^{(2)}(x)^2}. \quad (2.11)$$

If $(S^{(1)})^2$ and $(S^{(2)})^2$ are negligible compared with unity and $S^{(1)}$,

$$C_p = -2S^{(1)}(x). \quad \ldots \quad (2.12)$$

Since $S^{(1)}(x)$ can be written as a function of x multiplied by the thickness/chord ratio, t/c, of the aerofoil, by equation (2.7), it is only when the approximation of equation (2.12) is used that the pressure coefficient is proportional to the thickness-chord ratio. Fig. 3 shows in an example the various approximations; only the full relation (2.11) gives a satisfactory result over the whole chord.

2.2. *Application to the Sheared Wing.*—The flow past a sheared wing of infinite span, being essentially two-dimensional, is closely related to that past the two-dimensional unswept aerofoil. This is easily seen when considering the flow in a system, ξ, η, of co-ordinates which are normal and tangential to the direction of sweep, φ, Fig. 4. These co-ordinates are related to the rectangular system x, y, z, with x in the streamwise direction, by

$$\left.\begin{aligned} \xi &= x\cos\varphi - y\sin\varphi \\ \eta &= x\sin\varphi + y\cos\varphi \\ \zeta &= z \end{aligned}\right\}. \quad \ldots \quad (2.13)$$

The main stream velocity V_0 has then the components

$$V_{\xi 0} = V_0 \cos \varphi$$

and

$$V_{\eta 0} = V_0 \sin \varphi \, .$$

Obviously, the component $V_{\eta 0}$ parallel to the wing meets the condition that the wing surface is a stream surface whatever its shape. The remaining velocity components

$$V_\xi = V_0 \cos \varphi + v_\xi$$

and

$$V_z = v_z$$

in the ξ, z-plane, normal to the direction of sweep, must satisfy the streamline condition, which reads in analogy to equation (2.1),

$$\frac{dz(\xi)}{d\xi} = \frac{V_z}{V_\xi} = \frac{v_z(\xi,z)}{V_0 \cos \varphi + v_\xi(\xi,z)} \, . \quad .. \quad .. \quad .. \quad .. \quad .. \quad (2.14)$$

This is again simplified by ignoring v_ξ compared with $V_0 \cos \varphi$ and by calculating v_z on the chord-line instead of on the surface. Thus,

$$\frac{dz(\xi)}{d\xi} = \frac{1}{\cos \varphi} \frac{v_z(\xi,0)}{V_0} = \frac{1}{\cos \varphi} \frac{q(\xi)}{2V_0} \, , \quad .. \quad .. \quad .. \quad .. \quad .. \quad (2.15)$$

which determines the source distribution :—

$$q(\xi) = 2V_0 \cos \varphi \frac{dz(\xi)}{d\xi} = 2V_0 \frac{dz(x)}{dx} = q(x) \quad .. \quad .. \quad .. \quad (2.16)$$

by equation (2.13). We find that the two-dimensional aerofoil and the sheared wing with the same shape $z(x)$ in the streamwise section are produced by the same source distribution $q(x)$.

There is no velocity increment v_η along the wing. The velocity increment normal to the line of sweep induced by an infinite source filament $q(\xi)\, d\xi$ is given by

$$dv_\xi(\xi,0) = \frac{1}{2\pi} \frac{q(\xi')\, d\xi'}{\xi - \xi'} \, ,$$

so that, by integration,

$$\frac{v_\xi(\xi,0)}{V_0} = \frac{1}{2\pi V_0} \int_0^1 q(\xi') \frac{d\xi'}{\xi - \xi'} \, ,$$

in analogy to equation (2.4). With equations (2.13) and (2.16),

$$\frac{v_\xi(\xi,0)}{V_0} = \frac{1}{2\pi V_0} \int_0^1 q(x') \frac{dx'}{x - x'} = \frac{1}{\pi} \int_0^1 \frac{dz(x')}{dx'} \frac{dx'}{x - x'} = S^{(1)}(x) \, , \quad .. \quad .. \quad (2.17)$$

by equation (2.7). The velocity increments on the chord-line in the x- and y-directions are then :—

$$\left.\begin{aligned} v_x(x,0) &= \cos\varphi v_\xi(\xi,0) = \cos\varphi V_0 S^{(1)}(x) = \cos\varphi v_x(x,0)_{\varphi=0} \\ v_y(x,0) &= -\sin\varphi v_\xi(\xi,0) = -\sin\varphi V_0 S^{(1)}(x) = -\sin\varphi v_x(x,0)_{\varphi=0} \end{aligned}\right\} . \quad .. \quad (2.18)$$

The existence of a non-zero velocity component v_y in the transverse direction implies that the projections of the streamlines on to the plane of the wing are curved. Their shape can be obtained by integrating

$$\frac{dy(x)}{dx} = \frac{v_y}{V_0 + v_x} \simeq \frac{v_y}{V_0}$$

that is,

$$y(x) = \int_{-\infty}^{x} \frac{v_y}{V_0 + v_x}\,dx \simeq \int_{-\infty}^{x} \frac{v_y}{V_0}\,dx = -\sin\varphi \int_{-\infty}^{x} \frac{v_{x\,\varphi=0}}{V_0}\,dx \quad .. \quad .. \quad (2.19)$$

by equation (2.18). For points on the wing chord, $v_x(x,0)_{\varphi=0}$ can be determined from equation (2.7). We find that on the ' stagnation ' line, where $v_\xi = -V_0\cos\varphi$,

$$\frac{dy}{dx} = \frac{\sin\varphi\cos\varphi V_0}{V_0 - V_0\cos^2\varphi} = \cot\varphi$$

so that the air flows outwards along the nose of the wing. Further downstream, the streamlines curve round into the direction of the main stream which occurs when $v_x(x,0) = 0$. The streamlines are subsequently deflected inboard and the largest deflection angle is reached where v_x has its maximum, *i.e.*, at the peak-suction line. Downstream of that the streamlines gradually approach the direction of the free stream, reach it where $v_x = 0$, turn outwards, and finally form a parallel flow again, Fig. 2.

As on the two-dimensional aerofoil, the velocity on the chord-line does not give a sufficiently accurate approximation for the velocity on the surface. A better approximation, which is correct for ellipses, is obtained in analogy to equation (2.5) from

$$V_{\eta=0}(\xi,z) = \sqrt{(V_\xi^2 + V_z^2)} = \frac{V_0\cos\varphi + v_\xi(\xi,0)}{\sqrt{\left\{1 + \left(\frac{dz(\xi)}{d\xi}\right)^2\right\}}} = V_0\,\frac{\cos\varphi + S^{(1)}(x)}{\sqrt{\left\{1 + \left(\frac{S^{(2)}(x)}{\cos\varphi}\right)^2\right\}}} \quad .. \quad (2.20)$$

by equations (2.8), and (2.17). With $V_\eta = V_0\sin\varphi$, we obtain for the pressure coefficient

$$C_p(x,z) = 1 - \left(\frac{V_\xi}{V_0}\right)^2 - \left(\frac{V_\eta}{V_0}\right)^2 - \left(\frac{V_z}{V_0}\right)^2 = 1 - \frac{(\cos\varphi + S^{(1)}(x))^2}{1 + \left(\frac{S^{(2)}(x)}{\cos\varphi}\right)^2} - \sin^2\varphi$$

so that finally

$$C_p(x,z) = \frac{-2\cos\varphi\,S^{(1)}(x) - S^{(1)}(x)^2 + S^{(2)}(x)^2}{1 + \left(\frac{S^{(2)}(x)}{\cos\varphi}\right)^2} \quad .. \quad .. \quad .. \quad .. \quad (2.21)$$

The functions $S^{(1)}(x)$ and $S^{(2)}(x)$ can again be determined at discrete points along the chord from equations (2.7) and (2.8).

If this relation for the pressure coefficient is linearised by omitting quadratic terms in the functions $S^{(1)}(x)$ and $S^{(2)}(x)$, which contain t/c as a factor, then

$$C_p = -2 \cos \varphi \, S^{(1)}(x) = \cos \varphi \times C_{p\,\varphi=0} \quad \ldots \quad (2.22)$$

by equation (2.12). Only in this approximation are the pressures on a sheared wing reduced by a factor $\cos \varphi$ as compared with those on an unswept aerofoil. Fig. 3 illustrates that again only the full equation (2.21) gives adequate results. The results of the linearised theory become necessarily less accurate as the angle of sweep increases since the assumptions made in deriving equation (2.22) are

$$S^{(1)}(x) << \cos \varphi \text{ and } S^{(2)}(x) << \cos \varphi \, .$$

The thickness terms also become more important with sweep because they are proportional to $(t/c)/\cos \varphi$, t/c being measured along wind.

2.3. *Compressible Flow.—Critical Mach Number.*—Before extending the solutions described in the previous paragraphs to subcritical compressible flow, we shall have to determine the limit of this flow régime, *i.e.*, the so-called critical Mach number. If the Mach number of the free stream is increased, the flow will first become supersonic in a limited region near the body and eventually become supersonic everywhere, with the possible exception of a region near the nose of a rounded body. Subcritical flow is defined here as one where a body in it does not experience a drag force. It obeys a differential equation of the elliptic type. The differential equation must be of the hyperbolic type before there is any possibility of a drag. Such a drag force is the manifestation of an increase of entropy associated with shock-waves. We therefore call that free-stream Mach number at which the differential equation which governs the flow changes its type the critical Mach number $M_{0\,\mathrm{crit}}$ or M_{crit} for short. Whether such a drag will occur immediately when the critical Mach number is exceeded is not yet known and will not be discussed here.

The compressible, irrotational, inviscid flow is governed by the well-known equation for the velocity potential $\Phi(x,y,z)$. In the co-ordinate system ξ, η, z, defined by equation (2.13), the potential equation reads:—

$$\frac{\partial^2 \Phi}{\partial \xi^2}\left[1 - \frac{(\partial \Phi/\partial \xi)^2}{a^2}\right] - 2\frac{\partial^2 \Phi}{\partial \xi \, dz}\frac{(\partial \Phi/\partial \xi)(\partial \Phi/\partial z)}{a^2} + \frac{\partial^2 \Phi}{\partial z^2}\left[1 - \frac{(\partial \Phi/\partial z)^2}{a^2}\right] = 0 \, . \quad \ldots \quad (2.23)$$

The problem is essentially two-dimensional; thus only two variables appear. Critical conditions in the above sense prevail when equation (2.23) changes from elliptic type to hyperbolic type. The theory of partial differential equations shows that the equation is of the intermediate parabolic type when

$$\left[1 - \left(\frac{\partial \Phi/\partial \xi}{a}\right)^2\right]\left[1 - \left(\frac{\partial \Phi/\partial z}{a}\right)^2\right] - \left[\frac{(\partial \Phi/\partial \xi)(\partial \Phi/\partial z)}{a}\right]^2 = 0$$

(*see* R. Courant, K. O. Friedrichs[5], 1948). This gives

$$1 - \frac{(\partial \Phi/\partial \xi)^2 + (\partial \Phi/\partial z)^2}{a^2} = 0 \, . \quad \ldots \quad (2.24)$$

Now,

$$\left.\begin{aligned} \frac{\partial \Phi}{\partial \xi} &= V_\xi = V_0 \cos \varphi + v_\xi \\ \frac{\partial \Phi}{\partial z} &= V_z = v_z \end{aligned}\right\} \quad \ldots \quad (2.25)$$

so that the condition reads

$$V_\xi^2 + V_\zeta^2 = V_n^2 = a^2 \text{ or } V^2 - V_\eta^2 = V^2 - V_0^2 \sin^2\varphi = a^2 \quad \ldots \quad \ldots \quad (2.24a)$$

since the total velocity is $V^2 = V_\xi^2 + V_\eta^2 + V_\zeta^2$. This states that only the velocity component V_n normal to the direction of sweep must be sonic and not the total velocity which may, in fact, exceed sonic speed since $V^2 = a^2 + V_0^2 \sin^2\varphi \geqslant a^2$.

The various régimes occurring in the flow past an infinite sheared wing as the free-stream Mach number is increased are as follows :—Pure subsonic flow exists until the total velocity along the peak-suction line becomes sonic. If the wing has no sweep, this is also the end of the subcritical régime. If the wing is swept, subcritical flow exists until the velocity component normal to the peak-suction line becomes sonic ; this marking the end of the subcritical régime. This may thus include a Mach number range in which local supersonic regions exist. For a thin and highly swept wing it is also possible that subcritical conditions persist with supersonic free streams. The flow cannot have shock-waves in the subcritical régime, and it seems possible that there is a régime where the flow is supercritical without having shock-waves and a drag rise.

In order to determine the critical Mach number, the velocity, or pressure, at the critical condition must be related to the free-stream Mach number $V_0/a_0 = V_0\sqrt{(\rho_0/kp_0)}$

$$a^2 = a_0^2 + \frac{k-1}{2}(V_0^2 - V^2),$$

assuming isentropic flow. Hence, with equation (2.24a),

$$\left(\frac{V}{V_0}\right) = \left(\frac{V}{V_0}\right)_{\text{crit}} = \sqrt{\left\{1 + \frac{2}{(k+1)M_0^2}(1 - M_0^2\cos^2\varphi)\right\}}. \quad \ldots \quad \ldots \quad (2.26)$$

Introducing the static pressure

$$\frac{p}{p_0} = \left\{1 + \frac{k-1}{2}M_0^2\left[1 - \left(\frac{V}{V_0}\right)^2\right]\right\}^{k/(k-1)}$$

and the total head

$$\frac{H_0}{p_0} = \left\{1 + \frac{k-1}{2}M_0^2\right\}^{k/(k-1)},$$

as measured by a pitot-tube, for isentropic flow, we find

$$\left(\frac{p}{H_0}\right)_{\text{crit}} = \left(\frac{2}{k+1}\right)^{k/(k-1)}\left(\frac{1 + \frac{k-1}{2}M_0^2\cos^2\varphi}{1 + \frac{k-1}{2}M_0^2}\right)^{k/(k-1)} \quad \ldots \quad \ldots \quad \ldots \quad (2.27)$$

This implies that the air can expand over a swept wing more than the well-known St. Venant expansion which gives for the pressure ratio

$$\left(\frac{p}{H_0}\right)_{\text{crit}} = \left(\frac{2}{k+1}\right)^{k/(k-1)} = 0{\cdot}528$$

for $k = 1{\cdot}40$, as for the unswept wing. Instead of the critical pressure ratio, the critical pressure coefficient

$$C_p^* = \frac{p_{cri} - p_0}{\frac{1}{2}\rho_0 V_0^2}$$

may be used. This leads to

$$C_p^* = \frac{2}{kM_0^2}\left[\left(\frac{2}{k+1}\right)^{k/(k-1)}\left(1 + \frac{k-1}{2} M_0^2 \cos^2\varphi\right)^{k/(k-1)} - 1\right] \quad \ldots \quad \ldots \quad (2.28)$$

for isentropic flow.

The differential equation (2.23) is often simplified to read

$$\frac{\partial^2 \Phi}{\partial \xi^2}\beta^2 + \frac{\partial^2 \Phi}{\partial z^2} = 0\,, \text{ where } \beta^2 = 1 - \left(\frac{\partial \Phi/\partial \xi}{a}\right)^2. \quad \ldots \quad \ldots \quad \ldots \quad \ldots \quad \ldots \quad (2.29)$$

This makes it amenable to an analytic treatment. Equation (2.29) is correct for incompressible flow, where $\beta = 1$. It is normally used also for flat bodies in the subcritical flow range on the grounds that the mixed term in equation (2.23),

$$2\frac{\partial^2 \Phi}{\partial \xi\, \partial z}\frac{(\partial \Phi/\partial \xi)(\partial \Phi/\partial z)}{a^2} = 2\frac{\partial V_z}{\partial \xi}\frac{V_\xi V_z}{a^2}\,,$$

contains the cross-flow component V_z and its derivative, which can be assumed to be small compared with the velocity of sound (*see* L. Prandtl[8], 1936). The simplified equation (2.29) is further used at sonic conditions by Th. von Kármán[25], 1941, although the first term then vanishes, by equation (2.24), and equation (2.29) implies that the third term vanishes too. It would have to be shown in the general case that the solutions obtained from equation (2.29) lead to a mixed term in equation (2.23) which is still small compared with the other two terms (*see* also E. V. Laitone[10], 1951).

In the present paper, the simplified equation (2.29) will be used throughout the whole subcritical flow range. This leads to $\beta = 0$ as defining critical conditions and this is the same as equation (2.24) for flat bodies where $\partial \Phi/\partial z << a$.

2.4. *Approximate Solutions for Sub-critical Flow.*—The simplified potential equation (2.29) can readily be solved if some further simplifications, including linearisation, are introduced. The factor into the first term

$$\beta^2 = 1 - \frac{1}{a^2}\left(\frac{\partial \Phi}{\partial \xi}\right)^2 = 1 - \frac{V_\xi^2}{a^2}$$

can be approximated by

$$\beta^2 = 1 - \frac{V_n^2}{a^2} = 1 - \frac{V^2 - V_0^2 \sin^2\varphi}{a^2}$$

because for flat aerofoil sections, the term $(v_z/a)^2$ can be neglected compared with 1. The flow in the leading-edge region of bodies with rounded noses is thus excluded. Hence,

$$\beta^2 = 1 - \frac{V_0^2\cos^2\varphi + V^2 - V_0^2}{a_0^2 + \frac{k-1}{2}\left(V_0^2 - V^2\right)} = 1 - M_0^2\frac{\cos^2\varphi + \left(\frac{V}{V_0}\right)^2 - 1}{1 - \frac{k-1}{2}M_0^2\left[\left(\frac{V}{V_0}\right)^2 - 1\right]}\,. \quad (2.30)$$

Further, we may assume that the local velocity V is not very different from the free-stream velocity V_0, so that

$$\frac{k-1}{2} M_0^2 \left[\left(\frac{V}{V_0}\right)^2 - 1\right] << 1 .$$

In that case,

$$\beta^2 = 1 - M_0^2 \left\{\cos^2 \varphi + \left[\left(\frac{V}{V_0}\right)^2 - 1\right]\right\} . \quad .. \quad .. \quad .. \quad .. \quad .. \quad (2.31)$$

A simple solution of equation (2.29) can be obtained if β is assumed to be constant, *i.e.*, independent of ξ and z. The function $V(\xi,z)$ in equation (2.31) must then be replaced by a constant mean value, suitably chosen to represent the actual velocity over the suction region of the aerofoil.

In many cases, the velocity will be known only for incompressible flow*. The velocity term can then be replaced by a suitably chosen mean value of the pressure coefficient, C_{pi}, on the aerofoil in incompressible flow,

$$\left(\frac{V}{V_0}\right)^2 - 1 = - C_{pi} ,$$

so that

$$\beta^2 = 1 - M_0^2\{\cos^2 \varphi - C_{pi}\} = \text{const.} \quad .. \quad .. \quad .. \quad .. \quad .. \quad .. \quad (2.32)$$

This includes the well-known Prandtl-Glauert approximation as the special case $C_{pi} = 0$.

To solve equation (2.29) with β from equation (2.32) the transformation

$$\left.\begin{aligned} \xi_a &= \xi \\ z_a &= \beta z \end{aligned}\right\} \quad .. \quad .. \quad .. \quad .. \quad .. \quad .. \quad .. \quad .. \quad .. \quad (2.33)$$

of the wing into another, ' analogous ', sheared wing can be used. By this transformation, the perturbation potential $\Phi' = \Phi - V_0 \cos \varphi \, . \, \xi$ will also be changed and we put

$$\Phi_a' = \Phi_a - V_0 \cos \varphi \, . \, \xi_a = \lambda(\Phi - V_0 \cos \varphi \, . \, \xi) = \lambda \Phi' \quad .. \quad .. \quad .. \quad (2.34)$$

The factor λ is determined by the condition that both wings must be stream surfaces in their respective flows (' *Streamline analogy* ' of A. Busemann[6], 1928; and B. Göthert[7], 1941). By equations (2.1) and (2.25),

$$\frac{dz}{d\xi} = \frac{v_z}{V_\xi} = \frac{\partial\Phi/\partial z}{\partial\Phi/\partial\xi} \text{ and } \frac{dz_a}{d\xi_a} = \frac{v_{za}}{V_{\xi a}} = \frac{\partial\Phi_a/\partial z_a}{\partial\Phi_a/\partial\xi_a} . \quad .. \quad .. \quad .. \quad .. \quad (2.35)$$

This gives

$$\frac{dz}{d\xi} = \frac{dz_a}{d\xi_a}\frac{1}{\beta} = \frac{\lambda\, \partial\Phi/\partial z}{\beta^2(V_0 \cos \varphi + \lambda[\partial\Phi/\partial\xi - V_0 \cos \varphi])}$$

$$= \frac{\lambda\, \partial\Phi/\partial\xi}{\beta^2(V_0 \cos \varphi + \lambda[\partial\Phi/\partial\xi - V_0 \cos \varphi])}\frac{dz}{d\xi}$$

so that

$$\lambda \frac{\partial\Phi/\partial\xi}{V_0 \cos \varphi + \lambda[\partial\Phi/\partial\xi - V_0 \cos \varphi]} = \beta^2 .$$

* A method of iteration can also be used whereby the velocity V in equation (2·31) for β is replaced by its value in compressible flow as obtained from a first approximation. Using the Prandtl-Glauert rule to obtain a first approximation leads to the method of E. V. Laitone[10], 1951.

Here again we simplify matters by assuming that the velocity increment v_ξ is small as compared with $V_0 \cos\varphi$ so that $\partial\Phi/\partial\xi = V_0 \cos\varphi$, in which case

$$\lambda = \beta^2$$

and

$$\Phi_a' = \Phi_a - V_0 \cos\varphi \,.\, \xi_a = \beta^2(\Phi - V_0 \cos\varphi \,.\, \xi) = \beta^2\Phi' \,. \quad .. \quad .. \quad (3.34a)$$

The potential equation (2.29) reads then

$$\frac{\partial^2\Phi_a}{\partial\xi_a^2} + \frac{\partial^2\Phi_a}{\partial z_a^2} = 0 \,, \text{ or } \frac{\partial^2\Phi_a'}{\partial\xi_a^2} + \frac{\partial^2\Phi_a'}{\partial z_a^2} = 0 \,, \quad .. \quad .. \quad .. \quad .. \quad .. \quad (2.36)$$

i.e., it has been reduced to Laplace's equation.

A solution of equation (2.36) is given by equation (2.17) if we restrict ourselves again to thin bodies where the velocity increment can be calculated on the chord-line instead of on the surface. Using the expression for $S^{(1)}(x)$ from equation (2.7), we find

$$\frac{v_{\xi a}}{V_0} = S_a^{(1)}(x) = \sum_{\mu=1}^{N-1} s_{\mu\nu}^{(1)} z_{\mu a} \,.$$

Now, the aerofoil section of the analogous wing is thinner than that of the given wing by the factor β, by equation (2.33); hence,

$$\frac{v_{\xi a}}{V_0} = \beta \sum_{\mu=1}^{N-1} s_{\mu\nu}^{(1)} z_\mu = \beta \frac{v_{\xi i}}{V_0} \quad .. \quad .. \quad .. \quad .. \quad .. \quad .. \quad (2.37)$$

where $v_{\xi i}$ is the velocity increment on the given wing in incompressible flow, by equation (2.17). The velocity increment on the given wing in compressible flow is

$$\frac{v_\xi}{V_0} = \frac{\partial\Phi'}{\partial\xi} = \frac{1}{\beta^2}\frac{\partial\Phi_a'}{\partial\xi_a} = \frac{1}{\beta^2}\frac{v_{\xi a}}{V_0} \quad .. \quad .. \quad .. \quad .. \quad .. \quad .. \quad (2.38)$$

by equation (2.34a). Combining equations (2.37) and (2.38),

$$\frac{v_\xi}{V_0} = \frac{1}{\beta}\frac{v_{\xi i}}{V_0} \,. \quad .. \quad .. \quad .. \quad .. \quad .. \quad .. \quad .. \quad .. \quad (2.39)$$

By equations (2.18) and (2.22), the velocity increments in x- and y-direction and the pressure coefficients will also increase in the ratio $1/\beta$, within this approximation, so that

$$\frac{v_x}{V_0} = \frac{1}{\beta}\frac{v_{xi}}{V_0}; \quad \frac{v_y}{V_0} = \frac{1}{\beta}\frac{v_{yi}}{V_0}; \text{ and } C_p = \frac{1}{\beta}C_{pi} \,. \quad .. \quad .. \quad .. \quad (2.40)$$

The method described above follows the well-known procedure of L. Prandtl[8], 1936, and H. Glauert[9], 1928; it enables the calculation to be done for incompressible flow using the method described in section 2.2, and a compressibility correction applied afterwards. To obtain the Prandtl-Glauert rule, the value of β in equation (2.40) is taken from equation (2.32) with $C_{pi} = 0$, *i.e.*, the aerofoil is assumed to be so thin that the pressure coefficient can be ignored as compared with $\cos^2\varphi$. In this case,

$$\frac{v_x}{v_{xi}} = \frac{C_p}{C_{pi}} = \frac{1}{\sqrt{(1 - M_0^2\cos^2\varphi)}} \,. \quad .. \quad .. \quad .. \quad .. \quad .. \quad (2.41)$$

If C_{p_i} is not so small that it can be ignored altogether, it can be replaced by its mean value over the suction region, or by the peak value, in which case

$$\frac{v_x}{V_0} = \frac{C_p}{C_{p_i}} \sqrt{\{1 - M_0^2(\cos^2\varphi - C_{p_i})\}} \quad \ldots \quad (2.42)$$

This rule (2.42) was derived by J. Weber, 1948, and a similar relation was again proposed by E. V. Laitone[10], 1951, differing, however, by some terms with $M_0^4 C_{p_i}$ which cause the velocity to rise more steeply with Mach number. The Weber-Laitone rule represents the logical second-order refinement of the Prandtl-Glauert rule; it is consistent with the transonic similarity law of von Kármán.

Strictly, the rule (2.42) applies only to the velocity increase and not to the pressures. The velocity V in compressible flow should be determined first and the pressure coefficient afterwards from Bernoulli's equation for compressible flow:—

$$C_p = \frac{2}{kM_0^2}\left[1 - \left\{1 + \frac{k-1}{2} M_0^2\left[1 - \left(\frac{V}{V_0}\right)^2\right]\right\}^{k/(k-1)}\right]. \quad \ldots \quad (2.43)$$

To facilitate the calculation of C_p from equation (2.43), a diagram has been prepared, Fig. 5, from which the value of C_p in compressible flow can be read if the value of V/V_0 $(= 1 + v_x/V_0)$ is known.

The relation for C_p can be written as a power series in $(v_x/V_0)^2$, where $V = V_0 + v_x$ if

$$\frac{k-1}{2} M_0^2\left[1 - \left(\frac{V}{V_0}\right)^2\right] < 1.$$

In this case,

$$C_p = 1 - \left(\frac{V}{V_0}\right)^2 + \frac{M_0^2}{4}\left[1 - \left(\frac{V}{V_0}\right)^2\right]^2 + \frac{2-k}{24} M_0^4\left[1 - \left(\frac{V}{V_0}\right)^2\right]^3 + \ldots \quad \ldots \quad (2.44)$$

or

$$C_p = -2\frac{v_x}{V_0} - (1 - M_0^2)\left(\frac{v_x}{V_0}\right)^2 + \ldots \quad \ldots \quad (2.45)$$

There is little reliable evidence from experiments to check the accuracy of the various rules. The particular examples in Figs. 6 and 7 show that equation (2.42) agrees better with experimental values than either the Prandtl-Glauert rule or the rule of Th. von Kármán[11] (1941) for both unswept and swept-back aerofoils. The necessity of applying the rule to v_x and of evaluating the C_p afterwards can be seen.

By applying any of these rules, the pressure distribution from incompressible potential flow is multiplied by a factor and no overall drag results. The rules apply, therefore, only to subcritical flow, the range of which was discussed in section 2.3. In particular, the critical pressure coefficient is given by equation (2.28). Combining equations (2.42) and (2.28), the critical flight Mach number $M_{0\,\mathrm{crit}}$ can be found for any given value of C_{p_i} and φ. Charts on this basis are drawn in Fig. 8 to enable a quick estimate for the critical flight Mach number of sheared wings of infinite span.

3. *The Centre-section of a Swept Wing of Infinite Span.*—The peculiarities of the flow past the centre region of a swept wing may be more readily understood by considering first the properties of a kinked source line, as is done in section 3.1. From that a general formula for the velocity distribution over the centre-section of a swept wing is derived in section 3.2. The relation between

section shape and source distribution is considered in section 3.3. A simple method of calculation for practical purposes is then given in section 3.4 together with a brief discussion of the resulting aerodynamic properties. Very little is as yet known about the effects of compressibility; some approximate solutions for subcritical flow are given in section 3.5.

3.1. *Properties of a Kinked Source Line.*—Since the swept-back wing will be built up by a distribution of kinked source lines let us consider first a single kinked source line of strength E per unit length as indicated in Fig. 9. One semi-infinite side of the kinked line produces the following velocity components normal and tangential to the line:—

$$v_n = \frac{E}{4\pi r}(1 + \cos\varphi); \qquad v_t = -\frac{E}{4\pi r}\sin\varphi \quad . \quad . \quad . \quad . \quad . \quad . \quad . \quad . \quad (3.1)$$

For a given point on the line of symmetry we have

$$\varphi = -\eta + \frac{\pi}{2}$$

so that the total velocity on the centre-line, induced by the whole kinked line and directed along the main stream amounts to

$$\begin{aligned} v_1 &= 2(v_n \cos\eta + v_t \sin\eta) \\ &= \frac{E}{2\pi x \cos\varphi}[(1 + \sin\varphi)\cos\varphi - \cos\varphi \sin\varphi] \\ v_1 &= \frac{E}{2\pi x} \quad . \quad . \quad . \quad . \quad . \quad . \quad . \quad . \quad . \quad . \quad . \quad . \quad . \quad . \quad (3.2) \end{aligned}$$

This result, first shown by H. Ludwieg[12], 1946, in another way, states that at any point on the line of symmetry the velocity induced by a kinked source line is equal to that of a straight source line of infinite length through the kink point. Nothing can, however, be stated about the kink point itself. The important result follows that, for any given distribution of kinked source lines along the x-axis to represent a swept wing, the velocity increment v_x at a point x in the line of symmetry is equal to that of the corresponding distribution of straight source lines, representing an unswept wing, but for a contribution which may arise from the source element through the point $x' = x$ itself, which, in turn, must depend on the local source strength.

The singular kink point therefore requires special attention and to obtain the velocity there by integration of the contributions by a distribution of source lines the limit must be taken by approaching this point along a path outside any singularities, for instance the limit as $z \to 0$. For this purpose, we determine first the three velocity components which are induced at a point (x,y,z) by a single kinked source line as in Fig. 9.

The velocity dv at the point x,y,z (in the direction of the radius vector) induced by a source element Eds in x',y',z' has the direction of the radius vector and is

$$dv = \frac{Eds}{4\pi R^2} = \frac{E}{4\pi}\frac{1}{R^2}\frac{dy'}{\cos\varphi} \quad . \quad . \quad . \quad . \quad . \quad . \quad . \quad . \quad (3.3)$$

where

$$R = \sqrt{\{(x - x')^2 + (y - y')^2 + (z - z')^2\}} = \sqrt{\{(x - y'\tan\varphi)^2 + (y - y')^2 + z^2\}}.$$

This square root, being a geometric distance, is always positive. The streamwise component of the induced velocity is

$$dv_x = dV \cdot \frac{x - x'}{R} = \frac{E}{4\pi \cos\varphi} \frac{x - y' \tan\varphi}{R^3} dy' .$$

The total induced velocity component of a straight semi-infinite line—which can be regarded as the right-hand side of a kinked source line—is obtained by integration :—

$$v_x(x,y,z) = \frac{E}{4\pi} \frac{(x - y\tan\varphi)\left(\sqrt{(x^2 + y^2 + z^2)} + \frac{y}{\cos\varphi}\right) - \frac{\sin\varphi}{\cos^2\varphi} z^2}{\left\{(x - y\tan\varphi)^2 + \frac{z^2}{\cos^2\varphi}\right\}\sqrt{(x^2 + y^2 + z^2)}} .$$

The whole kinked source line as shown in Fig. 9 gives :—

$$v_x(x,y,z) = \frac{E}{4\pi}\left[\frac{(x - y\tan\varphi)\left(\sqrt{(x^2 + y^2 + z^2)} + \frac{y}{\cos\varphi}\right) - \frac{\sin\varphi}{\cos^2\varphi} z^2}{\left\{(x - y\tan\varphi)^2 + \frac{z^2}{\cos^2\varphi}\right\}\sqrt{(x^2 + y^2 + z^2)}}\right.$$

$$\left. + \frac{(x + y\tan\varphi)\left(\sqrt{(x^2 + y^2 + z^2)} - \frac{y}{\cos\varphi}\right) - \frac{\sin\varphi}{\cos^2\varphi} z^2}{\left\{(x + y\tan\varphi)^2 + \frac{z^2}{\cos^2\varphi}\right\}\sqrt{(x^2 + y^2 + z^2)}}\right] . \quad .. \quad .. \quad (3.4)$$

In the same way we find the induced velocity component v_y in the direction of the positive y-axis :—

$$v_y(x,y,z) = \frac{E}{4\pi\cos\varphi}\left[-\frac{(x - y\tan\varphi)(\sin\varphi\sqrt{(x^2 + y^2 + z^2)} + x) + z^2}{\left\{(x - y\tan\varphi)^2 + \frac{z^2}{\cos^2\varphi}\right\}\sqrt{(x^2 + y^2 + z^2)}}\right.$$

$$\left. + \frac{(x + y\tan\varphi)(\sin\varphi\sqrt{(x^2 + y^2 + z^2)} + x) + z^2}{\left\{(x + y\tan\varphi)^2 + \frac{z^2}{\cos^2\varphi}\right\}\sqrt{(x^2 + y^2 + z^2)}}\right] . \quad .. \quad .. \quad .. \quad (3.5)$$

and the induced velocity component v_z in the direction of the positive z-axis (downwards) :—

$$v_z(x,y,z) = \frac{E}{4\pi}\frac{z}{\cos^2\varphi}\left[\frac{\sqrt{(x^2 + y^2 + z^2)} + (x\sin\varphi + y\cos\varphi)}{\left\{(x - y\tan\varphi)^2 + \frac{z^2}{\cos^2\varphi}\right\}\sqrt{(x^2 + y^2 + z^2)}}\right.$$

$$\left. + \frac{\sqrt{(x^2 + y^2 + z^2)} + (x\sin\varphi - y\cos\varphi)}{\left\{(x + y\tan\varphi)^2 + \frac{z^2}{\cos^2\varphi}\right\}\sqrt{(x^2 + y^2 + z^2)}}\right] . \quad .. \quad .. \quad .. \quad .. \quad (3.6)$$

By integration these relations can be used to calculate the velocity components induced at any point by any distribution of such source lines. In the present paper, they are used only to determine the velocity increment at the centre-line of a swept wing.

3.2. *General Formula for the Streamwise Velocity Increment.*—The swept wing of infinite span with a kink at $y = 0$, as shown in Fig. 4, is replaced by a distribution of sources and sinks of strength $q(x,y)$ per unit area. These can be regarded as composed of single kinked source lines of constant strength E per unit length along the η-axis. The source strengths are related by the identity

$$E\,ds = E\,\frac{dy}{\cos\varphi} = q\,dx\,dy$$

so that

$$E = q\cos\varphi\,dx \quad . \quad . \quad . \quad . \quad . \quad . \quad . \quad . \quad . \quad . \quad (3.7)$$

With equation (3.4) we obtain

$$v_x(x,0,z) = \frac{\cos\varphi}{2\pi}\int_0^1 q(x')\,\frac{1}{(x-x')^2 + z^2/\cos^2\varphi} \times$$

$$\left\{x - x' - \sin\varphi\,\frac{z^2/\cos^2\varphi}{\sqrt{[(x-x')^2 + z^2]}}\right\} dx' \quad . \quad . \quad . \quad . \quad . \quad (3.8)$$

In this relation, all the co-ordinates are again non-dimensional with the wing chord. We can see already that the singularity at $x = x'$ as $z \to 0$ is not of such a kind that the principal value of the integral can be taken. The integration is therefore done first and the limit as $z \to 0$ is taken afterwards.

It is convenient to split the integral into two terms :—

$$\frac{2\pi}{\cos\varphi}\,v_x(x,0,z) = I_1(x,0,z) + I_2(x,0,z) \quad . \quad . \quad . \quad . \quad . \quad . \quad . \quad . \quad (3.9)$$

where

$$I_1(x,0,z) = \int_0^1 q(x')\,\frac{x-x'}{(x-x')^2 + (z/\cos\varphi)^2}\,dx' \quad , \quad . \quad . \quad . \quad . \quad . \quad (3.10)$$

$$I_2(x,0,z) = -\sin\varphi\int_0^1 q(x')\,\frac{(z/\cos\varphi)^2}{\{(x-x')^2 + (z/\cos\varphi)^2\}\sqrt{\{(x-x')^2 + z^2\}}}\,dx' \quad . \quad . \quad (3.11)$$

Putting $z = 0$ before integrating is permissible for the first integral, and the principal value must be taken:—

$$I_1(x,0,0) = \int_0^1 q(x')\,\frac{dx'}{x-x'} = 2\pi v_x(x,0)_{\varphi=0}$$

by equation (2.4). This leads to a first term

$$v_{x1}(x,0,0) = \cos\varphi\,.\,v_x(x,0)_{\varphi=0} = v_{xS}(x,0) \quad . \quad . \quad . \quad . \quad . \quad . \quad . \quad (3.12)$$

which is equal to the velocity increment $v_{xS}(x,0)$ of the sheared wing of infinite span. The existence of such a term has been predicted in section 3.1 from the properties of a kinked source line. The $\cos\varphi$ factor to $[v_x]_{\varphi=0}$ arises from the corresponding factor in equation (3.7).

In the second integral, z can be put equal to zero before integrating within two intervals not containing $x' = x$; that is from 0 to $x - a$ and from $x + a$ to $+1$; a being a finite positive number which is small compared with unity. Within these intervals, $I_2 \to 0$ as $z \to 0$. If $q(x)$

is a continuous function, it can be replaced by a constant value within the remaining interval $-a \leqslant x - x' \leqslant +a$, by its value at $x' = x$ say. $I_2(x,0,0)$ can then be written as

$$I_2(x,0,0) = -\sin\varphi \cdot q(x) \lim_{z\to 0} \int_{-a}^{+a} \frac{(z/\cos\varphi)^2}{\{(x-x')^2 + (z/\cos\varphi)^2\}\sqrt{\{(x-x')^2 + z^2\}}}\, d(x-x')$$

which gives

$$I_2(x,0,0) = -q(x) \lim_{z\to 0} \ln \frac{\sqrt{\{1 + (z/a)^2\}} + \sin\varphi}{\sqrt{\{1 + (z/a)^2\}} - \sin\varphi}$$

The limit as z tends to zero is independent of the choice of a, and we find

$$I_2(x,0,0) = -\pi q(x) f(\varphi) \text{ where } f(\varphi) = \frac{1}{\pi} \ln \frac{1+\sin\varphi}{1-\sin\varphi} \quad \ldots\ldots\ldots\ldots\ldots\ldots \quad (3.13)$$

This leads to a second term

$$v_{x2}(x,0,0) = -\frac{q(x)}{2} \cos\varphi\, f(\varphi) \quad \ldots\ldots\ldots\ldots\ldots\ldots\ldots\ldots \quad (3.14)$$

which depends only on the local source strength and on the angle of sweep, again as predicted above. $v_{x2} = 0$ for $\varphi = 0$. For small values of φ, the function $f(\varphi)$ can be expanded into a power series in φ:—

$$f(\varphi) = \frac{2}{\pi}\left(\varphi + \frac{\varphi^3}{6} + \ldots\right), \quad \ldots\ldots\ldots\ldots\ldots\ldots\ldots\ldots \quad (3.15)$$

of which the first term gives a good approximation up to about $\varphi = 30$ deg. The term v_{x2}, which is caused by the ' centre effect ' changes sign with the angle of sweep because $f(\varphi)$ changes its sign. Some numerical values of $f(\varphi)$ are given below:—

φ (deg)	$f(\varphi)$	φ (deg)	$f(\varphi)$	φ (deg)	$f(\varphi)$
0	0	30	0·350	60	0·838
5	0·056	35	0·416	65	0·959
10	0·112	40	0·486	70	1·105
15	0·169	45	0·561	75	1·291
20	0·227	50	0·643	80	1·551
25	0·287	55	0·735	85	1·993
				90	∞

The total induced velocity $v_x = v_{x1} + v_{x2}$ at the centre-line is then given by

$$v_x(x,0,0) = v_{x1} + v_{x2} = v_{xs}(x) - \frac{q(x)}{2} \cos\varphi\, f(\varphi) \quad \ldots\ldots\ldots\ldots\ldots \quad (3.16)$$

by equations (3.9), (3.12), and (3.14).

The type of solution, equation (3.16), and in particular the existence of an additional term proportional to the local source strength, may be illustrated by considering the midpoint of a uniform distribution of sources over a kinked strip, as shown in Fig. 10. In the two-dimensional

case, *i.e.*, for a straight strip without kink, the value v_z of the induced velocity at the midpoint would be zero, there being always a source element on one side of the midpoint to counterbalance the effect of another on the other side. With a kinked strip, however, only the sources in the shaded area counterbalance each other. Obviously, the remaining sources produce a velocity increment directed against the main stream, the magnitude of which is given by equation (3.14) as can be seen by considering $2a$ as the chord of the strip.

3.3. *The Vertical Velocity Component and the Shape of the Section.*—So far, the velocity distribution at the centre is known only in terms of the source distribution $q(x)$ which replaces the aerofoil. The next step is, therefore, to relate $q(x)$ to the shape of the aerofoil and, in particular to check whether equation (2.2) which holds for the unswept and the sheared wing of infinite span is still true.

v_z can be found from equation (3.6) by integration. Using equation (3.7), we have

$$v_z(x,0,z) = \frac{x}{2\pi \cos\varphi} \int_0^1 q(x') \frac{\sqrt{\{(x-x')^2 + z^2\}} + (x-x')\sin\varphi}{\{(x-x')^2 + (z/\cos\varphi)^2\}\sqrt{\{(x-x')^2 + z^2\}}}\, dx'$$

which it is convenient to split into two integrals:—

$$v_z(x,0,z) = \frac{1}{2\pi \cos\varphi} \int_0^1 q(x') \frac{z}{(x-x')^2 + (z/\cos\varphi)^2}\, dx'$$

$$+ \frac{\tan\varphi}{2\pi} \cdot z \int_0^1 q(x') \frac{x-x'}{\{(x-x')^2 + (z/\cos\varphi)^2\}\sqrt{\{(x-x')^2 + z^2\}}}\, dx'. \qquad .. \quad (3.17)$$

We are again chiefly interested in the limiting value of v_z as $z \to 0$. Splitting the range of integration into three intervals, as above, we note that $v_z \to 0$ as $z \to 0$ outside the interval $-a \leqslant x - x' \leqslant a$. Inside this interval, the second integral also vanishes because the integrand is antisymmetrical to $x = x'$. The first integral requires special treatment. In a small range about the point $x = x'$, $q(x)$ can again be replaced by its value at $x = x'$, so that

$$v_z(x,0,z) = \frac{q(x)}{2\pi \cos\varphi} \int_{-a}^{+a} \frac{z}{(x-x')^2 + (z/\cos\varphi)^2}\, d(x-x')$$

which gives

$$v_z(x,0,z) = \frac{q(x)}{\pi} \arctan \frac{a}{z/\cos\varphi}.$$

In the limit as $z \to 0$, provided z tends to zero more quickly than a,

$$v_z(x,0,0) = \pm \frac{q(x)}{2} \qquad .. \quad .. \quad .. \quad .. \quad .. \quad .. \quad .. \quad .. \quad .. \quad .. \quad (3.18)$$

which is the same result as equation (2.2). It may be noted that the derivation given here includes, of course, the straight wing as the special case $\varphi = 0$. Equation (3.18) allows a swept wing of constant chord and constant section to be represented by source lines of constant strength along the span.

It has been found, from a numerical evaluation of the integral (3.17) for the special case of a 30-deg swept-back wing with a biconvex parabolic section, $t/c = 0{\cdot}2$, that equation (3.18) still gives a good approximation for the actual distribution of $v_z(x,0,z)$ along the surface. Other cases,

in particular sections with rounded noses, still require to be investigated. Nor has it been checked whether the streamline condition (2.1) can be replaced by the simplified relation (2.3) with sufficient accuracy, and it is particularly questionable whether v_x can be ignored compared with the free-stream velocity V_0, now that v_x contains a term proportional to $q(x)$ which is tending to infinity at the leading edge of sections with rounded noses. In the following, however, we shall assume that equation (2.3) is adequate for practical purposes.

3.4. *Method of Calculating the Pressure Distribution and Evaluation of the Aerodynamic Characteristics.*—Combining equations (2.3), (3.16), and (3.18), we have

$$\frac{v_x(x,0,0)}{V_0} = \frac{v_{xS}(x,0,0)}{V_0} - \cos\varphi\, f(\varphi)\, \frac{dz(x)}{dx} \quad .. \quad .. \quad .. \quad .. \quad .. \quad (3.19)$$

or

$$\frac{v_x(x,0,0)}{V_0} = \left\{\left(\frac{v_x(x,0)}{V_0}\right)_{\varphi=0} - f(\varphi)\, \frac{dz(x)}{dx}\right\} \cos\varphi \; . \quad .. \quad .. \quad .. \quad .. \quad (3.19a)$$

The most important features of this relation are:

(*a*) that it contains a term which does not differ from that for an infinite sheared wing,

(*b*) that the additional term, the ' centre effect ', depends on the angle of sweep and the local slope of the aerofoil section only.

Thus, compared with the velocity increments of an infinite sheared wing, the velocity is decreased upstream, and increased downstream, of the maximum thickness position, for positive angles of sweep. Therefore the value and the chordwise location of the maximum velocity at the centre-section differ from those at the sheared wing, and this difference varies appreciably with the maximum thickness position and the trailing-edge angle. On swept-forward wings, the maximum value of the velocity at the centre is usually much higher than at a station which is not influenced by the centre effect; in this case, the nose thickness is the most important parameter. Generally, the velocity peak is shifted backwards for swept-back wings and forwards for swept-forward wings.

This change of flow near the centre of a swept wing was first pointed out by B. Göthert[13] (1942), who also measured the pressure distribution at the centre of a swept-forward wing. W. Krüger[14] (1946) showed the effect for the centre of a swept-back wing. Calculations have been made by R. T. Jones[15] (1947), S. Neumark[16] (1947) and F. Ursell[17] (1948) on the basis of linearised theory for the biconvex-parabolic and other related aerofoil sections. The general relations above were given by Küchemann (1947).

It is convenient for numerical calculations to introduce the functions $S^{(1)}(x)$ and $S^{(2)}(x)$ from equations (2.7) and (2.8) into equation (3.19a), which gives

$$\frac{v_x(x,0,0)}{V_0} = [S^{(1)}(x) - f(\varphi)\,.\,S^{(2)}(x)] \cos\varphi \; . \quad .. \quad .. \quad .. \quad .. \quad .. \quad (3.20)$$

With the coefficients given in Tables 1 and 2, $S^{(1)}$ and $S^{(2)}$ represent sums involving the given ordinates $z(x)$ of the aerofoil section. Equation (3.20) then represents a system of linear equations from which either the velocity distribution can be obtained for a given section shape, or the section shape defined for a given velocity distribution. In the latter case, certain conditions must be observed in order to obtain a reasonable section contour which closes and does not overlap (*see* also section 4.4.).

Since equation (3.20) is based on linearised theory and since it gives the velocity increment only on the chord-line, it is not normally accurate enough to put $V(x,z) = V_0 + v_x(x,0)$,

especially for round-nosed sections. An approximation* for the velocity along the surface of the aerofoil may be obtained by using equation (2.5), which gives

$$\frac{V(x,z)}{V_0} = \frac{1 + \left\{\left(\frac{v_x(x,0)}{V_0}\right)_{\varphi=0} - f(\varphi)\,\frac{dz(x)}{dx}\right\}\cos\varphi}{\sqrt{\left\{1 + \left(\frac{dz(x)}{dx}\right)^2\right\}}} \quad \ldots \quad (3.21)$$

or by equation (2.8),

$$\frac{V(x,z)}{V_0} = \frac{1 + (S^{(1)}(x) - f(\varphi)\,S^{(2)}(x))\cos\varphi}{\sqrt{\{1 + S^2(x)^2\}}} \quad \ldots \quad (3.22)$$

The pressure coefficient is then

$$C_p(x,z) = -\frac{2\cos\varphi\,(S^{(1)}(x) - f(\varphi)\,S^{(2)}(x)) - (S^{(1)}(x) - f(\varphi)\,S^{(2)}(x))^2\cos^2\varphi + S^{(2)}(x)^2}{1 + S^{(2)}(x)^2} \quad \ldots \quad (3.23)$$

It must be noted, however, that the use of equation (2.5) has been justified for two-dimensional aerofoils only and is correct for the line integral of the velocity around the aerofoil contour. It is not necessarily true at all chordwise positions at the centre of swept wings. An analytical check on its validity, which would be very tedious, has not yet been made.

A comparison between experimental values for the velocity at the centre of two swept-back wings and values calculated from equation (3.22), in Fig. 11, shows that a satisfactory approximation is obtained. It is possible that the slight deviations between the experimental and calculated results are genuinely due to an error introduced by using equation (2.5). It appears that the correction is too large near the nose of a swept-forward wing and too small near the nose of a swept-back wing. The values near maximum thickness (where $dz/dx = 0$) are not affected, however. At the centre of a swept-back wing the peak suction value may be higher (for sections with their maximum thickness far back) or lower (for sections with their maximum thickness further forward) than that for the same section on an infinite sheared wing (*see* Fig. 11).

The change of the pressure distribution near the centre of a swept wing causes a finite value of the local form drag, in spite of the assumed potential flow. This normal-pressure drag may be obtained by integration of the pressure distribution or, more conveniently, from the theorem of A. Betz[18] (1932) (analogous to the Kutta-Joukowsky theorem for the lift force)

$$\Delta C_D = \frac{\Delta D}{\frac{1}{2}\rho V_0^2 c} = -2\int_0^1 \frac{V_x(x)}{V_0}\,\frac{q(x)}{V_0}\,dx \,. \quad \ldots \quad (3.24)$$

---

* In this approximation, V is not zero at the leading edge. A better approximation near the leading edge is given by

$$\frac{V(x,z)}{V_0} = \frac{1 + \left\{\left(\frac{v_x(x,0)}{V_0}\right)_{\varphi=0} - f(\varphi)\,\frac{dz/dx}{\sqrt{\{1 + (dz/dx)^2\}}}\right\}\cos\varphi}{\sqrt{\{1 + (dz/dx)^2\}}} \quad \ldots \quad (3.21a)$$

or

$$\frac{V(x,z)}{V_0} = \frac{1 + \left(S^{(1)}(x) - f(\varphi)\,\frac{S^{(2)}(x)}{\sqrt{\{1 + S^{(2)}(x)^2\}}}\right)\cos\varphi}{\sqrt{\{1 + S^{(2)}(x)^2\}}} \quad \ldots \quad (3.22a)$$

Since, at the centre, $V_x = V_0 + v_{xS} - \cos\varphi\, f(\varphi)\,.\,dz/dx$, by equation (3.19), to a first approximation; and since no drag can result from the two-dimensional terms, we have

$$\Delta C_D = 4\cos\varphi\, f(\varphi) \int_0^1 \left(\frac{dz}{dx}\right)^2 dx\,, \qquad \ldots\ldots\ldots\ldots\ldots\ldots \quad (3.25)$$

using the relation $dz/dx = q/2V_0$. This can be refined for round-nosed sections by using equation (3.22):—

$$\Delta C_D = 4\cos\varphi\, f(\varphi) \int_0^1 \left(\frac{dz}{dx}\right)^2 \frac{dx}{\sqrt{\{1 + (dz/dx)^2\}}}\,. \qquad \ldots\ldots\ldots\ldots \quad (3.26)$$

Equation (3.25) applied to the biconvex parabolic section*

$$z(x) = 2\frac{t}{c}x(1 - x)$$

gives

$$\Delta C_D = \frac{16}{3}\left(\frac{t}{c}\right)^2 \cos\varphi\, f(\varphi) \qquad \ldots\ldots\ldots\ldots\ldots\ldots \quad (3.27)$$

and equation (3.26) applied to an elliptic section

$$z(x) = \frac{t}{c}\sqrt{\{x(1 - x)\}}\,,$$

as another extreme, gives

$$\Delta C_D = 4\left(\frac{t}{c}\right)^2 \cos\varphi\, f(\varphi)\, \frac{K(k) - E(k)}{k^2}\,, \qquad \ldots\ldots\ldots\ldots\ldots \quad (3.28)$$

where $\mathbb{K}(k)$ and $\mathbb{E}(k)$ are the complete elliptic integrals of the first and second kind respectively, with

$$k^2 = 1 - \left(\frac{t}{c}\right)^2.$$

The drag of the round-nose section is larger than that of the sharp-edged biconvex section. The following table gives some numerical values for the elliptic section:—

t/c	$\dfrac{\Delta C_D}{\left(\frac{t}{c}\right)^2 \cos\varphi\, f(\varphi)}$	
	Elliptic section	Biconvex section
0	∞	5·3 (= 16/3)
0·05	13·5	5·3
0·10	10·8	5·3
0·15	9·3	5·3
0·20	8·2	5·3

* The biconvex parabolic section represents a conveniently simple case where first-order solutions can easily be obtained. For example,

$$\frac{V(x,0)}{V_0} = 1 + \frac{v_{xs}}{V_0} - 2\frac{t}{c}\cos\varphi\, f(\varphi)(1 - 2x)$$

at the centre, which follows immediately from $z(x) = 2\frac{t}{c}x\,(1 - x)$; $dz/dx = 2\frac{t}{c}\,(1-2x)$; and equation (3.19).

For example, with $\varphi = 45$ deg, $t/c = 0{\cdot}1$, an elliptic section gives $\Delta C_D = 0{\cdot}043$; the centre effect on the normal pressure drag thus amounts to several times the ordinary profile drag.

The local drag, being proportional to the centre velocity increment v_{x2} from equation (3.16), can be used to define the spanwise extent of the centre effect. Obviously, v_{x2} and ΔC_D are both largest at the centre section and fade out gradually as the spanwise co-ordinate y increases. Measured and calculated values of ΔC_D for sections outside the centre have been plotted in Fig. 12, the calculations having been made for the special case of the biconvex section. These values do not differ greatly from one another, and the full line in Fig. 12 may be used to estimate the fading-out and the spanwise extent of the centre effect, giving the percentage of the value $v_{x2}(x,0)$, or C_D, which is left at a station y from the centre. This distance must be measured in terms of the wing chord c. No great accuracy is required for this interpolation. The centre effect does not reach farther than about half a chord from the centre-line.

3.5. *Approximate Solutions for Sub-critical Flow.*—A simple treatment of the compressible flow on a two-dimensional basis as for the sheared wing in section 2.4 is not possible for the centre-section of a swept wing because of the essentially three-dimensional character of the flow there. Instead of equation (2.23), the full potential equation

$$\frac{\partial^2\Phi}{\partial x^2}\left[1-\frac{1}{a^2}\left(\frac{\partial\Phi}{\partial x}\right)^2\right]+\frac{\partial^2\Phi}{\partial y^2}\left[1-\frac{1}{a^2}\left(\frac{\partial\Phi}{\partial y}\right)^2\right]+\frac{\partial^2\Phi}{\partial z^2}\left[1-\frac{1}{a^2}\left(\frac{\partial\Phi}{\partial z}\right)^2\right]$$

$$-\frac{2}{a^2}\frac{\partial^2\Phi}{\partial y\,\partial z}\frac{\partial\Phi}{\partial y}\frac{\partial\Phi}{\partial z}-\frac{2}{a^2}\frac{\partial^2\Phi}{\partial z\,\partial x}\frac{\partial\Phi}{\partial z}\frac{\partial\Phi}{\partial x}-\frac{2}{a^2}\frac{\partial^2\Phi}{\partial x\,\partial y}\frac{\partial\Phi}{\partial x}\frac{\partial\Phi}{\partial y}=0 \qquad \ldots \quad (3.29)$$

must now be used. At the centre-section, $\partial\Phi/\partial y = V_y = 0$, for reasons of symmetry. We may further restrict ourselves to flat bodies where

$$\left(\frac{\partial\Phi/\partial z}{a}\right)^2 << 1\,,$$

as in equation (2.29). We ignore again the mixed term

$$-\frac{2}{a^2}\frac{\partial^2\Phi}{\partial z\,\partial x}\frac{\partial\Phi}{\partial z}\frac{\partial\Phi}{\partial x}\,.$$

Equation (3.29) then reads:—

$$\frac{\partial^2\Phi}{\partial x^2}\beta^2+\frac{\partial^2\Phi}{\partial y^2}+\frac{\partial^2\Phi}{\partial z^2}=0\,, \qquad \ldots \quad (3.30)$$

where

$$\beta^2 = 1-\frac{1}{a^2}\left(\frac{\partial\Phi}{\partial x}\right)^2 = 1-\frac{V^2}{a^2} \qquad \ldots \quad (3.31)$$

again for flat bodies. As in section 2.4, β will be replaced by a constant value to make a solution of equation (3.30) possible. It is

$$\beta^2 = 1-\frac{V^2}{a_0^2+\frac{k-1}{2}(V_0^2-V^2)} = 1-M_0^2\frac{(V/V_0)^2}{1-\frac{k-1}{2}M_0^2\left[\left(\frac{V}{V_0}\right)^2-1\right]}\,. \qquad \ldots \quad (3.32)$$

which naturally differs from the corresponding relation (2.30) for the infinite sheared wing. Assuming again that the section is thin, so that

$$\frac{k-1}{2} M_0^2 \left[\left(\frac{V}{V_0} \right)^2 - 1 \right] << 1 ,$$

we have

$$\beta^2 = 1 - M_0^2 (V/V_0)^2 = 1 - M_0^2 (1 - C_{p\,i}) \qquad .. \quad .. \quad .. \quad .. \quad .. \quad (3.33)$$

if we restrict ourselves here to the problem of relating the velocity in compressible flow to that in incompressible flow (suffix i).

We follow again the Prandtl-Glauert procedure by transforming the wing into an analogous wing (suffix a) by means of

$$\left. \begin{aligned} x_a &= x \\ y_a &= \beta y \\ z_a &= \beta z \end{aligned} \right\} \quad . \quad .. \quad .. \quad .. \quad .. \quad .. \quad .. \quad .. \quad (3.34)$$

The perturbation potential functions of the two flows are related by

$$\Phi_a' = \Phi_a - V_0 x_a = \lambda(\Phi - V_0 x) = \lambda \Phi' .$$

The factor λ is so determined as to make both wings into stream surfaces, and in the same way as in section 2.4 and with the simplifying assumptions made there, we find $\lambda = \beta^2$, as before.

It may be noted that the transformations (3.34) imply that the analogous wing is thinner than the given wing:

$$\frac{t_a}{c} = \beta \frac{t}{c} ; \qquad .. \quad .. \quad .. \quad .. \quad .. \quad .. \quad .. \quad (3.35)$$

further, the analogous wing is more highly swept:

$$\left. \begin{aligned} \tan \varphi_a &= \frac{1}{\beta} \tan \varphi \\ \sin \varphi_a &= \frac{\tan \varphi}{\sqrt{(\beta^2 + \tan^2 \varphi)}} \\ \cos \varphi_a &= \frac{\beta}{\sqrt{(\beta^2 + \tan^2 \varphi)}} \end{aligned} \right\} \quad . \quad .. \quad .. \quad .. \quad .. \quad .. \quad (3.36)$$

With these transformations, equation (3.30) reduces to

$$\frac{\partial^2 \Phi_a}{\partial x_a^2} + \frac{\partial^2 \Phi_a}{\partial y_a^2} + \frac{\partial^2 \Phi_a}{\partial z_a^2} = 0 ; \quad \text{or} \quad \frac{\partial^2 \Phi_a'}{\partial x_a^2} + \frac{\partial^2 \Phi_a'}{\partial y_a^2} + \frac{\partial^2 \Phi_a'}{\partial z_a^2} = 0 , \qquad .. \quad .. \quad (3.37)$$

of which the solution is known to be, by equation (3.20),

$$\frac{v_{xa}}{V_0} = \left[S_a^{(1)}(x) - f(\varphi_a) S_a^{(2)}(x) \right] \cos \varphi_a$$

or, by equations (2.7), (2.8), (3.34), (3.35)

$$\frac{v_{xa}}{V_0} = \left[\beta S^{(1)}(x) - f(\varphi_a)\beta S^{(2)}(x)\right] \cos \varphi_a , \qquad \ldots \quad (3.38)$$

to a first approximation. With $\lambda = \beta^2$, the velocity increment of the given wing in compressible flow is

$$\frac{v_x(x,0,0)}{V_0} = \frac{1}{\beta^2} \frac{v_{xa}(x,0,0)}{V_0} \qquad \ldots \quad (3.39)$$

so that, with equations (3.36) and (3.38),

$$\frac{v_x}{V_0} = \frac{1}{\sqrt{(\beta^2 + \tan^2 \varphi)}} \left[S^{(1)}(x) - f(\varphi_a) S^{(2)}(x)\right] . \qquad \ldots \quad (3.40)$$

Using β as given by equation (3.33), we obtain finally

$$\frac{v_x}{V_0} = \frac{\cos \varphi}{\sqrt{\{1 - M_0^2(1 - C_{pi}) \cos^2 \varphi\}}} \left[S^{(1)}(x) - f(\varphi_a) S^{(2)}(x)\right] . \qquad \ldots \quad (3.41)$$

It is not possible to give a simple expression for the velocity ratio v_x/v_{xi} because the factor $f(\varphi_a)$ in the centre term in equation (3.40) depends on the angle of sweep of the analogous wing. Putting $C_{pi} = 0$ leads to an approximation which corresponds to the Prandtl-Glauert rule (2.41). It is suggested that equation (3.41) be used together with equation (2.43) for calculating the pressure coefficient in compressible flow.

It may be noted that the compressibility factor in equation (3.41) differs from that of the Weber rule (2.42) for the infinite sheared wing. This is due to the fact that the third mixed term in equation (3.29) is not zero for the sheared wing but gives a contribution to the term with $\partial^2\Phi/\partial x^2$. Since

$$\frac{\partial \Phi}{\partial y} = \left(\frac{\partial \Phi}{\partial x} - V_0\right) \tan \varphi$$

for the sheared wing, this mixed term can be written

$$-\frac{2}{a} \frac{\partial^2 \Phi}{\partial x \, \partial y} \frac{\partial \Phi}{\partial x} \frac{\partial \Phi}{\partial y} = -\frac{2}{a^2} \tan^2 \varphi \frac{\partial^2 \Phi}{\partial x^2} \frac{\partial \Phi}{\partial x} \left(\frac{\partial \Phi}{\partial x} - V_0\right).$$

Taking this together with the first term containing $\partial^2\Phi/\partial x^2$, we have

$$\frac{\partial^2 \Phi}{\partial x^2} \left\{1 - \frac{1}{a^2}\left(\frac{\partial \Phi}{\partial x}\right)^2 - \frac{2}{a^2} \tan^2 \varphi \frac{\partial \Phi}{\partial x}\left(\frac{\partial \Phi}{\partial x} - V_0\right)\right\} = \frac{\partial^2 \Phi}{\partial x^2} \beta^2 .$$

Ignoring quadratic terms in (v_x/V_0), we find

$$\beta^2 = 1 - M_0^2 \left(1 - \frac{C_{pi}}{\cos^2 \varphi}\right)$$

which gives for the compressibility factor in equation (3.40)

$$\frac{1}{\sqrt{(\beta^2 + \tan^2 \varphi)}} = \frac{\cos \varphi}{\sqrt{\{1 - M_0^2(\cos^2 \varphi - C_{pi})\}}} ,$$

which then leads to equation (2.42) for the sheared wing. This indicates, at the same time, an alternative derivation of equation (2.42), which does not resort to the transformations (2.13) that enable results from two-dimensional flow to be used.

There are as yet no experimental data available to check equation (3.41). The main error is likely to arise from the fact that the boundary condition that the aerofoil should be a streamline is not adequately fulfilled. Such an error may come in twice. First in the calculation of the incompressible flow past the analogous wing, as explained in section 3.3; and again in the transformation to compressible flow by putting $\lambda = \beta^2$.

An assessment of the critical conditions and of the critical Mach number, corresponding to the treatment of the sheared wing in section 2.3, cannot easily be made for the centre-section without considering the wing as a whole. Some remarks will, therefore, be left to a later stage, section 4.3 (*see* also the paper by G. H. Lee[19], 1950).

As an illustration, calculated velocity distributions for the centre-section of a 45-deg swept-back wing of large aspect ratio are compared in Fig. 14 with those on a 45-deg sheared wing of infinite aspect ratio. Fig. 13 shows that the pressure rise with Mach number at the centre differs from that at the sheared wing. $C_p = -2v_x$ has been assumed in calculating Fig. 13.

4. *Application of the Sheared Wing and Centre-Section Solutions to Special Problems.*—It is not in general possible to find an exact solution for the flow past a swept wing of given plan form and section shape. Existing papers deal with special cases where the generality has been restricted by the use of special section shapes, such as the biconvex parabolic section and by the application of linearised theory throughout (*see* S. Neumark and J. Collingbourne[20], 1949). Calculation methods are needed, however, which are applicable to any given section shape and which take second-order terms into account whenever the need arises. The procedure followed here is to combine the known solutions for the infinite sheared wing and for the centre-section to obtain an approximate solution for any other section on a given wing. This method is used first to investigate the flow over the wing tips, section 4.1, and is then applied to wings of finite aspect ratio, including those with taper in plan form or thickness, in section 4.2. Compressibility effects are briefly considered in section 4.3, and section 4.4 deals with the possibility of modifying the plan form, or the section shape, of a given wing in order to restore flow conditions which may appear desirable, such as sheared wing conditions.

4.1. *The Wing Tip.*—Since the velocity increment v_x at the centre of a swept wing of infinite aspect ratio is produced in equal parts by the two halves of the wing, as a first approximation half the value of v_x given by equation (3.19) would correspond to the velocity increment for a semi-infinite sheared wing at its tip section, the angle of sweep being reversed. However as this wing would be composed of source lines of equal strength along the span, its thickness would decrease in approaching the tip. This can easily be seen from equation (3.6); in particular, since the normal velocity v_z at the centre of a swept wing is produced in equal parts by the two halves of the wing, $v_z/V_0 = q/4$ at the tip instead of $q/2$ at the centre, by equation (3.18).

The decrease of v_z towards the tip spreads over an appreciable area inboard. To illustrate this, consider a parallel strip of semi-infinite length normal to the main stream and covered with a uniform distribution of sources as shown in Fig. 15. The induced normal velocity at and above the centre-line of the strip is, by equation (3.6), and integration,

$$v_z(0,y,z) = \frac{q}{2}\left(\frac{1}{\pi}\arctan\frac{1}{z} + \frac{1}{\pi}\arctan\frac{y}{z\sqrt{(1+y^2+z^2)}}\right) \quad \ldots \quad \ldots \quad (4.1)$$

Numerical values are shown in Fig. 15 where $v_z' = q/2$. It will be seen that, for $z \neq 0$, v_z/v_z' decreases steadily towards the tip. At the tip ($y = 0$) v_z has half the value of the two-dimensional case ($y \to \infty$), the latter itself being smaller than $q/2$ for $z \neq 0$, *i.e.*, for wings of

non-zero thickness. At $z = 0$, *i.e.*, wings of zero thickness, v_z jumps discontinuously from $q/2$ at $y \neq 0$ to $q/4$ at $y = 0$. Since any source distribution can be composed of such strips, this result has a general validity.

The reduction of the normal velocity component induced by a constant source distribution is related to a certain streamline pattern in a span-wise section through the wing. Fig. 16 shows the streamlines turned outwards near the tips of a wing of finite aspect ratio. This implies that there is also an induced velocity component v_y in a transverse direction, which is necessarily zero at the centre-line of a wing for reasons of symmetry. The existence of this cross-flow component adds considerably to the difficulties encountered in an analytical treatment of the flow near the wing tip. For example, we cannot take it for granted that the flow will form a closed contour at the tip if the wing is represented by the usual source-sink distribution. In a parallel flow, a closed body is obtained from a source and a sink only if these are of equal and opposite strength and, further, if they are directly behind one another. If the latter condition is not fulfilled, as in the case sketched in Fig. 17, the stagnation streamline will not be continued as the dividing streamline behind the body; in fact, no closed body is formed.

It will be helpful for a better understanding of the tip flow to consider the cross-flow component in more detail and, in particular, to investigate its magnitude. Consider a source distribution $q(x)$ between $x = 0$ and $x = 1$ in the plane $z = 0$, beginning at $y = 0$ and extending to $y = \infty$. The unswept wing which is produced by these sources in a parallel stream along the x-axis will not be of rectangular plan form, but will bulge out beyond the line $y = 0$, Fig. 18. We assume for the time being that the plan form, $y(x)$, of this end fairing forms a closed contour† and that it has a shape similar to that of the given aeroil section, $z(x)$:

$$y(x) = \sigma^* z(x) , \qquad (4.2)$$

where σ^* is a constant factor to be determined. The basic aerofoil shape is related to the source distribution by the streamline condition $dz/dx = q(x)/2V_0$; and the shape of the end fairing is similarly related to the cross-flow velocity v_y in the plane $z = 0$:—$dy/dx = v_y/V_0$. Hence, by equation (4.2),

$$\frac{v_y}{V_0} = \sigma^* \frac{1}{2} \frac{q(x)}{V_0} , \qquad (4.3)$$

i.e., the cross-flow velocity is proportional to the local source strength.

The value of the constant factor σ^* in equation (4.3) will be of the order 1. $\sigma^* = 1$ means that the end fairing is composed of semi-circles along $y = 0$, like the conventional fairing of wind-tunnel models. It is unlikely, from Fig. 18, that σ^* could be appreciably greater than 1. A lower limit for the value of σ^* can be obtained as follows:—Consider a cylinder of length dx and radius r around the edge $y = 0$. The spanwise extent of the sources forming the wing, which are enclosed by the cylinder, is r and the source material inside the cylinder is thus $q(x)r\,dx$. We now assume that all the source material flows out through the outer half of the cylinder with a constant radial velocity v_r. This would be similar to the flow condition on a body of revolution where the source material passes through the whole of the surface of the cylinder, and our assumption implies that the end fairing has the properties of a half-body of revolution, which may be regarded as an extreme case. Thus, by continuity,

$$q(x)r\,dx = \pi r\,dx\,v_r(x) ,$$

or

$$v_r(x) = \frac{1}{\pi} q(x) .$$

† In the conditions described further on, there is $\int_0^1 v_y\,dx = 0$, at least, by equation (4.3).

For $z = 0$, $v_r = v_y$, so that $\sigma^* = 2/\pi = 0{\cdot}64$ in this case. For $y = 0$, $v_r = v_z = q/\pi$, whereas the true value of v_z at this point will be smaller: linear theory gives $v_z(0) = q/4$. This implies that v_y at $z = 0$ will be greater than q/π, so that $\sigma^* > 0{\cdot}64$.

Analytically, the value of $v_y(x,y,z)$ is obtained from the integral

$$v_y(x,y,z) = \frac{1}{4\pi}\int_0^1 q(x') \frac{(x-x')^2 - z^2}{\{(x-x')^2 + z^2\}\sqrt{\{(x-x')^2 + y^2 + z^2\}}}\, dx' \quad .. \quad .. \quad (4.4)$$

which follows from equation (3.5). This can be written as

$$v_y(x,y,z) = \frac{1}{4\pi}\int_0^1 q(x') \frac{dx'}{\sqrt{\{(x-x')^2 + y^2 + z^2\}}} - \frac{z^2}{2\pi}\int_0^1 q(x) \frac{dx'}{\{(x-x')^2 + z^2\}\sqrt{\{(x-x')^2 + y^2 + z^2\}}}.$$

For $z = 0$,

$$v_y(x,y,0) = \frac{1}{4\pi}\int_0^1 q(x') \frac{dx'}{\sqrt{\{(x-x')^2 + y^2\}}} \quad .. \quad .. \quad .. \quad .. \quad .. \quad (4.5)$$

since the second integral vanishes. Thus v_y has a logarithmic infinity at the edge $y = 0$, as is to be expected since there is a non-zero source strength at $y = 0$. v_y falls to zero at either side of the edge. This shows that the linearised theory, in which the velocities are calculated in the plane of the source distribution and not on the surface of the wing, fails in the treatment of the cross-flow component of the induced velocity. Further, the velocity at the wing tip cannot be taken as $V = V_0 + v_x$, with v_x from linearised theory, because of the existence of an infinite v_y.

The integral in equation (4.5) occurs also in the treatment of the entirely different problem of finding the chordwise load distribution and the downwash at the centre of swept wings. It has been shown elsewhere (R. & M. 2935) that, on the wing contour $y(x)$, the value of the integral in equation (4.5) can be approximated by $v_y = \sigma^* q(x)/2$, in agreement with equation (4.3). In particular,

$$\sigma^* = \frac{\pi \tan\varphi + \pi f(\varphi)}{2\pi \sin\varphi},$$

with $f(\varphi)$ from equation (3.13). For $\varphi = 0$, using equation (3.15),

$$\sigma^* = \lim_{\varphi \to 0} \frac{\pi \tan\varphi + 2\varphi}{2\pi \sin\varphi} = 0{\cdot}82\,.$$

This is a reasonable value between the limits discussed above.

The above considerations confirm that the wing produced by sources of constant spanwise strength becomes appreciably thinner towards the tip as indicated in Fig. 18. Therefore, the source strength must be increased near the tip if a wing of constant thickness is to be produced. This in turn makes both normal and streamwise velocity increments greater than half the value of the two-dimensional aerofoil. The flow in the tip region is thus essentially three-dimensional, the tip representing an intermediate stage between a body of revolution, with the thickness of the body proportional to the square root of the source strength, and a two-dimensional body, with a linear relation between thickness and source strength.

There are no methods available for calculating the velocity distribution over the surface of such a body of given shape, and we must be content with a crude approximation. Since the

velocity at the tip section can be expected to lie between the full value obtained for the centre-section and half this value, we retain this type of distribution and put

$$\frac{v_x(x,\varphi)}{V_0} = \lambda\left(\frac{v_{xS}(x,\varphi)}{V_0} - \cos\varphi\, f(-\varphi)\,\frac{dz(x)}{dx}\right), \qquad \ldots \quad (4.6)$$

by analogy with equation (3.19). The centre term must be determined as for a wing of opposite sweep because, for a swept-back wing, the tip behaves similarly to the centre of a swept-forward wing. (*See* Fig. 2.) The factor λ must be determined from experiments. Its value is likely to be greater than $\frac{1}{2}$ (linearised theory) but smaller than 1 (full ' reflection ' of the flow, *i.e.*, straight streamlines, at the tip, Fig. 2). Several experiments indicate that a relation of the type of equation (4.6) is indeed sufficiently accurate for practical purposes. The value of λ obtained from the tests is $\lambda = 0{\cdot}7$ so that, at the tip,

$$\frac{v_x}{V_0} = 0{\cdot}7\left(\frac{v_{xS}(x,\varphi)}{V_0} - \cos\varphi\, f(-\varphi)\,\frac{dz(x)}{dx}\right). \qquad \ldots \quad (4.7)$$

Numerical values of v_x can be obtained by using the methods described in section 3.4. A simple approximation is

$$\frac{v_x}{V_0} = 0{\cdot}7\cos\varphi\,[S^{(1)}(x) - f(-\varphi)\,S^{(2)}(x)] \qquad \ldots \quad (4.8)$$

which corresponds to equation (3.20). A better approximation will be obtained from

$$\frac{V}{V_0} = \frac{1 + 0{\cdot}7\left(S^{(1)}(x) - f(-\varphi)\,\dfrac{S^{(2)}(x)}{\sqrt{\{1 + S^{(2)}(x)^2\}}}\right)\cos\varphi}{\sqrt{\{1 + S^{(2)}(x)^2\}}} \qquad \ldots \quad (4.9)$$

which corresponds to equation (3.22a). Some experimental evidence is shown in Figs. 19 and 25. It may be noted that this decrease in velocity to about $0{\cdot}7$ times the two-dimensional value has also been confirmed by tests on unswept wings.

In the absence of any evidence about the velocity rise with Mach number, equation (3.41) for the centre-section may be suitably modified to apply to the tip section. This leads to

$$\frac{v_x}{V_0} = \frac{0{\cdot}7\cos\varphi}{\sqrt{\{1 - M_0^2(1 - C_{p\,i})\cos^2\varphi\}}}\,[S^{(1)}(x) - f(-\varphi_a)\,S^{(2)}(x)], \qquad \ldots \quad (4.10)$$

where again the simplified terms corresponding to equation (4.8) can be replaced by the better approximation from equation (4.9). As an illustration, Fig. 14 shows calculated velocity distributions for a tip section at various Mach numbers. It will be seen from Fig. 13 that the pressure rise with Mach number is normally steeper at the tip than at either the sheared part of the wing or the centre. This may offer an explanation of the tip stalling tendency of swept-back wings at high Mach numbers.

The resemblance of the flow in the tip region to that in the centre region of a wing with opposite sweep implies the existence of non-zero drag forces there. For a swept-back wing, there is a drag force at the central region (section 4) and a thrust force in the tip regions. These two forces must exactly counterbalance each other on a wing of finite aspect ratio in inviscid flow. The thrust near the tip is caused by increased suction near the nose and lesser suction in the rear part of the section, Figs. 14 and 19. At the tip, the thrust force as given by equation (3.26) is only $0{\cdot}7$ times the drag force at the centre. As a consequence, the spanwise decrease of this local thrust is different from that near the centre, extending further inboard, as shown in Fig. 20.

The dotted line in Fig. 12, which has been obtained from various experiments, may be used to interpolate the tip term for stations between the tip and the sheared part of the wing, y being measured in this case from the tip inwards.

4.2. *Wings of Finite Aspect Ratio. Effect of Taper.*—It can be concluded from the previous considerations that the distortions of the centre and tip regions are localised and of limited spanwise extent. This should be measured in terms of the wing chord (Fig. 12), and it is not larger than about one chord in the direction of the y-axis, Fig. 3. In going either outboard from the centre or inboard from the tip, the flow conditions approach those of an infinite sheared wing. Thus all wings of aspect ratios greater than about 2 have well-defined and sometimes extensive regions about mid-semi-span with very nearly two-dimensional flow. It is convenient, therefore, to regard swept wings as basically sheared wings with modifications, or distortions, near the centre and the tips.

Such a sub-division of the wing into centre region, sheared part, and tip region is also suggested by the analytical expressions obtained above. The relations for the velocity increments both at the centre section, equations (3.20) or (3.22), and at the tip section, equations (4.8) or (4.9), contain a basic term, $\cos\varphi\, S^{(1)}(x)$, which is the velocity increment on the infinite sheared wing, the centre and tip terms being additive to the sheared wing term. It presents no difficulty, therefore, to interpolate between centre and sheared part of the wing and between sheared wing and tip by using the curve suggested in Fig. 12 to determine the magnitude of the centre and tip terms. Even if the centre and tip regions overlap, there must be one section along the span where centre and tip terms cancel each other all along the chord and sheared wing conditions exist. In this approximation, both centre and tip terms contain the same function of x.

This is borne out by the results of experiments on wings with constant chord, shown in Figs. 21 and 26. Isobars, *i.e.*, lines of constant pressure, have been drawn as a convenient means of describing the pressure distribution over the surface of the wing. These results from wings of aspect ratio 2 show that the isobars are straight and parallel to the leading edge in a narrow region around mid-semi-span, so that the pattern for a similar wing of greater aspect ratio can be obtained by lengthening this parallel portion (*see* also Fig. 2). With wings of aspect ratio less than about 2, this region vanishes and the centre and tip distortions merge, as shown in Fig. 21. The full geometric sweep of the wing is then never achieved by the isobars. It will be noted, however, that the pressure distributions at the centre and at the tip are not affected by the aspect ratio. It was found experimentally, Fig. 19, that, at aspect ratios 1 and 2, they are still the same as those calculated for infinite aspect ratio. Further tests are needed to confirm this for other aspect ratios and angles of sweep, in particular for unswept wings. The analytical treatment of wings of very small aspect ratio is difficult for the reasons mentioned in section 4.1 in connection with the three-dimensional flow near the wing tips ; the applicability of linearised theory, in particular, becomes doubtful.

The above solutions for wings of constant chord can be applied also to tapered wings*, to a first approximation. The definition of the ' angle of sweep ' of a wing tapered in plan form presents some difficulty. For wings of moderate taper, it is usually adequate to take the angle of sweep as that of the maximum-thickness line†. A refined solution can be obtained by considering a ' local ' angle of sweep which varies along the chord. Lines of equal local sweep are obtained by connecting points of equal percentage of the local chord at the different spanwise positions (Fig. 22). These lines contain the maximum-thickness line as well as the leading edge and the trailing edge, and the angle of sweep varies along the chord between that of the leading edge and that of the trailing edge. It is convenient in such cases to measure the co-ordinate x from the local leading edge in terms of the local chord. In calculating the velocity distribution, the relations derived above can be used with φ being replaced by its local value $\varphi(x)$.

* ' Cranked ' wings where the angle of sweep changes at one or several spanwise stations must be excluded here.

† The quarter-chord line is, of course, not relevant to the present considerations.

Physically, this procedure implies the substitution of the given wing by a fictitious one which incorporates the correct chord at any given spanwise station and the correct angle of sweep at any chordwise position on that station but does not represent any changes of the chord at neighbouring stations. If a section is near the centre of the wing, the centre of the fictitious wing is made to coincide with the centre of the real wing, the wing chord, however, being that of the station considered (*see* Fig. 22). This procedure is not new but in fact the same as that tacitly assumed in calculating the velocity distribution over the surface of an unswept wing of finite aspect ratio where the flow at any spanwise station is assumed to be like that over a two-dimensional aerofoil section.

The chordwise velocity distribution obtained by this method is usually not very different from that obtained by taking a constant mean angle of sweep. This is shown in Fig. 23 for the example of a highly tapered wing of delta plan form, where it will be seen that the proposed calculation method is adequate.

The fictitious wing to replace the given wing has a constant absolute thickness along the span whereas the given wing has not. Even for a delta wing, this is a reasonable approximation for the part of the wing near mid-semi-span since the effects of the increasing thickness on one side of a given station are neutralised roughly by the effects of the decreasing thickness on the other side. But the approximation is clearly not good enough near the centre and tips of the wing. At the centre, the absolute thickness of a tapered wing decreases on either side and replacing the wing by another without any ' thickness taper ' must lead to calculated velocities which are too high.

To find the order of this velocity reduction at the centre due to absolute thickness taper, the velocity at the mid-chord point on the centre-line has been calculated for several rectangular wings with biconvex-parabolic sections. The thickness of all these wings decreased linearly from a maximum value at the centre-line to zero at the wing tips. The result is expressed as the ratio, τ, between the velocity at the wing with thickness taper to that at the corresponding two-dimensional aerofoil of the same thickness as that at the centre of the tapered wing. The value of τ depends on the ratio, s/c_0, between the spanwise distance s from the centre line at which the thickness falls to zero to the centre-line chord c_0. $s/c_0 = A/4$ for delta wings with pointed tips. Numerical values are :—

s/c_0	0·25	0·50	0·75	1·0	1·50	2·0	2·5	∞
τ	0·48	0·65	0·74	0·79	0·85	0·89	0·91	1·00

For the present this may be used also when the wing is swept, in which case

$$\frac{V}{V_0} = \frac{1 + \tau((S^{(1)}(x) - f(\varphi)\, S^{(2)}(x))\cos\varphi}{\sqrt{\{1 + S^{(2)}(x)^2\}}} \qquad \ldots \quad (4.11)$$

by equation (3.22). Clearly, a more detailed investigation is needed, which takes into account separately the effects of section shape, thickness taper, plan-form taper, and angle of sweep.

Experimental velocity distributions from the centre-line of delta wings, of which Fig. 24 gives an example, show good agreement with calculations by equation (4.11) using the values of τ given above. In the case of Fig. 24, τ is about 0·8; this velocity reduction is large enough not to be ignored.

Near the tips of a tapered wing the greater thickness on the inboard side of a given section more than compensates for the smaller thickness on the outboard side. Hence the local velocities on the outer part of a tapered wing should be higher than those found on a corresponding wing of constant chord and thickness. This effect has been little investigated so far owing to the obvious theoretical and experimental difficulties.

4.3. *Compressibility Effects.*—Consider an untapered swept wing of large aspect ratio. A considerable portion of such a wing should show straight isobars swept at the geometric angle of sweep of the wing, thus signifying that sheared-wing conditions prevail. For this part of the wing the considerations of sections 2.3 and 2.4 concerning compressibility effects will apply. Critical conditions, as defined in section 2.3, occur at the peak-suction line when the velocity component normal to the peak-suction line is equal to the local velocity of sound, equation (2.24a). This leads to a critical pressure coefficient C_p^* given by equation (2.28). At the centre-section, however, critical conditions occur when $\beta = 0$ in equation (3.30) so that the streamwise velocity V is equal to the local velocity of sound, by equation (3.31). The critical pressure is still given by equation (2.28) but with $\varphi = 0$; its value is then much smaller (*see* Fig. 13). Critical conditions will again occur first at the point of peak suction.

There will be a region of transition between the ' unswept ' centre and the sheared part of the wing. It can be assumed that this region coincides roughly with that part of the wing where the peak-suction line curves round and where the isobars deviate from straight parallel lines (*see* Figs. 21 and 26). A crude estimate of the critical Mach number can therefore be obtained by determining that free-stream Mach number at which the velocity component normal to the peak-suction line equals the local velocity of sound, *i.e.*, at which the minimum pressure coefficient reaches the value given by equation (2.28) where φ is the angle of sweep of the peak-suction line. Available experimental evidence has supported this procedure so far.

Similar considerations apply to the regions near the tips of a swept wing. There is again an appreciable portion of the wing inboard of the tip where the isobars deviate from straight parallel lines and where the peak-suction line curves round to a direction normal, or nearly normal, to the free stream. The position is aggravated by the fact that the peak-suction value is often higher at the tip than anywhere else on the wing (*see* Figs. 14 and 19) and that the pressure rises more steeply with Mach number (*see* Fig. 13).

It may be repeated that exceeding the critical Mach number does not imply that shock-waves and a drag rise associated with them should immediately occur. The development of the supersonic region is not considered here.

4.4. *Modifications to the Wing to Improve the Flow.*—It follows from the above considerations that any deviations from the straight isobar pattern of the sheared wing, such as occur on swept wings with constant section in the centre and tip regions, are normally detrimental to the performance of the wing at high subsonic speeds. Centre and tip effects reduce the benefit to be obtained from sweeping the wing. To obtain the full effect of a chosen angle of sweep over the whole of the wing, at least as far as the attainment of a certain critical Mach number is concerned, it is necessary to modify the aerofoil sections or the wing plan form to offset the distortions of the isobars in the centre and tip regions, as suggested by Küchemann (1947).

The peak-suction line in the central region can be straightened by enlarging the wing chord there. This amounts to a leading-edge fillet for swept-back wings, and to a trailing-edge fillet for swept-forward wings. The extent and shape of the fillet can be found by successive approximations, calculating for each step the position of the peak suction at the centre from equation (3.23). The isobars obtained by this method need not be straight. The fact that the local angle of sweep in the central region is somewhat higher than the original one must be taken into account. The spanwise extent of the fillet can be estimated from Fig. 12, the interpolation curve being used also for the fading-out of the chord extension at the centre. Care must be taken to avoid cranks (*i.e.*, sudden changes of sweep, for instance in the leading edge) away from the centre, since increased suction peaks will arise there.

Another way of straightening the peak-suction line is to modify the aerofoil section, leaving the plan-form unaltered. In this case, the ordinates of the centre-section can be determined so as to give a velocity distribution which appears to be desirable. To make it equal to the velocity distribution on the sheared part of the wing is an obvious choice; in that case, the peak-suction line and the isobars would be straight right up to the centre. Another choice would

be to have the peak-suction line straight but the whole velocity level lower at the centre than further out ; in that case, possible supersonic regions on the two wing halves would be separated by a central strip without local supersonic flow.

An approximate shape for the modified centre-section can be found by assuming the wing to have a uniform aerofoil section of the modified shape. Then equation (3.22) can be applied, the values of $z(x)$ which occur in the functions $S^{(1)}(x)$ and $S^{(2)}(x)$, equations (2.7), (2.8), being calculated for given values of $V(x)$. If the simplified equation (3.20) is used, this process involves the solution of a system of 15 linear equations ; this may be done by an iteration. Because of the changes occurring due to compressibility effects, it is better to do such a calculation not for incompressible flow but for the design Mach number. This means that the modifications to the analogous wing are first determined and then the shape of the real wing, using equations (3.34) to (3.38).

The resulting section for the centre of a swept-back wing is in general of about the same thickness/chord ratio as the original section, but the maximum thickness is further forward, giving a large nose thickness. The trailing-edge angle is much smaller. An example is shown in Fig. 25. It may happen that the resulting modified section shows an unreasonable shape in which the upper and lower surfaces cross over near the trailing edge. In that case the required velocity distribution cannot be achieved. If the section is further modified arbitrarily so as to give a finite trailing edge angle, it appears essential to retain the distinctive inflexion of the profile shape aft of the maximum thickness which normally occurs.

If the use of thickened wing roots is contemplated, it implies that the absolute thickness tapers down in going out from the centre. The reduction factor τ should be taken into account and equation (4.11) applied.

If, for such a calculation, the angle of sweep is taken as that of the unmodified wing, the velocity increments at the centre are lower than those required. This happened in the example shown in Fig. 25 and can be explained as follows. The shift of the maximum-thickness position, being greatest at the centre-section, fades out towards the sides according to a function which can be approximated by the interpolation curve of Fig. 12. Thus the maximum-thickness line possesses an increased effective sweep in the central region, which amounts to about 48 deg at the centre instead of 40 deg further out on the wing in the example shown in Fig. 25. It can be seen that the curve, calculated from equation (3.22) with $\varphi = 48$ deg, agrees well with the measured values. To obtain a better approximation, the calculation of the modified shape should be repeated, taking the increased sweep into account. Mathematically, the attainment of perfectly straight isobars right into the centre presents great difficulties, as has been shown by F. Ursell[17] (1949).

An estimate of the magnitude of the shift of the maximum-thickness position and the change of thickness/chord ratio which result from such modifications can be obtained by considering the special case of the biconvex parabolic section. Although results obtained for this section are often misleading if applied directly to conventional aerofoil shapes, the section is sufficiently general for the present purpose where only changes of section shape are investigated. The results derived here have also been checked against those obtained for conventional sections with rounded noses and maximum thickness further forward, and satisfactory agreement was found.

To find explicit relations for the profile parameters we begin with the source distribution and put

$$\frac{q(x)}{2V_0} = \sigma_1(1 - 2x) + \sigma_2 \frac{1 - 2(1 - 2x)^2}{\sqrt{\{1 - (1 - 2x)^2\}}}, \qquad \ldots \quad (4.12)$$

where σ_1 and σ_2 are two constants to be determined later to give the required velocity distribution. The first term in equation (4.12) would give a biconvex parabolic section on an infinite sheared

wing ; the second term allows for centre modifications. The velocity increment produced at the centre by a source distribution is

$$\frac{v_x}{V_0} = \tau \cos\varphi \left(\frac{1}{\pi} \int_0^1 \frac{q(x')}{2V_0} \frac{dx'}{x - x'} - f(\varphi) \frac{q(x)}{2V_0} \right)$$

by equations (3.16) and (4.11), if we restrict ourselves to linearised theory. With equation (4.12),

$$\frac{v_x}{V_0} = \tau \cos\varphi \left\{ \frac{2}{\pi} \sigma_1 \left(1 - \frac{1 - 2x}{2} \ln \frac{1 - x}{x} \right) - 2\sigma_2 (1 - 2x) \right.$$

$$\left. - \sigma_1 f(\varphi)(1 - 2x) - \sigma_2 f(\varphi) \frac{1 - 2(1 - 2x)^2}{\sqrt{\{1 - (1 - 2x)^2\}}} \right\} . \quad .. \quad .. \quad .. \quad (4.13)$$

At the sheared part of the wing,

$$\frac{q_S}{2V_0} = 2 \left(\frac{t}{c} \right)_S (1 - 2x)$$

and

$$\frac{v_{xs}}{V_0} = \frac{4}{\pi} \left(\frac{t}{c} \right)_S \left(1 - \frac{1 - 2x}{2} \ln \frac{1 - x}{x} \right) \cos\varphi_S . \quad .. \quad .. \quad .. \quad .. \quad (4.14)$$

This has its maximum at $x = \frac{1}{2}$ and its value there is

$$\frac{v_{xs}(\frac{1}{2})}{V_0} = \frac{4}{\pi} \left(\frac{t}{c} \right)_S \cos\varphi_S .$$

The conditions to determine σ_1 and σ_2 are that v_x from equation (4.13) has its maximum at $x = \frac{1}{2}$ and that its value there is equal to $v_{xs}(\frac{1}{2})$. This gives

$$\left[\frac{d}{dx} \left(\frac{v_x}{V_0} \right) \right]_{x = 1/2} = \tau \cos\varphi \, (4\sigma_2 + 2\sigma_1 f(\varphi)) = 0 ,$$

so that

$$\frac{\sigma_2}{\sigma_1} = -\frac{f(\varphi)}{2} ; \quad .. \quad .. \quad .. \quad .. \quad .. \quad .. \quad .. \quad .. \quad (4.15)$$

and

$$\frac{v_x(\frac{1}{2})}{V_0} = \tau \cos\varphi \left(\frac{2}{\pi} \sigma_1 - \sigma_2 f(\varphi) \right) = \frac{4}{\pi} \left(\frac{t}{c} \right)_S \cos\varphi_S . \quad .. \quad .. \quad .. \quad .. \quad (4.16)$$

From equations (4.15) and (4.16),

$$\sigma_1 = \frac{2}{\tau} \left(\frac{t}{c} \right)_S \frac{\cos\varphi_S}{\cos\varphi} \frac{1}{1 + \frac{1}{4}\pi f(\varphi)^2} ; \quad \sigma_2 = -\frac{1}{\tau} \left(\frac{t}{c} \right)_S \frac{\cos\varphi_S}{\cos\varphi} \frac{f(\varphi)}{1 + \frac{1}{4}\pi f(\varphi)^2} . \quad (4.17)$$

The velocity at the centre becomes, by equation (4.13),

$$\frac{v_x}{V_0} = \frac{4}{\pi} \left(\frac{t}{c} \right)_S \cos\varphi_S \frac{1}{1 + \frac{1}{4}\pi f(\varphi)^2} \left\{ 1 + \frac{1 - 2x}{2} \ln \frac{1 - x}{x} + \frac{\pi}{4} f(\varphi)^2 \frac{1 - 2(1 - 2x)^2}{\sqrt{\{1 - (1 - 2x)^2\}}} \right\} . \quad (4.18)$$

This velocity distribution differs slightly from the required one as given by equation (4.14); but the differences are small in the range of angles of sweepback in practical use and, of course, disappear entirely at the maximum velocity. Thus no further refinement is required.

The shape of the aerofoil section at the centre can be derived by integration from equation (2.3), with $q(x)$ from equation (4.12). This gives :—

$$z(x) = \int_0^x \frac{q(x)}{2V_0}\,dz$$

$$= \frac{2}{\tau}\left(\frac{t}{c}\right)_S \frac{\cos\varphi_S}{\cos\varphi}\,\frac{1}{1+\frac{1}{4}\pi f(\varphi)^2}\left(x - x^2 + \frac{f(\varphi)}{4}(1-2x)\sqrt{\{1-(1-2x)^2\}}\right). \quad \ldots \quad (4.19)$$

$z = 0$ at $x = 0$ and at $x = 1$. The maximum thickness of this section is

$$\frac{t}{c} = \frac{(t/c)_S}{\tau}\,\frac{\cos\varphi_S}{\cos\varphi}\,\frac{1+\sqrt{\{1+f(\varphi)^2\}}}{2+\frac{1}{2}\pi f(\varphi)^2}, \quad \ldots \quad (4.20)$$

and its maximum thickness is shifted forward (for $\varphi > 0$) from $x = \frac{1}{2}$ by the amount

$$\Delta x = \frac{1}{2\sqrt{2}}\sqrt{\left[1 - \frac{1}{\sqrt{\{1+f(\varphi)^2\}}}\right]}. \quad \ldots \quad (4.21)$$

The effective angle of sweep, φ, at the centre of the modified wing is greater than the angle of sweep, φ_S, of the sheared part of the wing. If we assume that the centre modification fades out in practice at $y = c/2$, and if the maximum-thickness line is replaced, for the present purpose, by a straight line from the new maximum-thickness position at the centre-line to a point on the original maximum-thickness line at $y = c/2$, we find

$$\tan\varphi = \tan\varphi_S + 2\Delta x\,. \quad \ldots \quad (4.22)$$

These relations can be simplified for estimation purposes by using the expansion of $f(\varphi)$ for small φ given by equation (3.15). In that case, ignoring terms in φ^4,

$$\frac{t}{c} = \frac{(t/c)_S}{\tau}\left(1 + \frac{{\varphi_S}^2}{2(\pi-1)^2}\right) = \frac{(t/c)_S}{\tau}(1 + 0{\cdot}1{\varphi_S}^2) \quad \ldots \quad (4.23)$$

and

$$\Delta x = \frac{\varphi}{2\pi}\,. \quad \ldots \quad (4.24)$$

This shows that the change in thickness is less significant than the shift of the maximum-thickness position. t/c is independent of the angle of sweep, to a first order, except when thickness taper is introduced. In that case, the wing root can be considerably thickened, provided that the increased thickness is made to fade out rapidly enough to give the necessary value of τ (*see* section 4.2). This means in practice that any thickening of the sections in the centre region of a swept-back wing should extend over only a comparatively small part of the wing span. Whether there are any detrimental effects in the region where the thickened part joins the basic wing has not yet been investigated.

The aerofoil sections in the tip regions can be modified by the same method using equation (4.7). If the velocity increments at the tip are to be equal to those of the infinite sheared wing, the resulting section shape will have a considerably larger thickness/chord ratio than the original one because of the reduction factor 0·7 in equation (4.7). This possibility is unlikely to be

exploited in practice; in special cases, the thickened wing tip could be made use of for storage purposes. Reducing the thickness/chord ratio of the modified section to that of the original section also reduces the velocity increments, Fig. 25, so that some of the isobars form closed loops, Fig. 26. There is as yet no experimental evidence to decide whether this is detrimental at high Mach numbers or whether it is sufficient to have the peak-suction line swept.

With the thickness/chord ratio kept constant, the nose thickness of the modified tip section becomes rather small and the trailing-edge angle correspondingly large (*see* Fig. 25). These are undesirable features for high lift. An alternative method of improving the tip region, with beneficial effects on the lift distribution too, is to alter the plan form of the wing, leaving the (streamwise) section shape unaltered. Fig. 26 shows the leading edge curved parabolically while the trailing edge is kept straight in this case. The curved part of the leading edge extends inboard by 25 per cent of the tip chord. The idea behind such a shape is to produce the unavoidable tip thrust not by increasing the suction but by reducing the positive pressure near the leading edge. Although this modification does not straighten the isobars completely, it appears to be satisfactory for practical purposes. A combination of a curved leading-edge tip with modifications to the section shape would seem to provide a perfect solution. In this case, only a slight thickening of the rear of the section and no reduction of the nose radius is needed.

5. *Body Interference.*—In the following, the methods explained so far are extended to wing–body combinations. The treatment is restricted to bodies of circular cross-section in a midwing position on the line of symmetry of the wing. Asymmetrical wing–fuselage arrangements and nacelles outboard on the wing show basically similar flow phenomena but some extension of the method is required. This is not discussed here. The effect of the shape of the intersection line in the junction between wing and body is considered in section 5.1 and the additional effects introduced by wing sweep in section 5.2. An alternative, in some respects, to the wing modifications discussed in section 4.4 is the modification of the shape of the body as originally suggested in 1947; this is investigated in section 5.3. A brief discussion of compressibility effects is given in section 5.4. Much of this work was done together with D. E. Hartley.

5.1. *The Junction Effect.*—If a fuselage is fitted to a wing, one might expect that (to a first approximation) the velocity fields could be superimposed, that is the velocity increments v_W of the wing alone, and v_B, of the body alone would be added. This method was tried by J. Liese and F. Vandrey[21] (1942). The source distribution representing a fuselage was superimposed upon another representing an unswept wing. It was found that the resulting shape of the wing–body combination differed from that aimed at by a bulge in the region of the junction. This indicates that a simple addition of the two component velocities is not sufficient to represent the conditions at the intersection of a given body with a given wing. There will be an additional velocity increment dependent on the shape of the wing–fuselage intersection.

Consider the use of an unswept wing with a long cylindrical body mounted in a symmetrical position, Figs. 27, 28. The intersection line is not straight but curved, and if the body is large enough the streamlines follow the shape of this intersection line. Generally, this means a divergence of the streamlines on the wing and a corresponding reduction in velocity. This velocity decrement, $-v_J$, is related to the shape of the junction.

If the body height is not fairly large compared with the wing thickness, the streamlines may not follow exactly the intersection line. v_J is then not determined only by the shape of this line.

Although this junction effect has usually been ignored altogether in previous studies of body interference, its magnitude is nevertheless appreciable. Fig. 29 shows some experimental results for cylindrical bodies on an unswept rectangular wing. The effect is larger on the smaller of the two bodies investigated, since the intersection line is more curved in that case, the depth of the ' waist ' being about twice the depth of the waist of the large body. The ratio of the body diameter to the wing thickness, D/t, is the main parameter in this respect.

Two methods have been used to calculate the junction velocity increment v_J:

(*a*) ' Vortex method '. Ring vortices are placed on the surface of the body, and their strength is determined from the condition that their induced radial velocities are proportional to the slope dr/dx of the intersection line. Their induced axial velocity is equal to v_J.

(*b*) ' Source method '. Since part of the wing is ' inside the body ', a fictitious body, obtained by subtracting the wing thickness inside the body from the given body thickness, is considered and replaced by a source distribution. This induces a velocity increment equal to $v_B + v_J$.

In the second method, the displacement flow round the wing–body junction is considered to be the determining characteristic, whereas the first method emphasises the curved flow in the intersection line.

In the first method, a number (n) of standard distributions $\gamma_\nu(x)$ of ring vortices on a cylinder* (diameter D, length L) are used :—

$$\gamma(x) = \sum_\nu \gamma_\nu(x) \qquad \ldots\ldots\ldots\ldots\ldots\ldots\ldots\ldots \quad (5.1)$$

where $\gamma_\nu(x) = c_\nu \cdot f_\nu(x)$; the c_ν are constant coefficients to be determined later. Suitable functions $\gamma_\nu(x)$ are given in Table 3. The velocity increments, induced on the outer surface of the cylinder, are :—

$$\frac{v_x}{V_0} = \sum_\nu c_\nu \frac{v_{x\nu}^*}{V_0}\,; \qquad \ldots\ldots\ldots\ldots\ldots\ldots\ldots\ldots \quad (5.2)$$

and

$$\frac{v_r}{V_0} = \sum_\nu c_\nu \frac{v_{r\nu}^*}{V_0}. \qquad \ldots\ldots\ldots\ldots\ldots\ldots\ldots\ldots \quad (5.3)$$

Values of the function $v_{x\nu}^*$ and $v_{r\nu}^*$ are tabulated in Tables 4 and 5 for a number of special functions $\gamma_\nu(x)$. The velocity components on the stream surface are assumed to be the same as those on the cylinder.

If the shape of the intersection line is given, the deviations

$$\Delta y = y_{\text{junction}} - R_{\text{body}} \qquad \ldots\ldots\ldots\ldots\ldots\ldots\ldots\ldots \quad (5.4)$$

along the y-axis (normal to x, Fig. 28) are known; they are usually taken as deviations Δr of the radius of the cylinder†. These are related to v_r by the streamline condition :—

$$\Delta r(x) = \sum_\nu \int_{x_0}^{x} \frac{v_{r\nu}(x)}{V_0}\, dx\,, \qquad \ldots\ldots\ldots\ldots\ldots\ldots\ldots\ldots \quad (5.5)$$

x_0 being the value of x where $\Delta r = 0$. Values of the functions $\Delta r_\nu(x)$ are given in Table 6. The coefficients c_ν can be obtained from the system of equations (5.5), using equation (5.3). The velocity increments v_x are then obtained from equation (5.2) and these are identical with v_J.

This method can also be used to solve the reverse problem. If $v_x(x)$ is given, the values c_ν are determined from equation (5.2) and the junction shape from equation (5.5). In either case, the equations are satisfied at a number (n) of points along the chord.

---

* Placing the vortices on a cylinder instead of on the actual stream surface reduces the amount of work considerably. This is justified for shallow stream surfaces, and the approximation corresponds to the usual method of calculation for two-dimensional or annular cambered aerofoils (*see* Ref. 22).

† This assumption means that the body is supposed to have the waisted intersection shape round the whole of its circumference.

The vortex method has been used to calculate the velocity distributions in the junctions for the examples in Fig. 29, and it is seen that a good approximation is obtained. For a body with elliptical cross-sections, however, the method of ring vortices on a circular cylinder is not suitable. Noticeable discrepancies between the results of this method and experimental values were found for a body the height of which was twice its width. In such cases, the method may be modified and two plane vortex sheets used, placed at $0 \leqslant x \leqslant c\,;\, y = \pm y_0\,;\, -\infty < z < \infty$. The strength of the vortices may be constant along the z-axis. The distribution $\gamma(x)$ can be obtained, as for the ring vortices, by adding standard distributions $\gamma_r(x)$, and the corresponding induced velocity components v_{xr} and v_{yr}. The vortex strips were placed at the ends of the minor axis of the ellipse, and the results were found to agree well with experimental values. Numerical tables for the velocity components induced by the standard vortex distributions from equation (5.1) are given in Ref. 22.

Using the source method, the wing cross-section area inside the body, at a station x, is subtracted from the cross-section area A of the given body ; and a smaller cross-section area $\bar{A}$ is obtained. The source distribution per unit length which produces such a body is

$$E(x) = V_0 \frac{d\bar{A}(x)}{dx}, \qquad \ldots\ldots\ldots\ldots\ldots\ldots\ldots\ldots \quad (5.6)$$

assuming a thin body with a slight waist*. A further assumption must be made as to the position of this source distribution. In general, a single line of sources and sinks along the x-axis can be used. This produces a velocity increment v_x at a given point (x,r) :—

$$\frac{v_x(x,r)}{V_0} = \frac{1}{4\pi} \int_0^L \frac{x - x'}{\{(x - x')^2 + r^2\}^{3/2}} \frac{d\bar{A}(x')}{dx'}\, dx' . \qquad \ldots\ldots\ldots\ldots \quad (5.7)$$

For long cylindrical bodies, only the contribution of the waist differs from zero, and the integration is done only for the length of the waist, that is the wing chord. Generally, the integral (5.7) has to be evaluated graphically. The induced velocity should not be calculated on the surface of the body of area $\bar{A}$ but on the actual body.

The value of v_x in equation (5.7) represents the sum of v_B and v_J. The value of v_J can be obtained directly by calculating in the same way the velocity increment of a body which has the same volume as that part of the wing which is ' inside the body '.

The source method in this simplified form tends to overestimate the junction effect slightly; but it is capable of further refinement, in particular as to the position of the sources. The source method usually involves more work than the vortex method, and the calculation of a body shape to give a certain velocity distribution in the junction is more complicated and has to be done by trying out a series of shapes. But there are cases where the vortex method fails and where the source method can be used with advantage. An instructive example is the intersection of two wings without fairing. Here the vortex method is not adequate, but the source method gives a satisfactory solution. The velocity increment is the sum of the velocity increments of the single wings, minus the velocity induced by a body in the line of symmetry the cross-section area of which is equal to the area common to the two wings.

5.2. *The Reflection Effect with Swept Wings.*—The junction velocity increment v_J is assumed to be the same for both straight and swept wings if the shape of the intersection line is the same. But the sum of the velocity increment v_S of the sheared wing and v_J does not give the velocity increment in the junction of a swept wing with a body, as is shown in two examples† in Fig. 30.

* This approximation is known to fail in the stagnation region of conventional bodies of revolution of finite length; but this region is of little interest in the present case.

† The shape of the tested bodies, as shown in Fig. 28, is such as to ensure that the velocity increment v_B of the body alone is small.

There exists another velocity increment which is plotted in Fig. 31 as the difference between the experimental value of the velocity in the junction and the calculated value of $v_S + v_J$, for a number of bodies. The points lie on one curve which can be approximated by the velocity increment $v_x = v_C$, found at the centre of a swept wing alone, *see* section 3.4. This effect can be interpreted as the body wall acting like a reflection plate. The reflection effect is, generally, not quite complete in the rear of the junction, Fig. 21. The effect exists even if the body diameter is very small so that a full reflection would not be expected. But, since the junction is then near the centre-line of the wing, there will be some ' centre effect ' from the wing itself.

Thus the total velocity in the body junction of a swept wing can be approximated by these additive terms:

V_0, free-stream velocity;

v_S, increment of undisturbed (sheared) wing;

v_B, increment of body alone ;

v_J, increment at junction, depending on the junction shape and not on the angle of sweep;

v_C, increment at the junction due to the centre effect and depending on the angle of sweep.

The sum of these terms gives a fairly accurate approximation for the total velocity, as can be seen from Fig. 30. The approximation may be improved by assuming only a partial reflection in the rear of the junction, about 80 per cent say.

The effect of the body on the isobar pattern on the wing is that v_J reduces the velocity near the body, and that v_C reduced the effective angle of sweep. In particular, the maximum-velocity line has generally no sweep near the junction.

5.3. *Modifications to the Body Shape to Improve the Flow.*—The distortion of the isobar pattern near the body may have a detrimental effect on the characteristics of the wing-body combination at high Mach numbers; this is, generally, slightly relieved by the reduction of the velocity due to the junction effect. Since the different effects are independent of each other, one may counteract the other. For example, by suitably shaping the body, $v_B + v_J$ can be made equal and of opposite sign to v_C. This gives straight isobars on the wing, to a first approximation.

The vortex method of section 5.1 can be used to design a junction shape for this purpose. If the body is long enough for v_B to be neglected, equation (5.2) is used to determine the values of c_v so as to make $v_J = -v_C$, where v_C is obtained from equation (3.22) for the given wing section and angle of sweep. The modification $\Delta r(x)$ of the body shape is then obtained from equations (5.3) and (5.5). In the junction, this deviation is to be regarded as a function $\Delta y(x)$, y being normal to the centre plane and $x = 0$ at the local leading edge. The corresponding deviation of the spanwise ordinate is $\Delta\eta(x)$, where

$$\eta = y/\cos\varphi\ , \qquad \ldots\ \ldots\ \ldots\ \ldots\ \ldots\ \ldots \quad (5.8)$$

and φ is the local angle of sweep in the case of tapered wings.

Modified body shapes have been designed for a 45-deg swept-back wing with bodies of different basic size, Fig. 32:—

Small body	$D/t = 1{\cdot}5$	$\sigma = 3{\cdot}7$
Medium body	$D/t = 2{\cdot}0$	$\sigma = 2{\cdot}3$
Large body	$D/t = 3{\cdot}0$	$\sigma = 1{\cdot}7$
Elliptical body	$D/t = 1{\cdot}5/3{\cdot}0$	$\sigma = 0{\cdot}8$

The shape parameter σ is defined below.

The junction shape to give the sheared-wing velocity distribution is nearly the same for all three sizes of body. The modification is such that the variation in width of the body does not exceed 10 per cent of the wing chord for a 12 per cent thick 45-deg swept-back wing, Fig. 34. The shape is rather similar to that of the streamline of the infinite sheared wing. This streamline is the correct shape for bodies of very large diameters.

The experimental results for these bodies, Fig. 33 top, show that only the body with elliptical cross-sections gives the required distribution. The reason for the discrepancies on the other bodies was found to be the small height of the bodies above the wing surface. Obviously, the flow does not follow the intersection lines in these cases. When the bodies were heightened above the wing so as to prevent any flow across the inter-section lines, the junction pressures for all the combinations tested agreed and coincided with the distribution on the sheared part of the wing (Fig. 33 bottom). The actual junction shape was kept the same when the body was heightened. A suitable parameter, characterising the flatness of the top of the body, is the ratio σ between half the width $W/2$ and the height H of that part of the body which is above the wing, measured at the maximum thickness of the wing, Fig. 32:

$$\sigma = W/2H \, .$$

It is convenient to shape this cross-section of the body as a semi-ellipse, the ratio of the axes being σ; but the same result can be achieved with a body of circular cross-section, provided the intersection line is the same and the value of σ is not smaller. As a rough rule, a value of $\sigma \leqslant 1 \cdot 5$ ensures that the flow will follow the intersection line. It is not certain, however, whether such a modification to the top of the body is necessary to give the same results at high Mach numbers; even the modification of the junction alone results in a reasonable pressure distribution in the junction where the suction peak is roughly at the same chordwise position as on the undisturbed wing (Fig. 33 top).

Figs. 29 and 30 also show some velocity distributions along the top of the body. Generally, these can be estimated by calculating the velocity due to the wing alone, at that distance from the wing, and adding the corresponding velocity due to the body alone. This suggests that there is only little interference between the top of the body and the junction.

Low velocities are usually found on the straight-topped bodies near the leading edge of the wing so that the cabin can profitably be placed in this low-velocity area. This gives, at the same time, a high angle of sweep to the isobars across the body. On the other hand, the low velocities might separate the regions of high suctions on the wing and on the body by a belt of low suction in between. Which of the two possibilities is more suitable for delaying the drag rise at high Mach numbers is not yet known.

Relatively high velocities on the body near the trailing edge of the wing may be reduced by means of a suitably faired dorsal fin.

In all these tests, the theoretical intersection line has been realised on the model only in the region from the leading edge of the wing up to 80 per cent of the wing chord (Fig. 34). The deviation near the trailing edge appears to be of little importance as far as the velocities at and upstream of the peak-suction line are concerned. Behind the peak-suction line, however, the velocities are higher than on the sheared wing, Fig. 33, and the sweep of the isobars is reduced in that region. The deviation from the theoretical curve near the leading edge gives a proper stagnation point at the leading edge, in contrast to the flow round an infinite sheared wing where a velocity component $V_0 \sin \varphi$ remains at the leading edge (*see* section 2.2). This is of little consequence for a body on a swept-back wing, since the flow along the leading edge in the outwards direction is accelerated. Serious effects would, however, arise from such a modified body on a swept-forward wing. By stopping and diverting the inflow, $V_0 \sin \varphi$, the body wall would create a region of high velocities. Therefore, on a swept-forward wing, either the calculated

body shape must be realised ahead of the leading edge, or the slope of the intersection line with the wing has to be exaggerated and curved more than otherwise necessary in an attempt to neutralise this effect.

So far, the modifications to the body shape aim at a given velocity distribution in the junction between wing and body. There is some indication that the effects, induced by the body, fade out more quickly than those induced by the centre effect of the wing. For example, if the shape of the body has been chosen to give a satisfactory reduction in the velocity in the junction, there is a possibility that the velocity farther from the centre is still too high. But experimental evidence so far has shown that this occurs only to a degree which is of no great practical importance Generally, this can only be overcome by modifying also the wing shape.

The modification of the wing section is an alternative means of compensating for the wing–body interference. Since, with swept-back wings, the necessary alteration usually results in a thickening of the wing root in the front part, it provides an opportunity of installing air intakes there. The general method of designing the wing section has been explained in section 4.4. It should be noted that a modification of the wing section causes a change in the shape of the intersection line. Conclusive experiments have not yet been made, but preliminary tests show that the thickness/chord ratio of the root section can be considerably increased (by about 33 per cent in one case) as compared with that of the basic wing. Special care must be taken in designing the rate of decrease of the wing thickness in going outwards from the junction. If the decrease is not sufficiently rapid the sections are too thick and tend to produce local suction peaks exceeding those on the basic wing (*see* section 4.2).

The effects mentioned above also occur with nacelles or other bodies on the wing at any spanwise position off the centre-line. The effects are different on either side of the nacelle: the wing has to be regarded as swept-back on one side and swept-forward on the other; and the intersection lines and thus the junction effect may differ. As a first approximation it is suggested that the separate sides should be treated as though independent of each other. The methods explained above can then be applied. There are no extensive experimental results available. These concepts have been successfully applied in designing an underslung nacelle on a 35 deg swept-back wing, described in Ref. 22. Tests have also confirmed that in other cases the respective velocity increments are additive (*e.g.*, struts fixed to a wing, even when their chords differ considerably from that of the wing); and that the same effects occur and the same rules apply to the design of a body at a spanwise position away from the centre (*e.g.*, at the wing tip) as have been described for a central fuselage.

5.4. *Compressibility Effects.*—In practice, the task is either to investigate the properties of a given wing–body combination at a given Mach number, or to make a design for a given Mach number. Therefore, the above methods, which are valid only for incompressible flow, have to be adapted for this purpose.

If the incompressible flow round a given wing–body combination is known, the simplest method of estimating the critical Mach number is to use one of the various rules, relating the incompressible velocity increment to that at a given subcritical Mach number, the angle of sweep being that of the peak-suction line. For example, applying equation (2.42) to the tested wing–body combinations in Fig. 28, it is found that the critical Mach number for the swept-back wing alone would drop from 0·96 on the undisturbed (sheared) part of the wing to 0·78 at the centre-section. In the junctions with the cylindrical bodies, Fig. 30, there would be a slightly higher value of M_{crit} of about 0·80. This is roughly the same for all cylindrical bodies tested. The modifications to the body shape will increase M_{crit} in the junction to at least 0·92. The diagrams in Fig. 8 can be used for this purpose.

These estimates can only give a crude guide since they are based on a supposedly two-dimensional flow. Regarding the various velocity increments, the actual velocity rise with Mach number is likely to be different for the separate terms.

As discussed in section 3.5 the compressible flow round a given body can be calculated from the incompressible flow round an analogous body. This applies also to wing–fuselage combinations, and the analogous combination is obtained by reducing the y- and z-co-ordinates of the given combination by the factor $\sqrt{(1 - M_0^2)}$; then the x-component v_x of the velocity increment on the given combination is $1/(1 - M_0^2)$ times the incompressible value v_{xa} of this analogous combination. This procedure corresponds to the ordinary Prandtl-Glauert analogy, as explained in section 2.4.

In certain simple cases a relation between v_{xa} and v_{xi} of the analogous and the given combination, both in incompressible flow, can be found and thus a function $v_x = f(v_{xi}; M_0)$. The sheared wing of infinite span has been treated this way in section 2.4, and the centre-section of a swept wing in section 3.5. Isolated bodies of revolution have also been dealt with, and Ref. 23 gives for bodies similar to ellipsoids:

$$v_B = \frac{v_{Bi}}{(1 - M_0^2)^{1/4}}; \qquad \ldots\ldots\ldots\ldots\ldots \quad (5.9)$$

and A. D. Young and S. Kirkby[24], 1947, for bodies with pronounced velocity peaks:—

$$v_B = \frac{v_{Bi}}{\sqrt{(1 - M_0^2)}}. \qquad \ldots\ldots\ldots\ldots\ldots \quad (5.10)$$

The velocity increment v_J due to the junction also varies with Mach number. In the first instance, ignoring the alteration of L/D, the intersection line on the analogous combination is similar to that on the given one, only flatter; the ratio D/t is left unaltered. Therefore:

$$v_{Ja} = v_{Ji}\sqrt{(1 - M_0^2)}$$

and

$$v_J = \frac{v_{Ji}}{\sqrt{(1 - M_0^2)}}. \qquad \ldots\ldots\ldots\ldots\ldots \quad (5.11)$$

There are appreciable differences between the rates of increase with Mach number of the various terms, as can be seen from the example in Fig. 35.

It follows from the above that low-speed tests cannot give direct information with regard to the flow at high Mach numbers. For example, a low-speed model with straight isobars cannot be expected to show straight isobars also at high Mach numbers. It will be necessary to split the measured total velocity into separate terms and to treat them separately, using the above method as a first approximation. A more accurate result would be obtained by testing the analogous wing–fuselage combination at low speeds, instead of the given one, and applying the factor $1/(1 - M_0^2)$ to the measured velocity increments.

Accepting the Prandtl-Glauert method, the design of a wing–body combination for a given Mach number is comparatively straightforward. The basic geometry of the analogous combination is worked out first; the junction shape of this analogous combination is then determined according to a given velocity distribution; and, finally, the analogous combination is transformed back by applying the factor $1/\sqrt{(1 - M_0^2)}$ to all y_a and z_a-values and the factor $1/(1 - M_0^2)$ to all velocity increments.

LIST OF SYMBOLS

x, y, z		Rectangular co-ordinates; x-axis in direction of the main flow, y-axis spanwise
r		Radial co-ordinate
ξ, η		Rectangular co-ordinates, normal and parallel to the leading edge; $\eta = y/\cos\varphi$
t		Thickness of the aerofoil section
c		Wing chord
L		Length of vortex cylinder
D		Maximum diameter of body; or diameter of vortex cylinder
σ		*See* Fig. 32
A		Aspect ratio
φ		Angle of sweep
$f(\varphi)$		*See* equation (3.13)
V		Total local velocity
V_0		Velocity of the free stream
V_x		Velocity component in the direction of the x-axis
V_n		Velocity component normal to the leading edge
v	=	$V - V_0$; velocity increment
$v_x, v_y, v_z, v_\xi, v_r$		Velocity increments in the directions of the respective axes
v_S		Velocity increment for the sheared wing
v_B		Velocity increment for the body alone
v_J		Velocity increment due to the junction shape
v_C		Velocity increment at the centre of a swept wing ($= v_{x2}$ from equation (3.14)); or velocity increment at the junction due to the wing being swept
v_{xi}, v_{yi}		Velocity increments in incompressible flow
a		Local velocity of sound
a_0		Velocity of sound in the free stream
M	=	V/a; Mach number
M_0	=	V_0/a_0; free-stream Mach number
M_n	=	V_n/a
M_{crit}		Free-stream Mach number at which critical conditions occur on the wing
p		Local static pressure
p_0		Free-stream static pressure
C_p	=	$(p - p_0)/\frac{1}{2}\rho V_0^2$; pressure coefficient
C_{pi}		Pressure coefficient in incompressible flow
C_p^*		Pressure coefficient at critical conditions

LIST OF SYMBOLS—*continued*

D		Normal-pressure drag
C_D	$=$	$D/\frac{1}{2}\rho V_0^2 c$; local drag coefficient
Φ		Potential function
Φ'		Perturbation potential
E		Strength of source line
q		Strength of source distribution
γ		Strength of vortex distribution
c_ν		Parameter to signify the intensity of the vortex distribution γ_ν
τ		Reduction factor due to thickness taper
$S_\nu^{(1)}$, $S_\nu^{(2)}$		*See* equations (2.7) and (2.8)
k	$=$	C_p/C_v; ratio of specific heat coefficients
μ, ν, n		Integer numbers

Suffixes :—

i	Incompressible flow
a	Analogous flow
crit	Critical condition
S	Sheared wing
C	Centre of swept wing
B	Body
J	Junction between wing and body

REFERENCES

No.	*Author*	*Title, etc.*
1	R. C. Pankhurst and H. B. Squire ..	Calculated pressure distributions for the R.A.E. 100–104 aerofoil sections. C.P. 80. March, 1950.
2	S. Goldstein	A theory of aerofoils of small thickness. C.P. 68. May, 1942.
3	H. Multhopp	Die Berechnung der Auftriebsverteilung von Tragflügeln. *L.F.F.*, Vol. 15, p. 153. 1938. Translated as A.R.C. 8516.
4	F. Riegels and H. Wittich	Zur Berechnung der Druckverteilung von Profilen. *Jahrbuch* 1942 *d. deutschen Luftfahrtforschung*, I, p. 120.
5	R. Courant and K. O. Friedrichs ..	*Supersonic flow and shock-waves.* Interscience Publishers, New York. 1949.
6	A. Busemann	Profilmessungen bei Geschwindigkeiten nahe der Schallgeschwindigkeit. *Jahrb. d. Wiss. Ges. f. Luftfahrt.* 1928.
7	B. Göthert	Ebene und raümliche Strömung bei hohen Unterschallgeschwindigkeiten. *Jahrb.* 1941 *d. deutschen Luftfahrtforschung*, I, p. 156.

REFERENCES—*continued*

No.	*Author*	*Title, etc.*
8	L. Prandtl	Allgemeine Betrachtungen über die Strömung zusammendrückbarer Flüssigkeiten. Atti dei Convegni 5 (1936), R. Acad. d' Italia (Volta Congress), p. 180. Also *Z.A.M.M.*, Vol. 16, p. 129. 1936.
9	H. Glauert	The effect of compressibility on the lift of an aerofoil. *Proc. Roy. Soc.* A, Vol. 118, p. 113. 1928.
10	E. V. Laitone..	New compressibility correction for two-dimensional subsonic flow. *J.Ae.Sci.*, Vol. 18, p. 350. May, 1951.
		Also: Use of the local Mach number in the Prandtl-Glauert method. *J.Ae.Sci.*, Vol. 18, p. 842. December, 1951.
11	Th. von Kármán	Compressibility effects in aerodynamics. *J.Ae.Sci.*, Vol. 8, p. 337. July, 1941.
12	H. Ludwieg	Improvement of the critical Mach number of aerofoils by sweepback. Ministry of Supply (Völkenrode) R. & T. 84. 1946.
13	B. Göthert	Hochgeschwindigkeitsmessungen an einem Pfeilflügel. *Lilienthal Ges. f. Luftfahrtforschung*, Bericht 156, p. 30. 1942.
14	W. Krüger	Wind tunnel investigations on a 35° sweptback wing with various high-lift devices. Part II.—Measurements of pressure distribution on wing without high lift devices in symmetrical flow. Ministry of Supply (Völkenrode) R. & T. 847. November, 1947.
15	R. T. Jones	Subsonic flow over thin oblique airfoils at zero lift. N.A.C.A. Tech. Note 1340. June, 1947.
16	S. Neumark	Velocity distribution on straight and sweptback wings of small thickness and infinite aspect ratio at zero incidence. R. & M. 2713. May, 1947.
17.	F. Ursell	Notes on the linear theory of incompressible flow round symmetrical sweptback wings at zero lift. *Aero. Quart.*, Vol. 1, p. 101. 1949.
18	A. Betz	Singularitäten Verfahren zur Ermittlung der Kräfte und Momente auf Körper in Potentialströmungen. *Ing. Archiv*, Vol. 3, p. 454. 1932.
19	G. H. Lee	Estimation of critical Mach number. *The Aeroplane*, Vol. 79, pp. 110 and 216. 1950.
20	S. Neumark and J. Collingbourne ..	Velocity distribution on untapered sheared and sweptback wings of small thickness and finite aspect ratio at zero incidence. R. & M. 2717. March, 1949.
21	J. Liese and F. Vandrey	Theoretische Untersuchungen über die Druckverteilung einesMitteldeckers in der Nähe des Rumpf-Flügelüberganges. *Jahrb.* 1942 *d. deutschen Luftfahrtforschung*, I, p. 326.
22	D. Küchemann and J. Weber ..	*Aerodynamics of Propulsion.* McGraw-Hill Book Company, New York, London. 1953.
23	D. Küchemann	A simple rule for the velocity rise with Mach number on ellipsoids of revolution. *J.Ae.Sci.*, Vol. 18, p. 770. November, 1951.
24	A. D. Young and S. Kirkby ..	Application of the linear perturbation theory to compressible flow about bodies of revolution. Cranfield Report No. 11. 1947.
25	Th. von Kármán	The similarity law of transonic flow. *J. Math. Phys.*, Vol. 26, p. 182. 1947.

TABLE 1

Coefficients $s_{\mu\nu}^{(1)}$ for $N = 16$

μ	ν 1	2	3	4	5	6	7	8	9	10	11	12	13	14	15
1 ..	+82·013	−15·061	0	− 0·651	0	− 0·136	0	− 0·051	0	− 0·026	0	− 0·017	0	− 0·013	0
2 ..	−29·544	+41·810	−11·203	0	− 0·705	0	− 0·180	0	− 0·076	0	− 0·044	0	− 0·031	0	− 0·026
3 ..	0	−16·265	+28·799	− 8·980	0	− 0·690	0	− 0·201	0	− 0·094	0	− 0·059	0	− 0·045	0
4 ..	− 2·360	0	−11·430	+22·627	− 7·698	0	− 0·674	0	− 0·217	0	− 0·111	0	− 0·075	0	− 0·062
5 ..	0	− 1·532	0	− 9·052	+19·243	− 6·954	0	− 0·673	0	− 0·236	0	− 0·130	0	− 0·095	0
6 ..	− 0·646	0	− 1·147	0	− 7·727	+17·318	− 6·563	0	− 0·692	0	− 0·262	0	− 0·157	0	− 0·124
7 ..	0	− 0·462	0	− 0·935	0	− 6·968	−16·314	− 6·442	0	− 0·735	0	− 0·301	0	− 0·196	0
8 ..	− 0·260	0	− 0·362	0	− 0·810	0	− 6·569	+16·000	− 6·569	0	− 0·810	0	− 0·362	0	− 0·260
9 ..	0	− 0·196	0	− 0·301	0	− 0·735	0	− 6·442	+16·314	− 6·968	0	− 0·935	0	− 0·462	0
10 ..	− 0·124	0	− 0·157	0	− 0·262	0	− 0·692	0	− 6·563	+17·318	− 7·727	0	− 1·147	0	− 0·646
11 ..	0	− 0·095	0	− 0·130	0	− 0·236	0	− 0·673	0	− 6·954	+19·243	− 9·052	0	− 1·532	0
12 ..	− 0·062	0	− 0·075	0	− 0·111	0	− 0·217	0	− 0·674	0	− 7·698	+22·627	−11·430	0	− 2·360
13 ..	0	− 0·045	0	− 0·059	0	− 0·094	0	− 0·201	0	− 0·690	0	− 8·980	+28·799	−16·265	0
14 ..	− 0·026	0	− 0·031	0	− 0·044	0	− 0·076	0	− 0·180	0	− 0·705	0	−11·203	+41·810	−29·544
15 ..	0	− 0·013	0	− 0·017	0	− 0·026	0	− 0·051	0	− 0·136	0	− 0·651	0	−15·061	+82·013

TABLE 2

Coefficients $s_{\mu\nu}^{(2)}$ for $N = 16$

μ	ν 1	2	3	4	5	6	7	8	9	10	11	12	13	14	15
1 ..	+25·769	+17·917	− 4·703	+ 2·016	− 1·104	+ 0·706	− 0·506	+ 0·398	− 0·338	+ 0·310	− 0·305	+ 0·327	− 0·388	+ 0·535	− 1·020
2 ..	−68·941	+ 6·309	+14·908	− 4·993	+ 2·499	− 1·531	+ 1·071	− 0·828	+ 0·697	− 0·634	+ 0·622	− 0·664	+ 0·785	− 1·082	+ 2·060
3 ..	+38·144	−31·420	+ 2·694	+12·636	− 4·844	+ 2·680	− 1·780	+ 1·336	− 1·104	+ 0·991	− 0·963	+ 1·021	− 1·203	+ 1·654	− 3·143
4 ..	−26·486	+17·048	−20·468	+ 1·414	+11·224	− 4·718	+ 2·816	− 2·000	+ 1·598	− 1·405	+ 1·347	− 1·414	+ 1·654	− 2·266	+ 4·295
5 ..	+20·046	−11·798	+10·849	−15·519	0·804	+10·411	− 4·704	+ 2·993	− 2·259	+ 1·918	− 1·800	+ 1·862	− 2·158	+ 2·937	− 5·548
6 ..	−15·836	+ 8·922	− 7·411	+ 8·054	−12·854	+ 0·448	+10·043	− 4·828	+ 3·261	− 2·613	+ 2·369	− 2·398	+ 2·739	− 3·696	+ 6·946
7 ..	+12·797	− 7·033	+ 5·548	− 5·418	+ 6·546	−11·318	+ 0·203	+10·055	− 5·126	+ 3·675	− 3·143	+ 3·075	− 3·439	+ 4·581	− 8·551
8 ..	−10·453	+ 5·657	− 4·330	+ 4·000	− 4·330	+ 5·657	−10·453	0	+10·453	− 5·657	+ 4·330	− 4·000	+ 4·330	− 5·657	+10·453
9 ..	+ 8·551	− 4·581	+ 3·439	− 3·075	+ 3·143	− 3·675	+ 5·126	−10·055	− 0·203	+11·318	− 6·546	+ 5·418	− 5·548	+ 7·033	−12·797
10 ..	− 6·946	+ 3·696	− 2·739	+ 2·398	− 2·369	+ 2·613	− 3·261	+ 4·828	−10·043	− 0·448	+12·854	− 8·054	+ 7·411	− 8·922	+15·836
11 ..	+ 5·548	− 2·937	+ 2·158	− 1·862	+ 1·800	− 1·918	+ 2·259	− 2·993	+ 4·704	−10·411	− 0·804	+15·519	−10·849	+11·798	−20·046
12 ..	− 4·295	+ 2·266	− 1·654	+ 1·414	− 1·347	+ 1·405	− 1·598	+ 2·000	− 2·816	+ 4·718	−11·224	− 1·414	+20·468	−17·048	+26·486
13 ..	+ 3·143	− 1·654	+ 1·203	− 1·021	+ 0·963	− 0·991	+ 1·104	− 1·336	+ 1·780	− 2·680	+ 4·844	−12·636	− 2·694	+31·420	−38·144
14 ..	− 2·060	+ 1·082	− 0·785	+ 0·664	− 0·622	+ 0·634	− 0·697	+ 0·828	− 1·071	+ 1·531	− 2·499	+ 4·993	−14·908	− 6·309	+68·941
15 ..	+ 1·020	− 0·535	+ 0·388	− 0·327	+ 0·305	− 0·310	+ 0·338	− 0·398	+ 0·506	− 0·706	+ 1·104	− 2·016	+ 4·703	−17·917	−25·769

TABLE 3

Numerical Values of Several Vortex Distribution Functions

$$\gamma_2\left(\frac{x}{L}\right) = 2\pi V_0 c_2 \sqrt{\left\{1-\left(1-\frac{2x}{L}\right)^2\right\}}$$

$$\gamma_3\left(\frac{x}{L}\right) = 2\pi V_0 c_3 \left(1-\frac{2x}{L}\right)\sqrt{\left\{1-\left(1-\frac{2x}{L}\right)^2\right\}}$$

$$\gamma_6\left(\frac{x}{L}\right) = 2\pi V_0 c_6 \left\{1-\left(1-\frac{2x}{L}\right)^2\right\}^{1/4}$$

$$\gamma_7\left(\frac{x}{L}\right) = 2\pi V_0 c_7 \left(1-\frac{2x}{L}\right)\left\{1-\left(1-\frac{2x}{L}\right)^2\right\}^{1/4}$$

$$\gamma_8\left(\frac{x}{L}\right) = 2\pi V_0 c_8 \left[1-\left(1-\frac{2x}{L}\right)^2\right]$$

$$\gamma_9\left(\frac{x}{L}\right) = 2\pi V_0 c_9 \left(1-\frac{2x}{L}\right)\left[1-\left(1-\frac{2x}{L}\right)^2\right]$$

x/L	$\frac{\gamma_2(x)}{2\pi V_0 c_2}$	$\frac{\gamma_3(x)}{2\pi V_0 c_3}$	$\frac{\gamma_6(x)}{2\pi V_0 c_6}$	$\frac{\gamma_7(x)}{2\pi V_0 c_7}$	$\frac{\gamma_8(x)}{2\pi V_0 c_8}$	$\frac{\gamma_9(x)}{2\pi V_0 c_9}$
0	0	0	0	0	0	0
0·05	0·436	0·392	0·660	0·594	0·190	0·171
0·10	0·600	0·480	0·775	0·620	0·360	0·288
0·15	0·714	0·500	0·845	0·592	0·510	0·357
0·20	0·800	0·480	0·894	0·537	0·640	0·384
0·25	0·866	0·433	0·931	0·465	0·750	0·375
0·30	0·917	0·367	0·957	0·383	0·840	0·336
0·35	0·954	0·286	0·977	0·293	0·910	0·273
0·40	0·980	0·196	0·990	0·198	0·960	0·192
0·45	0·995	0·100	0·998	0·100	0·990	0·099
0·50	1·000	0	1·0	0	1·0	0

TABLE 4

Induced Axial Velocity Components v_x of the Vortex-ring Distributions*

$$\frac{v_{x2}^*}{V_0} = \frac{1}{c_2}\frac{v_{x2}}{V_0}$$

x/L	L/D			
	2	3	4	5
−0·50	0·16	0·09	0·05	0·03
−0·20	0·41	0·29	0·20	0·14
−0·10	0·61	0·48	0·38	0·31
−0·05	0·76	0·64	0·54	0·47
0	0·95	0·89	0·81	0·72
0·05	−0·14	−0·13	−0·14	−0·13
0·10	−0·41	−0·33	−0·30	−0·28
0·15	−0·55	−0·43	−0·37	−0·33
0·20	−0·64	−0·48	−0·39	−0·34
0·25	−0·70	−0·50	−0·40	−0·34
0·30	−0·73	−0·50	−0·39	−0·33
0·35	−0·75	−0·50	−0·38	−0·31
0·40	−0·76	−0·49	−0·36	−0·29
0·45	−0·77	−0·48	−0·34	−0·28
0·50	−0·77	−0·47	−0·33	−0·26

$$\frac{v_{x3}^*}{V_0} = \frac{1}{c_3}\frac{v_{x3}}{V_0}$$

x/L	L/D			
	2	3	4	5
−0·50	0·04	0·03	0·02	0·01
−0·20	0·15	0·13	0·11	0·08
−0·10	0·25	0·24	0·22	0·18
−0·05	0·32	0·33	0·32	0·30
0	0·43	0·49	0·51	0·50
0·05	−0·65	−0·52	−0·44	−0·38
0·10	−0·84	−0·68	−0·57	−0·49
0·15	−0·87	−0·70	−0·59	−0·50
0·20	−0·82	−0·65	−0·54	−0·46
0·25	−0·72	−0·55	−0·45	−0·37
0·30	−0·60	−0·43	−0·33	−0·27
0·35	−0·46	−0·31	−0·22	−0·17
0·40	−0·31	−0·20	−0·13	−0·09
0·45	−0·15	−0·09	−0·05	−0·03
0·50	0	0	0	0

* These include the term $-\frac{1}{2}\gamma(x)$ and thus represent the velocities at the outer surface of the cylinder.

TABLE 4—*continued*

$$\frac{v_{x6}^*}{V_0} = \frac{1}{c_6}\frac{v_{x6}}{V_0}$$

x/L	L/D			
	2	3	4	5
−0·50	0·18	0·10	0·06	0·04
−0·20	0·50	0·35	0·25	0·18
−0·10	0·74	0·60	0·48	0·39
−0·05	0·91	0·80	0·71	0·64
0	1·14	1·10	1·06	1·03
0·05	−0·65	−0·58	−0·52	−0·47
0·10	−0·76	−0·60	−0·51	−0·43
0·15	−0·77	−0·57	−0·45	−0·38
0·20	−0·76	−0·54	−0·41	−0·34
0·25	−0·74	−0·50	−0·37	−0·30
0·30	−0·73	−0·48	−0·35	−0·28
0·35	−0·72	−0·46	−0·33	−0·26
0·40	−0·71	−0·44	−0·31	−0·24
0·45	−0·71	−0·43	−0·30	−0·23
0·50	−0·71	−0·43	−0·30	−0·23

$$\frac{v_{x7}^*}{V_0} = \frac{1}{c_7}\frac{v_{x7}}{V_0}$$

x/L	L/D			
	2	3	4	5
−0·50	0·06	0·04	0·03	0·02
−0·20	0·19	0·17	0·14	0·11
−0·10	0·32	0·33	0·30	0·25
−0·05	0·43	0·45	0·44	0·42
0	0·57	0·69	0·74	0·77
0·05	−1·14	−0·93	−0·77	−0·67
0·10	−1·13	−0·89	−0·73	−0·62
0·15	−1·02	−0·79	−0·64	−0·53
0·20	−0·89	−0·67	−0·53	−0·43
0·25	−0·74	−0·53	−0·41	−0·33
0·30	−0·58	−0·40	−0·30	−0·24
0·35	−0·43	−0·28	−0·20	−0·15
0·40	−0·28	−0·17	−0·11	−0·07
0·45	−0·13	−0·07	−0·04	−0·02
0·50	0	0	0	0

TABLE 4—*continued*

$$\frac{v_{x8}^*}{V_0} = \frac{1}{c_8}\frac{v_{x8}}{V_0}$$

x/L	L/D			
	2	3	4	5
−0·50	0·12	0·07	0·04	0·02
−0·20	0·33	0·22	0·15	0·11
−0·10	0·48	0·36	0·27	0·21
−0·05	0·59	0·47	0·38	0·31
0	0·72	0·63	0·55	0·48
0·05	0·32	0·28	0·22	0·17
0·10	0	0·02	0·02	0·01
0·15	−0·26	−0·17	−0·13	−0·10
0·20	−0·47	−0·30	−0·23	−0·18
0·25	−0·63	−0·40	−0·30	−0·24
0·30	−0·75	−0·47	−0·35	−0·28
0·35	−0·84	−0·53	−0·39	−0·31
0·40	−0·90	−0·58	−0·43	−0·34
0·45	−0·94	−0·61	−0·45	−0·35
0·50	−0·95	−0·61	−0·45	−0·35

$$\frac{v_{x9}^*}{V_0} = \frac{1}{c_9}\frac{v_{x9}}{V_0}$$

x/L	L/D			
	2	3	4	5
−0·50	0·03	0·01	0·01	0
−0·20	0·11	0·09	0·07	0·05
−0·10	0·16	0·15	0·13	0·11
−0·05	0·20	0·20	0·19	0·17
0	0·27	0·29	0·30	0·29
0·05	−0·18	−0·12	−0·08	−0·06
0·10	−0·45	−0·34	−0·29	−0·25
0·15	−0·62	−0·48	−0·40	−0·34
0·20	−0·69	−0·53	−0·43	−0·36
0·25	−0·68	−0·52	−0·42	−0·35
0·30	−0·61	−0·46	−0·37	−0·31
0·35	−0·50	−0·36	−0·29	−0·24
0·40	−0·35	−0·24	−0·19	−0·15
0·45	−0·18	−0·12	−0·09	−0·07
0·50	0	0	0	0

TABLE 5

Induced Radial Velocity Components v_r of the Vortex-ring Distributions

$$\frac{v_{r2}^*}{V_0} = \frac{1}{c_2} \cdot \frac{v_{r2}}{V_0}$$

x/L	L/D			
	2	3	4	5
−0·50	−0·07	−0·03	−0·02	−0·01
−0·20	−0·32	−0·16	−0·10	−0·07
−0·10	−0·62	−0·37	−0·26	−0·20
−0·05	−0·94	−0·65	−0·50	−0·40
0	−2·04	−1·73	−1·53	−1·39
0·05	−1·75	−1·41	−1·20	−1·05
0·10	−1·49	−1·16	−0·96	−0·81
0·15	−1·25	−0·95	−0·77	−0·64
0·20	−1·03	−0·77	−0·61	−0·51
0·25	−0·83	−0·61	−0·48	−0·40
0·30	−0·64	−0·47	−0·36	−0·30
0·35	−0·47	−0·34	−0·26	−0·21
0·40	−0·31	−0·22	−0·17	−0·14
0·45	−0·15	−0·11	−0·08	−0·07
0·50	0	0	0	0

$$\frac{v_{r3}^*}{V_0} = \frac{1}{c_3} \cdot \frac{v_{r3}}{V_0}$$

x/L	L/D			
	2	3	4	5
−0·50	−0·03	−0·01	−0·01	0
−0·20	−0·17	−0·09	−0·06	−0·05
−0·10	−0·36	−0·24	−0·18	−0·14
−0·05	−0·56	−0·45	−0·37	−0·30
0	−1·52	−1·40	−1·31	−1·23
0·05	−0·96	−0·86	−0·77	−0·70
0·10	−0·49	−0·44	−0·40	−0·36
0·15	−0·11	−0·12	−0·12	−0·12
0·20	0·21	0·14	0·09	0·06
0·25	0·47	0·35	0·26	0·21
0·30	0·67	0·51	0·40	0·33
0·35	0·83	0·63	0·51	0·43
0·40	0·94	0·72	0·59	0·50
0·45	1·01	0·78	0·64	0·54
0·50	1·03	0·81	0·66	0·56

TABLE 5—*continued*

$$\frac{v_{r6}^*}{V_0} = \frac{1}{c_6} \cdot \frac{v_{r6}}{V_0}$$

x/L	L/D			
	2	3	4	5
−0·50	−0·08	−0·04	−0·02	−0·01
−0·20	−0·38	−0·21	−0·12	−0·08
−0·10	−0·76	−0·49	−0·35	−0·27
−0·05	−1·21	−0·89	−0·71	−0·59
0	−3·71	−3·57	−3·43	−3·29
0·05	−1·87	−1·52	−1·27	−1·09
0·10	−1·39	−1·04	−0·82	−0·68
0·15	−1·10	−0·76	−0·58	−0·47
0·20	−0·87	−0·56	−0·41	−0·32
0·25	−0·67	−0·41	−0·28	−0·22
0·30	−0·50	−0·30	−0·19	−0·14
0·35	−0·36	−0·20	−0·12	−0·09
0·40	−0·23	−0·12	−0·07	−0·05
0·45	−0·11	−0·06	−0·03	−0·02
0·50	0	0	0	0

$$\frac{v_{r7}^*}{V_0} = \frac{1}{c_7} \cdot \frac{v_{r7}}{V_0}$$

x/L	L/D			
	2	3	4	5
−0·50	−0·04	−0·02	−0·01	−0·01
−0·20	−0·22	−0·12	−0·09	−0·07
−0·10	−0·49	−0·35	−0·27	−0·22
−0·05	−0·84	−0·69	−0·57	−0·49
0	−3·44	−3·36	−3·20	−3·08
0·05	−1·13	−0·89	−0·75	−0·67
0·10	−0·39	−0·27	−0·21	−0·18
0·15	0·04	0·08	0·10	0·10
0·20	0·36	0·33	0·30	0·27
0·25	0·60	0·52	0·44	0·38
0·30	0·79	0·65	0·53	0·45
0·35	0·93	0·74	0·60	0·50
0·40	1·02	0·80	0·64	0·53
0·45	1·07	0·84	0·67	0·56
0·50	1·09	0·86	0·69	0·57

TABLE 5—*continued*

$$\frac{v_{r8}^*}{V_0} = \frac{1}{c_8} \cdot \frac{v_{r8}}{V_0}$$

x/L	L/D			
	2	3	4	5
−0·50	−0·05	−0·02	−0·01	0
−0·20	−0·23	−0·12	−0·06	−0·04
−0·10	−0·43	−0·25	−0·16	−0·12
−0·05	−0·63	−0·40	−0·28	−0·22
0	−1·04	−0·78	−0·63	−0·53
0·05	−1·42	−1·11	−0·92	−0·81
0·10	−1·45	−1·16	−0·96	−0·84
0·15	−1·40	−1·11	−0·92	−0·80
0·20	−1·28	−1·00	−0·82	−0·71
0·25	−1·10	−0·86	−0·70	−0·60
0·30	−0·91	−0·70	−0·57	−0·49
0·35	−0·70	−0·53	−0·43	−0·37
0·40	−0·48	−0·36	−0·29	−0·25
0·45	−0·24	−0·18	−0·15	−0·13
0·50	0	0	0	0

$$\frac{v_{r9}^*}{V_0} = \frac{1}{c_9} \cdot \frac{v_{r9}}{V_0}$$

x/L	L/D			
	2	3	4	5
−0·50	−0·02	−0·01	0	0
−0·20	−0·10	−0·06	−0·03	−0·02
−0·10	−0·20	−0·14	−0·10	−0·07
−0·05	−0·32	−0·25	−0·19	−0·14
0	−0·63	−0·54	−0·47	−0·41
0·05	−0·77	−0·70	−0·62	−0·55
0·10	−0·55	−0·53	−0·49	−0·45
0·15	−0·31	−0·30	−0·29	−0·28
0·20	−0·06	−0·05	−0·07	−0·08
0·25	0·20	0·17	0·13	0·10
0·30	0·46	0·37	0·30	0·25
0·35	0·67	0·54	0·45	0·37
0·40	0·82	0·66	0·55	0·46
0·45	0·92	0·74	0·61	0·51
0·50	0·95	0·76	0·63	0·53

TABLE 6

Radial Increments Δr Produced by the Vortex-ring Distributions

$$\frac{1}{c_2} \cdot \frac{\Delta r_2}{L}$$

x/L	L/D			
	2	3	4	5
$-\infty$	0	0	0	0
−0·5	−0·025	−0·01	−0·005	0
−0·2	−0·075	−0·035	−0·02	−0·01
−0·1	−0·12	−0·055	−0·035	−0·025
0	−0·225	−0·135	−0·095	−0·07
0·1	−0·395	−0·28	−0·22	−0·18
0·2	−0·52	−0·37	−0·295	−0·245
0·3	−0·605	−0·43	−0·345	−0·285
0·4	−0·65	−0·465	−0·37	−0·305
0·5	−0·665	−0·475	−0·38	−0·31

$$\frac{1}{c_3} \cdot \frac{\Delta r_3}{L}$$

x/L	L/D			
	2	3	4	5
$-\infty$	0	0·01	0·02	0·025
−0·5	−0·005	0·005	0·02	0·02
−0·2	−0·03	−0·005	0·01	0·015
−0·1	−0·055	−0·02	0·00	0·01
0	−0·12	−0·075	−0·045	−0·03
0·1	−0·215	−0·16	−0·125	−0·105
0·2	−0·23	−0·175	−0·14	−0·12
0·3	−0·18	−0·14	−0·115	−0·095
0·4	−0·10	−0·08	−0·065	−0·055
0·5	0	0	0	0

TABLE 6—*continued*

$$\frac{1}{c_6}\cdot\frac{\Delta r_6}{L}$$

x/L	L/D			
	2	3	4	5
$-\infty$	0	0	0	0
−0·5	−0·025	−0·01	−0·005	0
−0·2	−0·08	−0·04	−0·02	−0·01
−0·1	−0·14	−0·075	−0·04	−0·025
0	−0·28	−0·185	−0·13	−0·105
0·1	−0·485	−0·36	−0·28	−0·23
0·2	−0·595	−0·435	−0·335	−0·28
0·3	−0·665	−0·475	−0·365	−0·30
0·4	−0·70	−0·495	−0·375	−0·31
0·5	−0·71	−0·50	−0·38	−0·315

$$\frac{1}{c_7}\cdot\frac{\Delta r_7}{L}$$

x/L	L/D			
	2	3	4	5
$-\infty$	0·055	0·025	0·02	0·025
−0·5	0·04	0·02	0·02	0·02
−0·2	0·01	0·005	0·01	0·015
−0·1	−0·02	−0·015	−0·01	0
0	−0·125	−0·105	−0·085	−0·065
0·1	−0·26	−0·215	−0·18	−0·15
0·2	−0·26	−0·21	−0·17	−0·14
0·3	−0·20	−0·16	−0·125	−0·105
0·4	−0·105	−0·085	−0·065	−0·055
0·5	0	0	0	0

TABLE 6—*continued*

$$\frac{1}{c_8} \cdot \frac{\Delta r_8}{L}$$

x/L	L/D			
	2	3	4	5
$-\infty$	0	0	0	0
−0·5	−0·015	−0·005	−0·005	0
−0·2	−0·05	−0·02	−0·01	−0·005
−0·1	−0·08	−0·04	−0·02	−0·01
0	−0·15	−0·085	−0·055	−0·035
0·1	−0·29	−0·19	−0·14	−0·115
0·2	−0·425	−0·30	−0·23	−0·19
0·3	−0·535	−0·385	−0·30	−0·255
0·4	−0·605	−0·435	−0·345	−0·29
0·5	−0·63	−0·455	−0·36	−0·30

$$\frac{1}{c_9} \cdot \frac{\Delta r_9}{L}$$

x/L	L/D			
	2	3	4	5
$-\infty$	0	0	0	0·005
−0·5	−0·01	−0·005	0	0·005
−0·2	−0·025	−0·01	−0·005	0·005
−0·1	−0·04	−0·02	−0·01	0
0	−0·075	−0·05	−0·03	−0·02
0·1	−0·145	−0·11	−0·09	−0·07
0·2	−0·175	−0·14	−0·115	−0·095
0·3	−0·155	−0·125	−0·105	−0·085
0·4	−0·09	−0·075	−0·06	−0·05
0·5	0	0	0	0

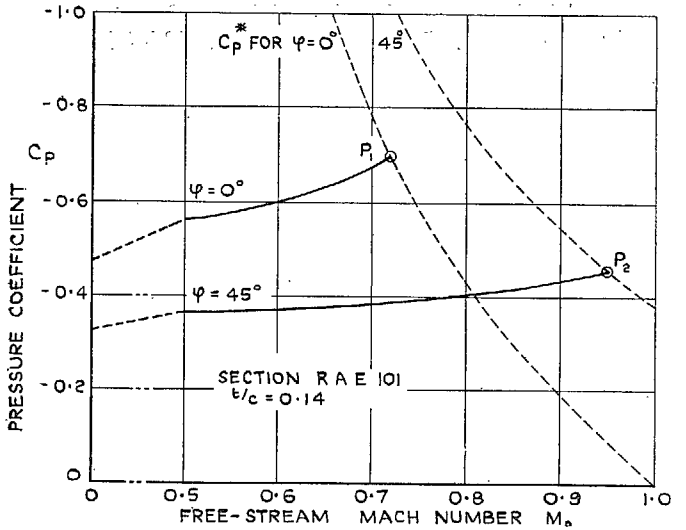

FIG. 1. Increase of pressure coefficient with Mach number for an unswept and for a sheared wing, according to the Prandtl-Glauert rule, equation (2·45).

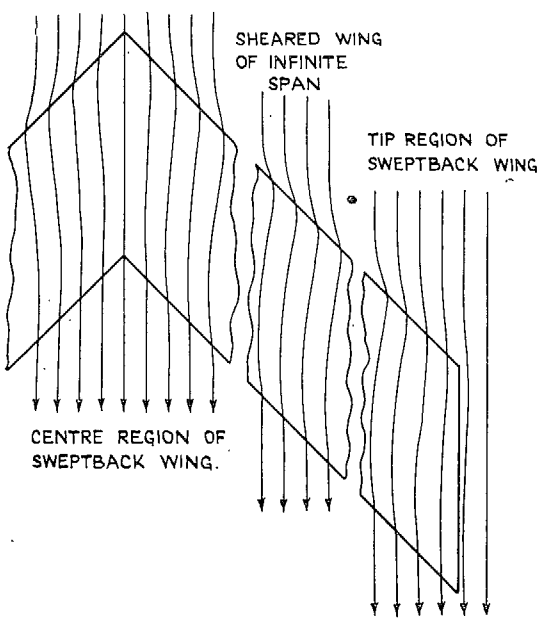

FIG. 2. Flow patterns over the various parts of a swept-back wing.

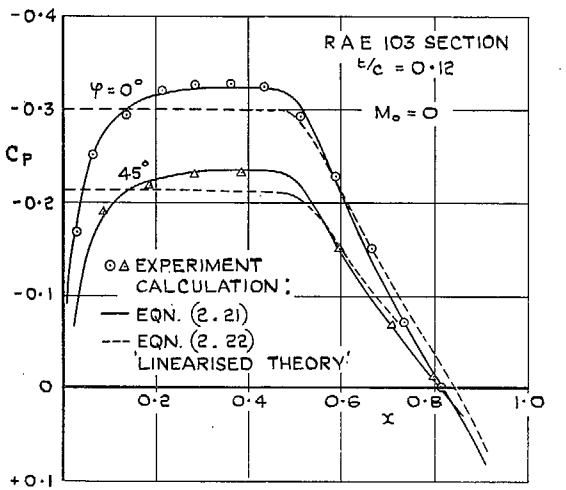

FIG. 3. Pressure distributions along chord for an unswept wing and for the sheared part of a 45-deg swept-back wing.

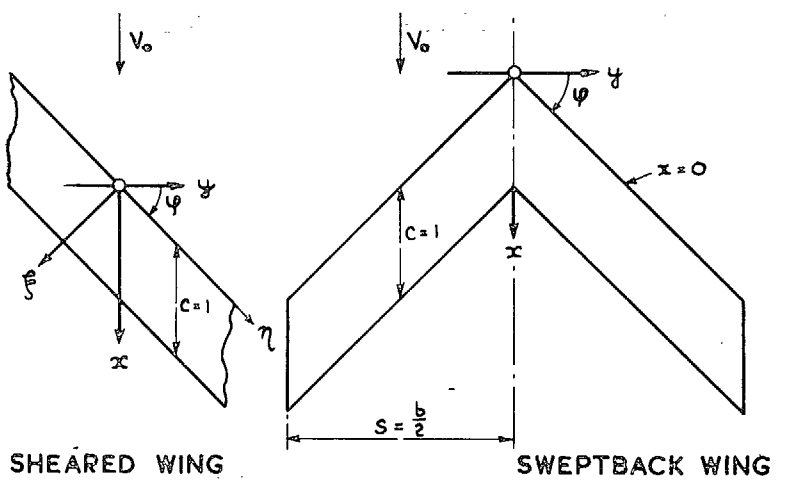

FIG. 4. Co-ordinate systems.

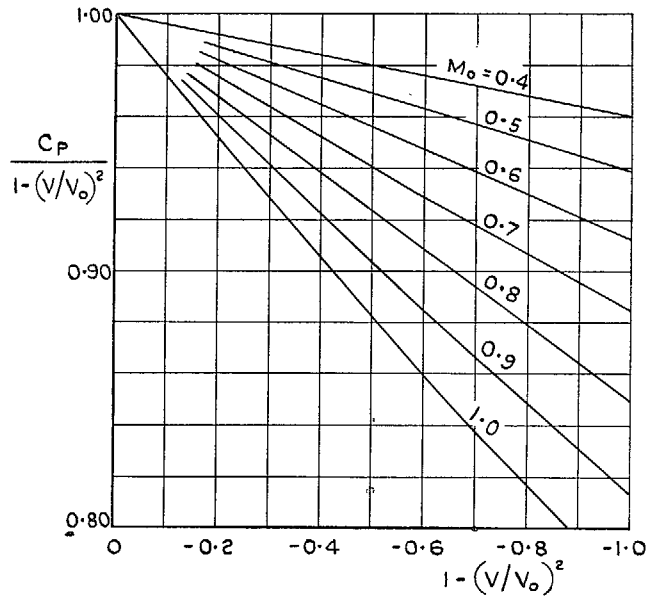

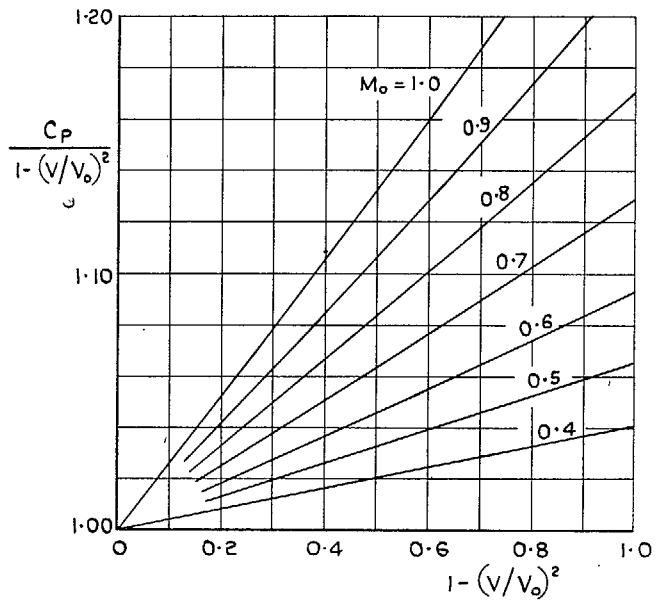

FIG. 5. Diagram for determining the pressure coefficient for a given velocity ratio.

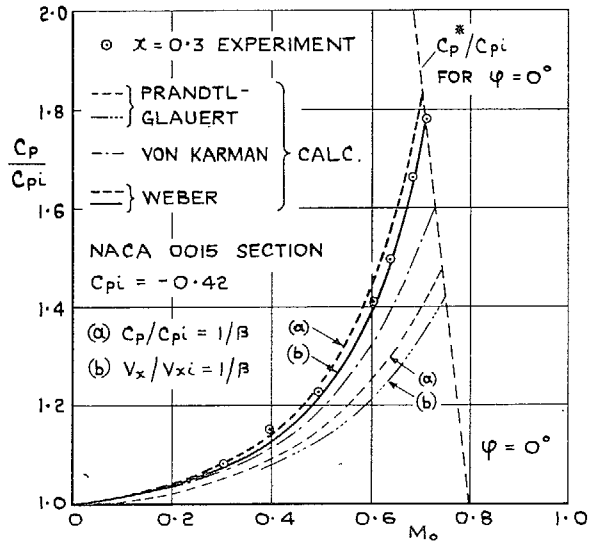

FIG. 6. Pressure rise with Mach number on an unswept wing spanning a closed tunnel.

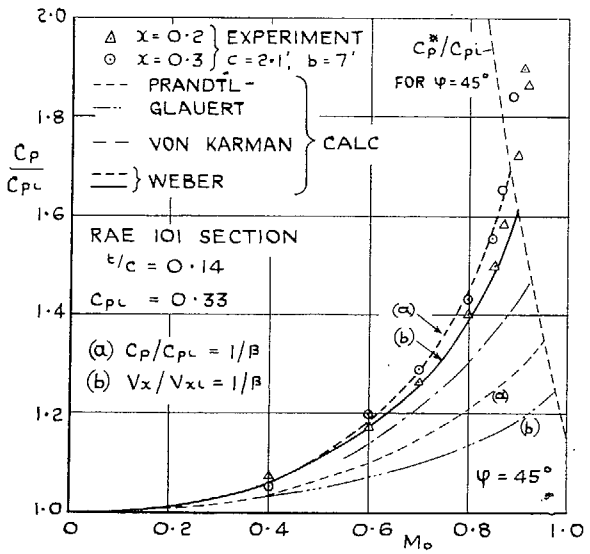

FIG. 7. Pressure rise with Mach number on a 45-deg swept-back wing spanning a closed tunnel.

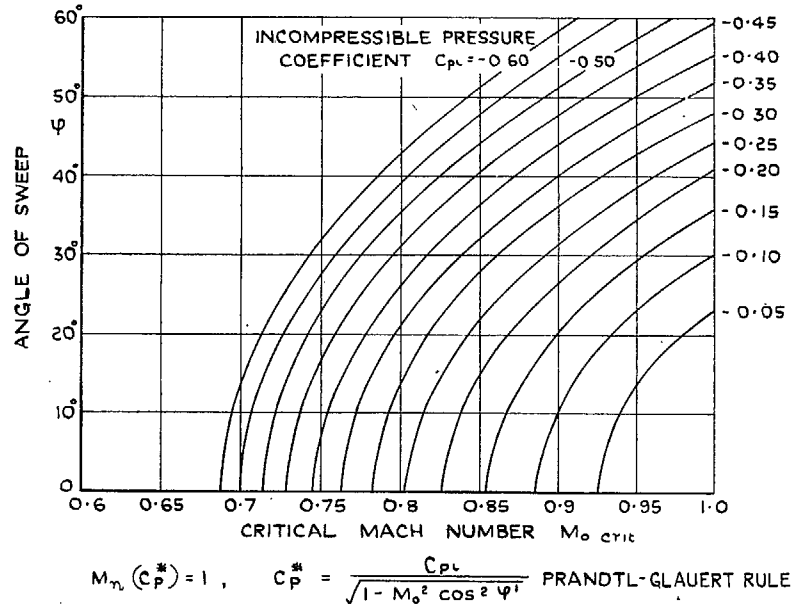

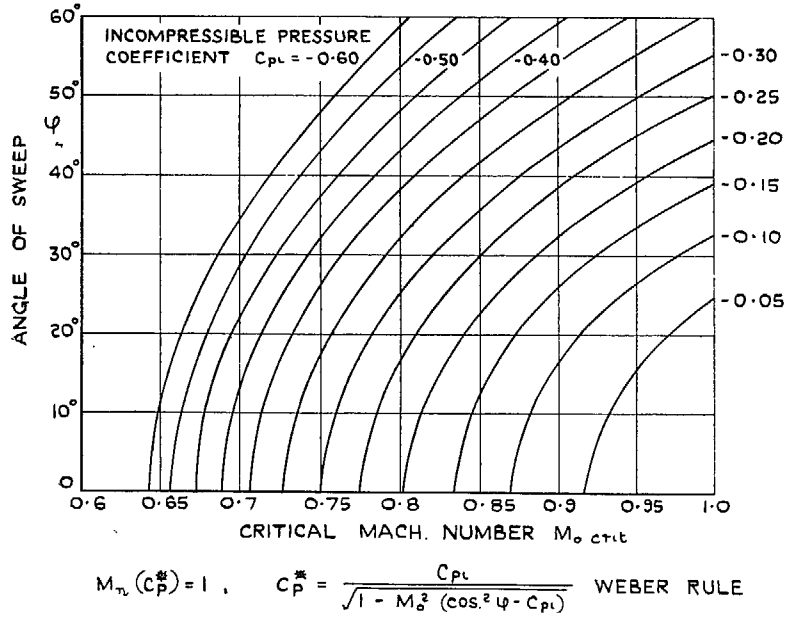

FIG. 8. Critical Mach numbers for two-dimensional flow.

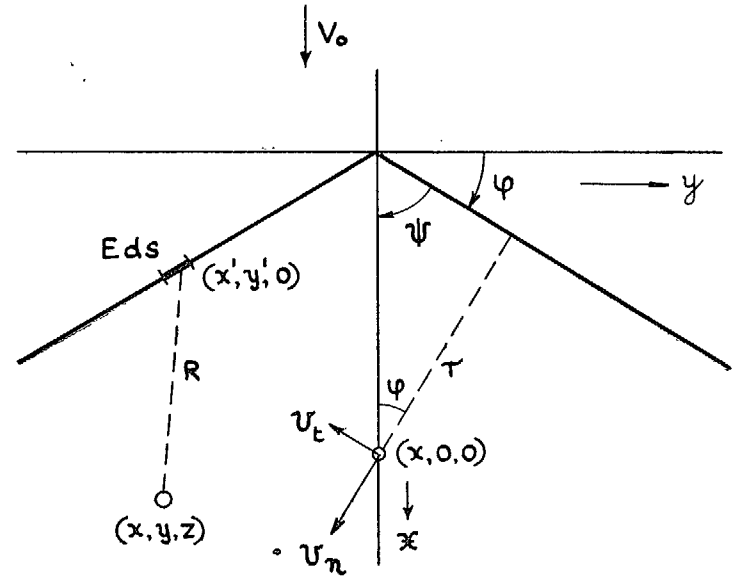

FIG. 9. Kinked source line.

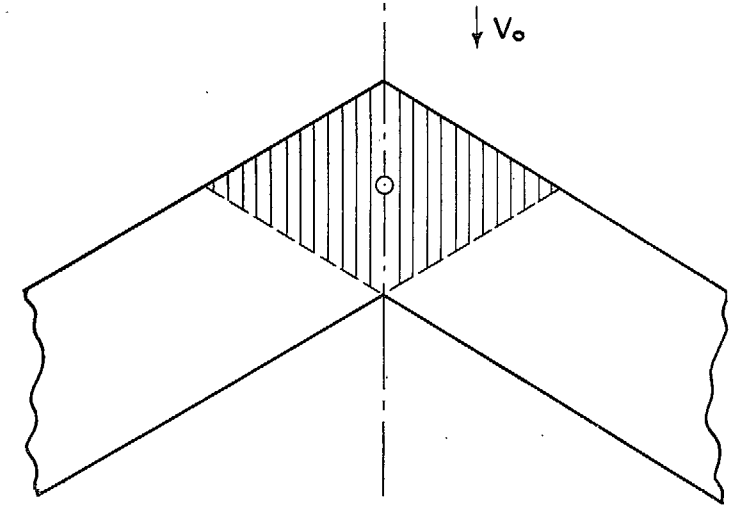

FIG. 10. Kinked strip with uniform source distribution.

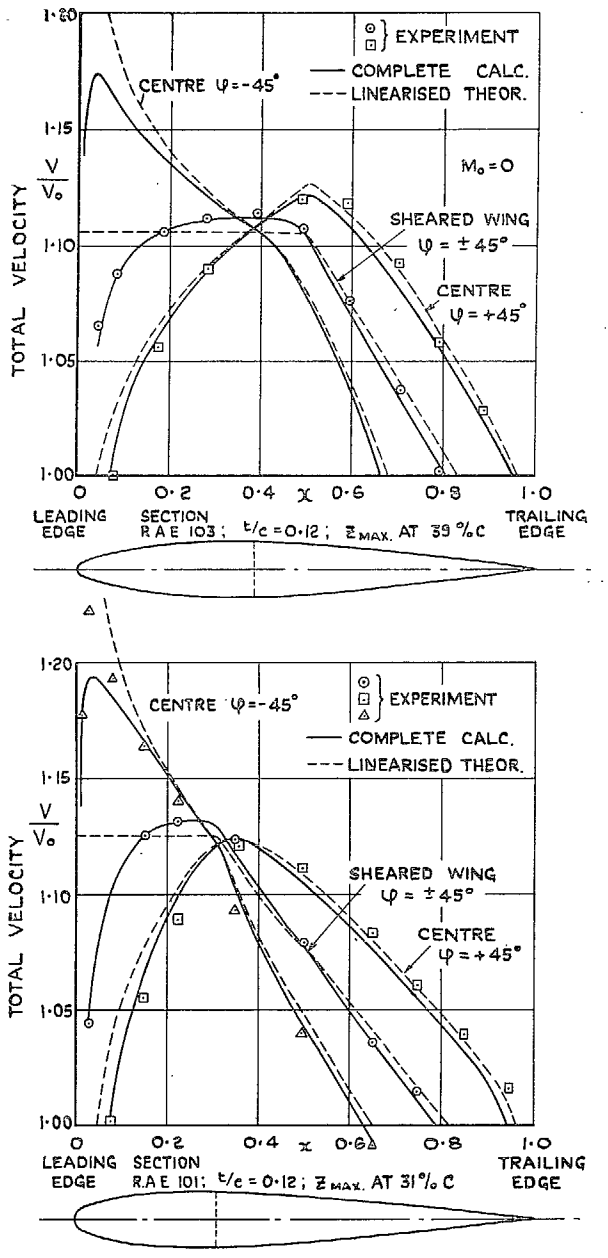

FIG. 11. Velocity distributions for two different aerofoil sections.

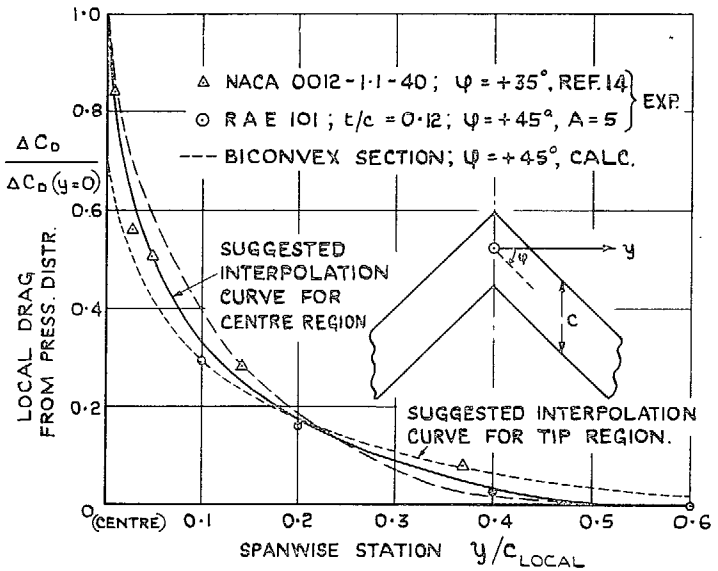

FIG. 12. Spanwise decrease of local drag coefficient.

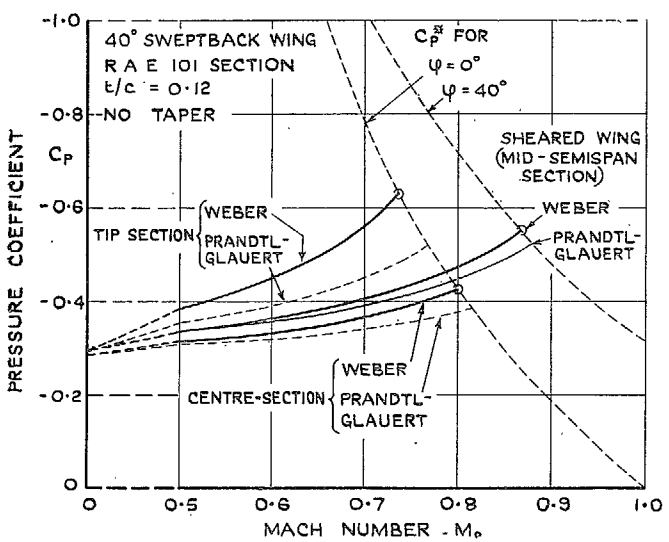

FIG. 13. Increase of pressure coefficient with Mach number for various spanwise stations on a 40-deg swept-back wing.

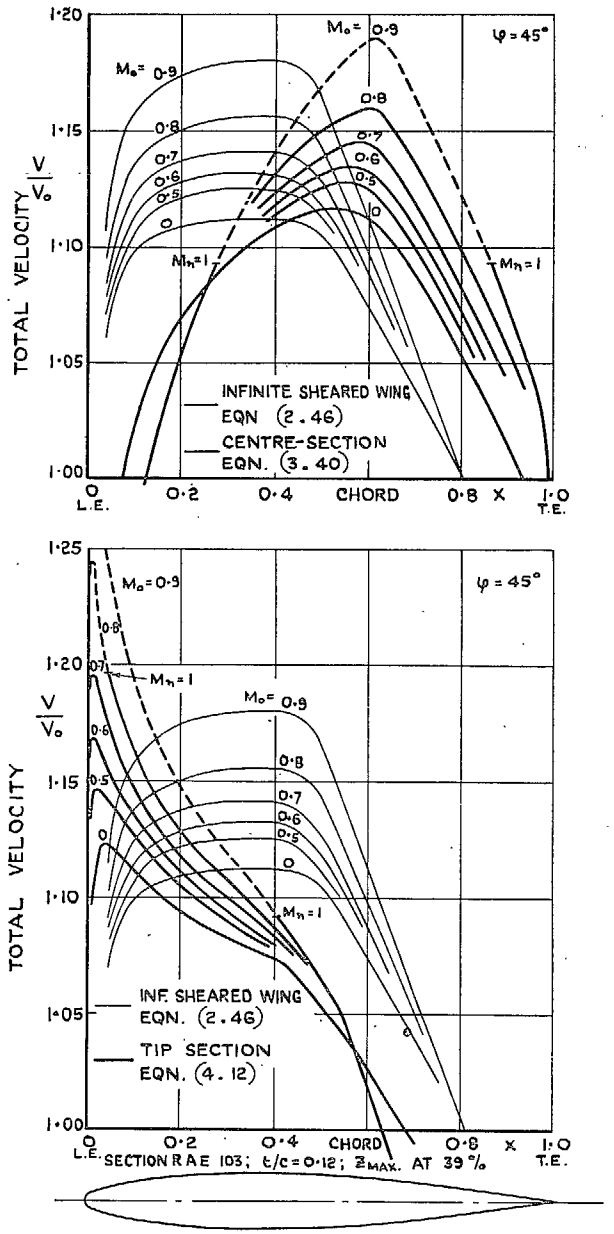

FIG. 14. Influence of Mach number on chordwise velocity distributions (calculated).

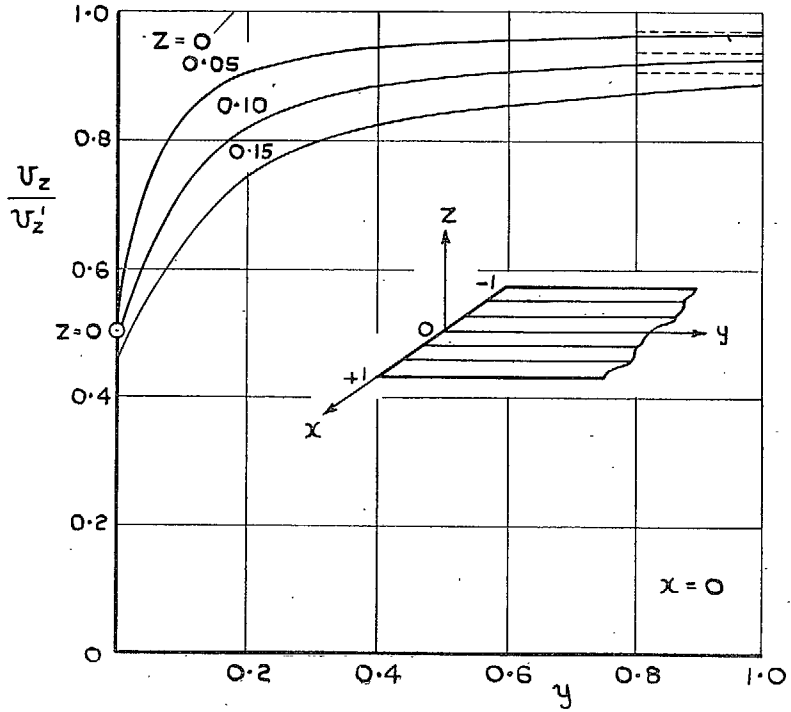

FIG. 15. Normal velocity produced by a semi-infinite strip covered uniformly with sources.

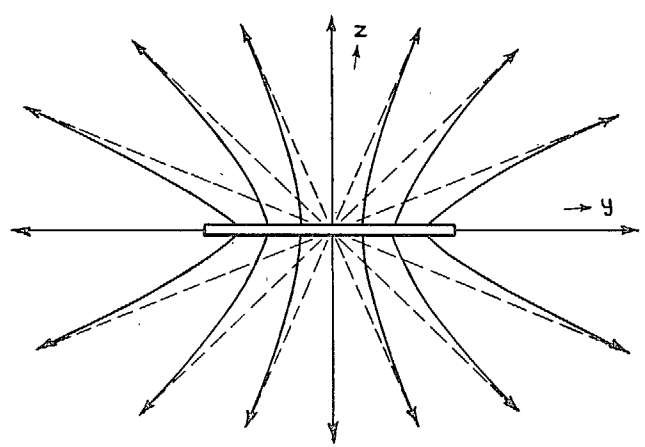

FIG. 16. Streamlines of a source element of finite span.

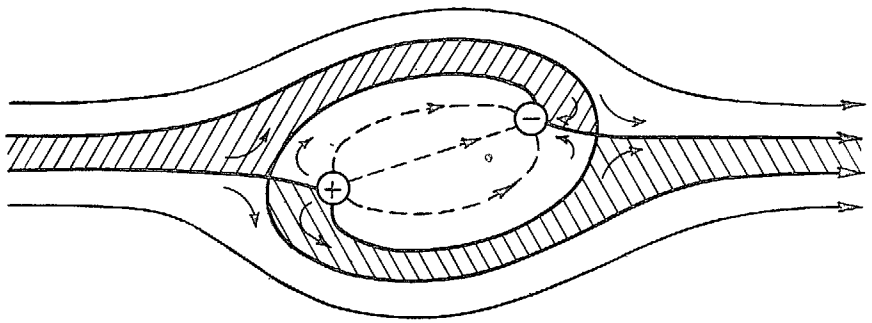

FIG. 17. Streamlines about a yawed source-sink pair.

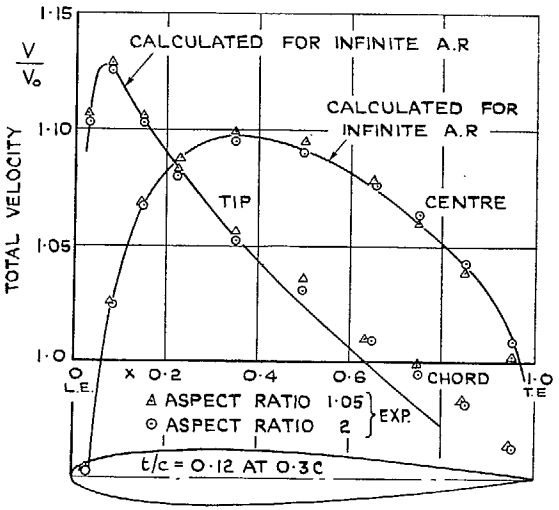

FIG. 19. Velocity distributions at centre and tip sections of two 53-deg swept-back wings with constant chord (square-cut tips).

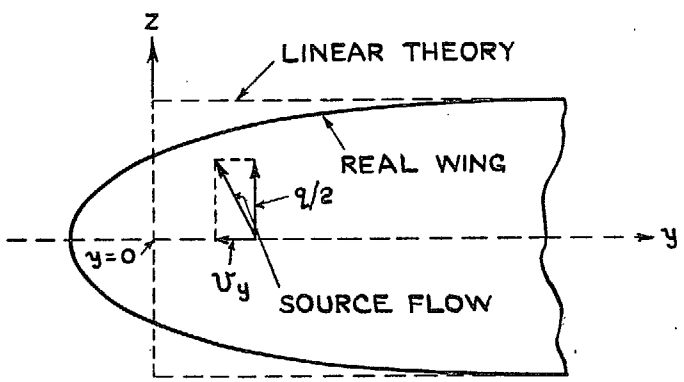

FIG. 18. Spanwise section of a wing produced by a source distribution which is constant along span.

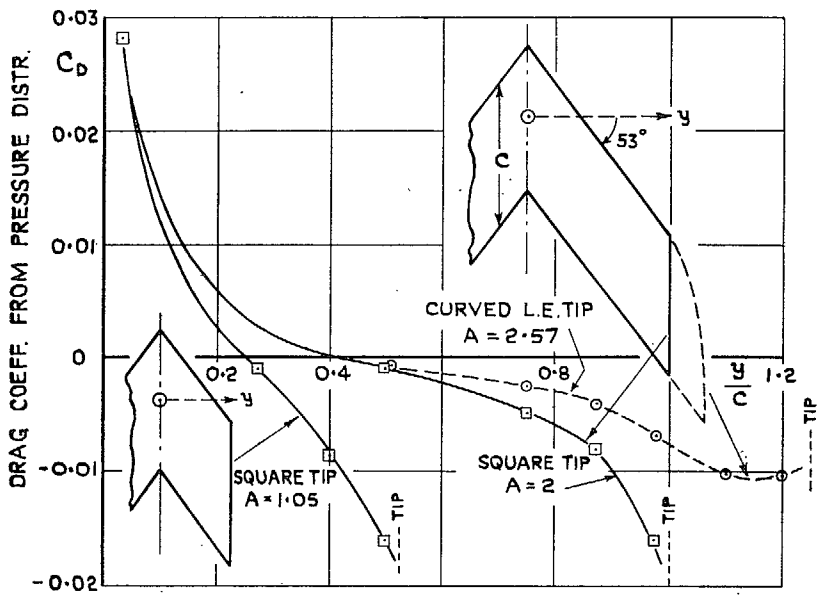

FIG. 20. Coefficient of local form drag along the span of some 53-deg swept-back wings with constant chord.

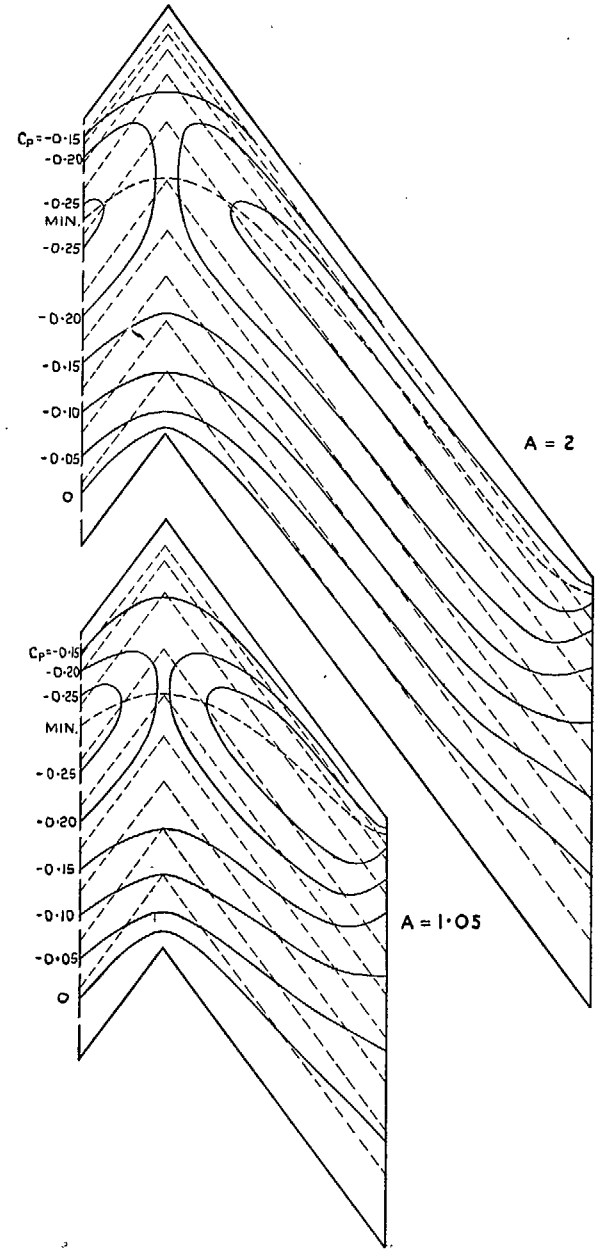

FIG. 21. Isobars on two 53-deg swept-back wings of different aspect ratios (square-cut tips).

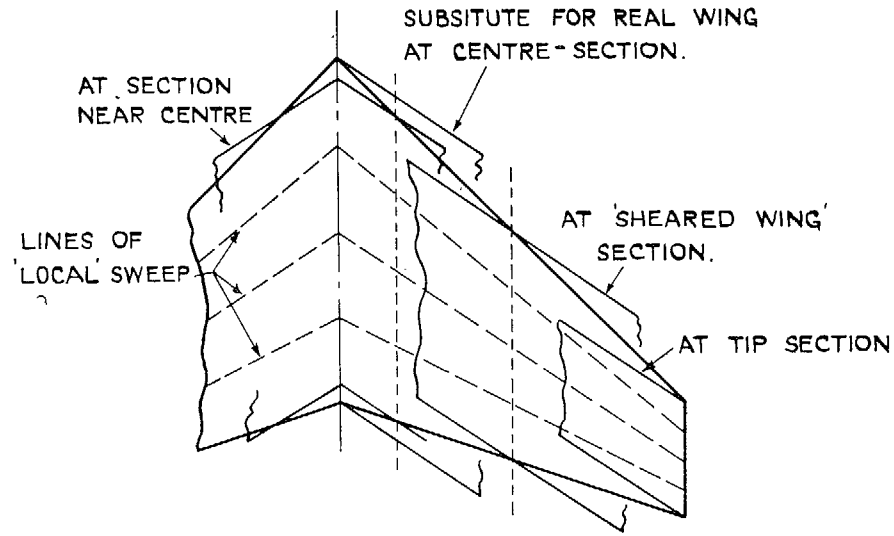

FIG. 22. Substitutes for real wing at various spanwise stations.

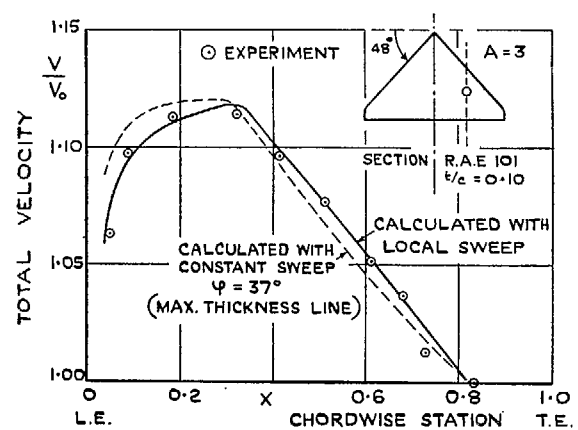

FIG. 23. Velocity distribution at about mid-semi-span on a delta wing.

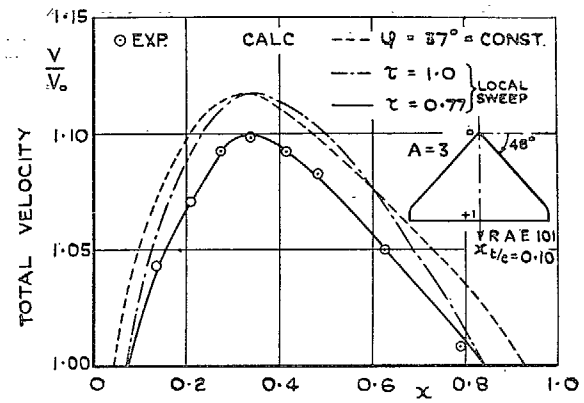

FIG. 24. Velocity distribution at the centre-section of a delta wing.

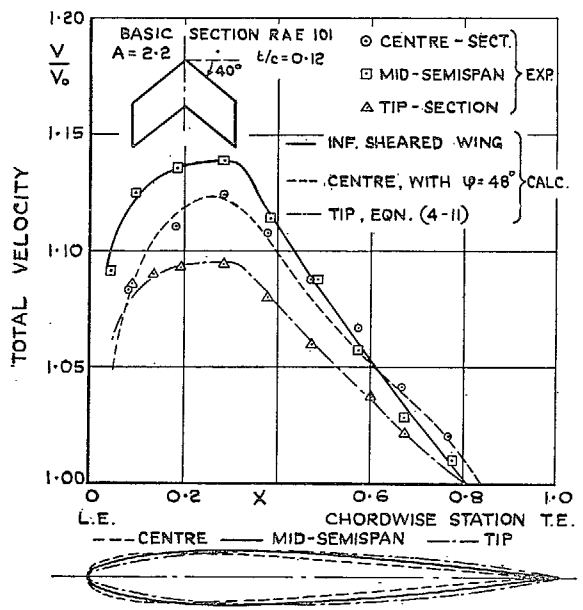

FIG. 25. Velocity distributions at three spanwise stations on a 40-deg swept-back wing of constant chord with modified section shapes.

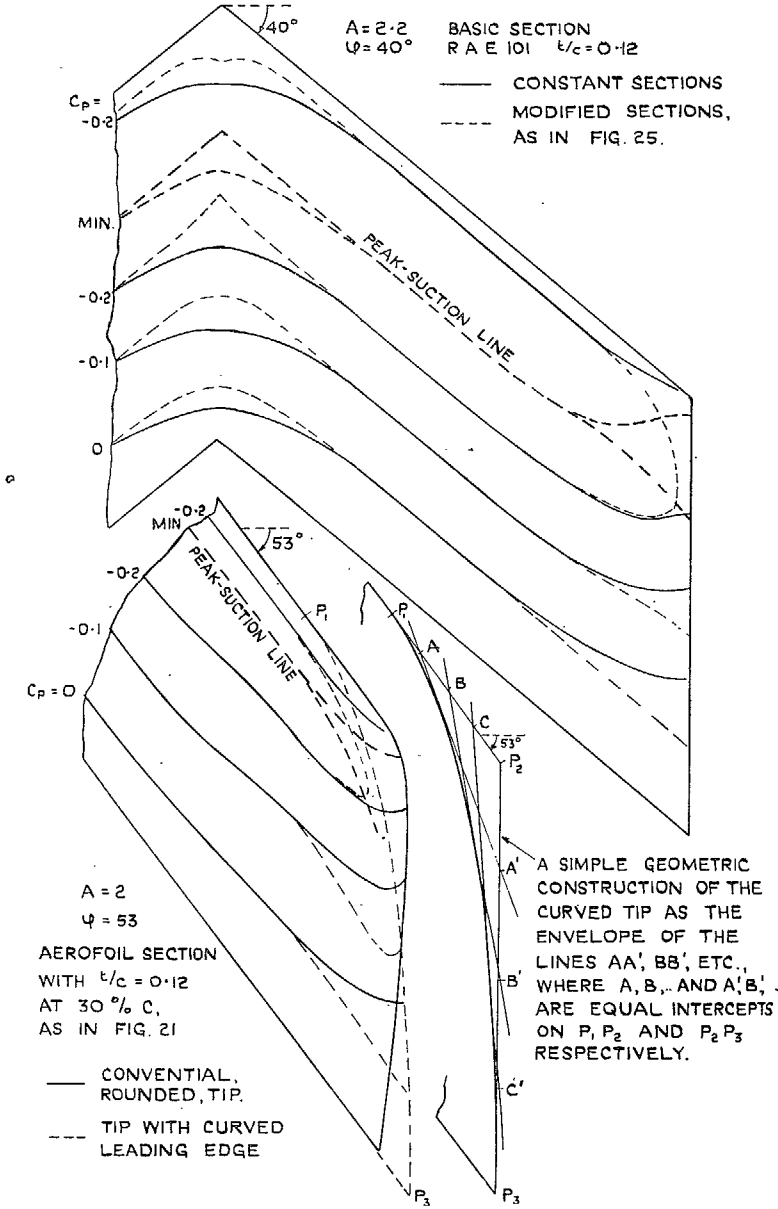

FIG. 26. Isobar patterns on two swept-back wings.
Above: Modification of the aerofoil section.
Below: Modification of the plan form in tip region.

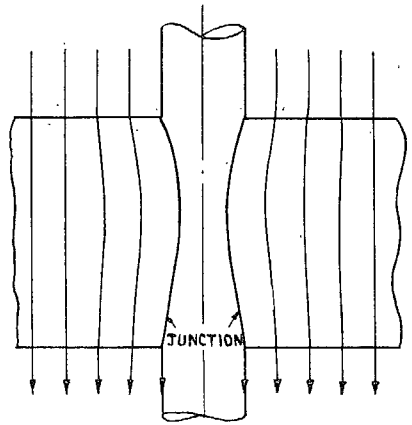

FIG. 27. Flow pattern near the junction of a body with an unswept wing.

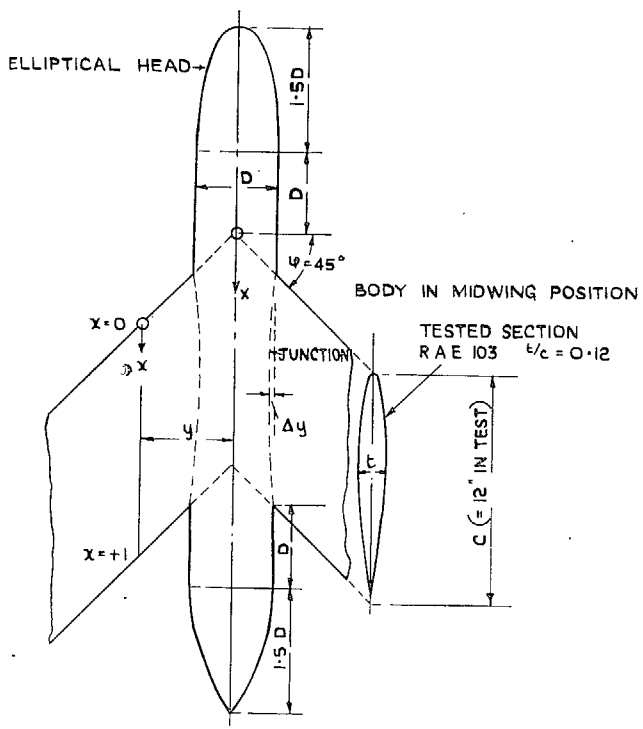

FIG. 28. Cylindrical body on 45-deg swept-back wing. Nomenclature.

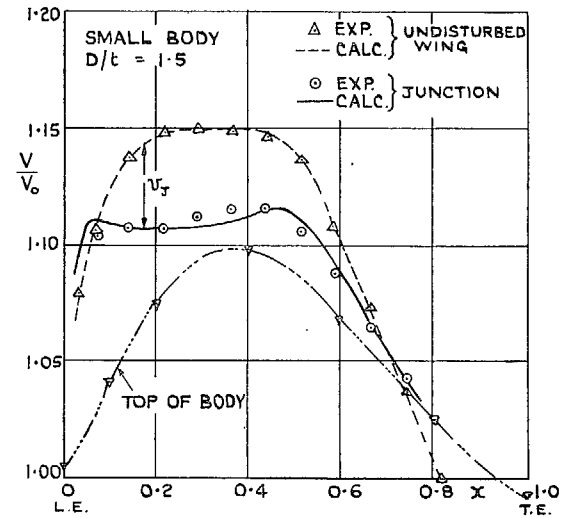

WING SECTION : R A E 103 ; t/c = 0·12 , φ = 0°

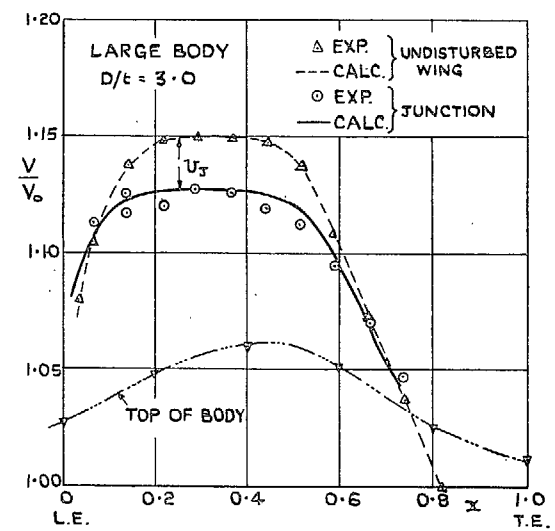

FIG. 29. Velocity distributions on an unswept wing with cylindrical bodies.

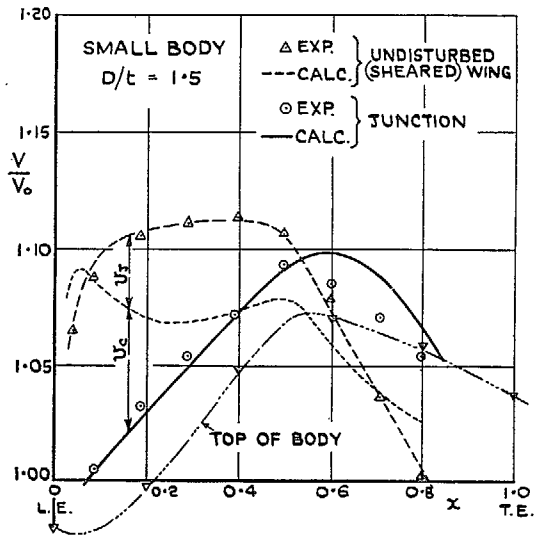

FIG. 30. Velocity distributions on a 45-deg swept-back wing with cylindrical bodies.

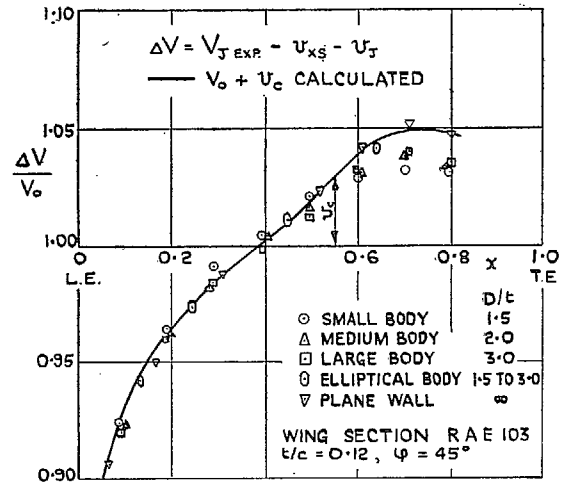

FIG. 31. Velocity increments due to reflection in the junctions of cylindrical bodies with a 45-deg swept-back wing.

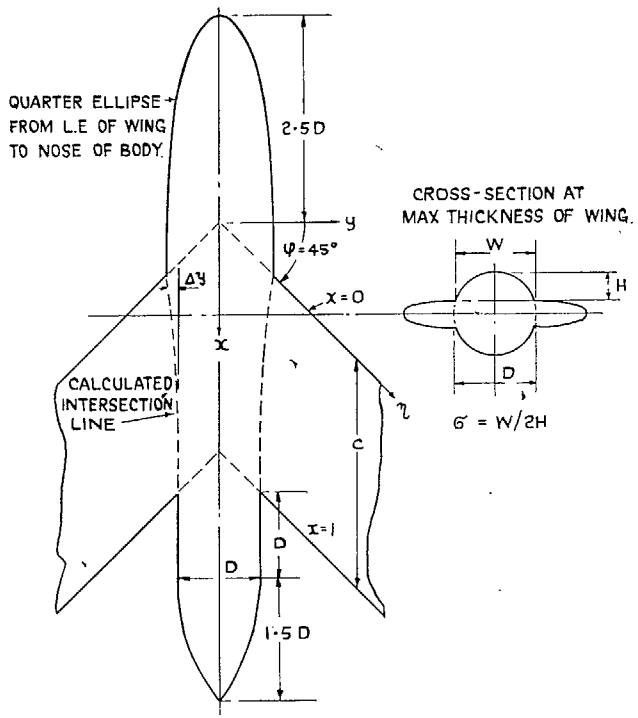

FIG. 32. Modified body on 45-deg swept-back wing.

(1277) Wt.18/9696 K.7 5/59 Hw.

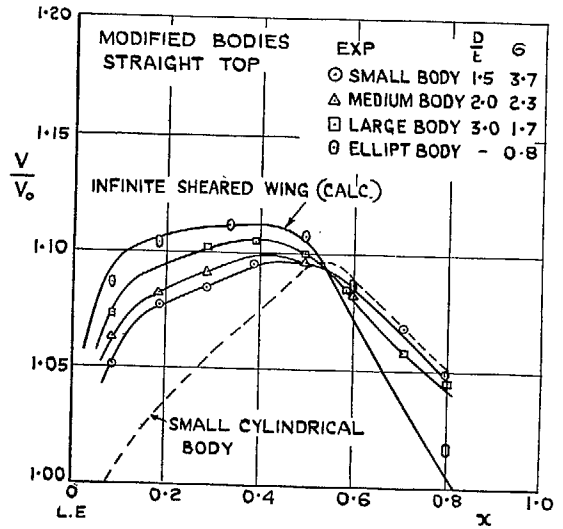

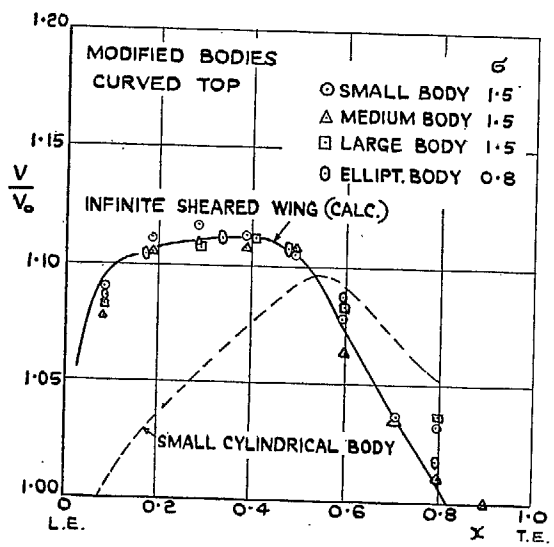

FIG. 33. Velocity distributions in the junctions of a 45-deg swept-back wing with modified bodies.

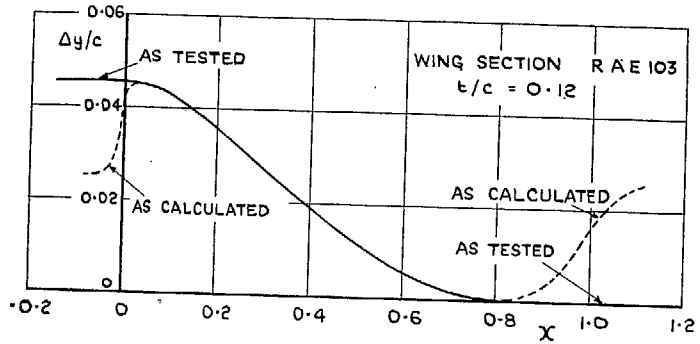

FIG. 34. Junction shape of modified bodies on 45-deg swept-back wing. Calculations from vortex method.

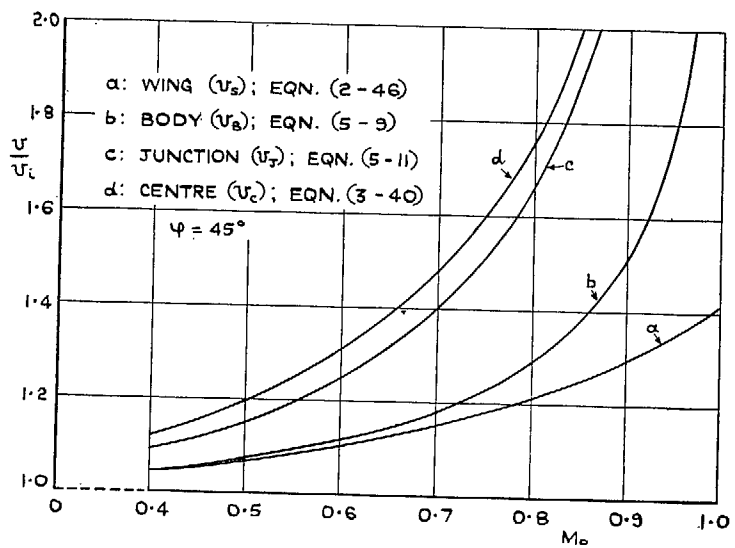

FIG. 35. Approximations for the velocity rise with Mach number.

Publications of the Aeronautical Research Council

ANNUAL TECHNICAL REPORTS OF THE AERONAUTICAL RESEARCH COUNCIL (BOUND VOLUMES)

1938 Vol. I. Aerodynamics General, Performance, Airscrews. 50*s*. (51*s*. 2*d*.)
Vol. II. Stability and Control, Flutter, Structures, Seaplanes, Wind Tunnels, Materials. 30*s*. (31*s*. 2*d*.)

1939 Vol. I. Aerodynamics General, Performance, Airscrews, Engines. 50*s*. (51*s*. 2*d*.)
Vol. II. Stability and Control, Flutter and Vibration, Instruments, Structures, Seaplanes, etc. 63*s*. (64*s*. 2*d*.)

1940 Aero and Hydrodynamics, Aerofoils, Airscrews, Engines, Flutter, Icing, Stability and Control. Structures, and a miscellaneous section. 50*s*. (51*s*. 2*d*.)

1941 Aero and Hydrodynamics, Aerofoils, Airscrews, Engines, Flutter, Stability and Control Structures. 63*s*. (64*s*. 2*d*.)

1942 Vol. I. Aero and Hydrodynamics, Aerofoils, Airscrews, Engines. 75*s*. (76*s*. 3*d*.)
Vol. II. Noise, Parachutes, Stability and Control, Structures, Vibration, Wind Tunnels. 47*s*. 6*d*. (48*s*. 8*d*.)

1943 Vol. I. Aerodynamics, Aerofoils, Airscrews. 80*s*. (81*s*. 4*d*.)
Vol. II Engines, Flutter, Materials, Parachutes, Performance, Stability and Control, Structures. 90*s*. (91*s*. 6*d*.)

1944 Vol. I. Aero and Hydrodynamics, Aerofoils, Aircraft, Airscrews, Controls. 84*s*. (85*s*. 8*d*.)
Vol. II. Flutter and Vibration, Materials, Miscellaneous, Navigation, Parachutes, Performance, Plates and Panels, Stability, Structures, Test Equipment, Wind Tunnels. 84*s*. (85*s*. 8*d*.)

Annual Reports of the Aeronautical Research Council—

1933–34	1*s*. 6*d*. (1*s*. 8*d*.)	1937	2*s*. (2*s*. 2*d*.)
1934–35	1*s*. 6*d*. (1*s*. 8*d*.)	1938	1*s*. 6*d*. (1*s*. 8*d*.)
April 1, 1935 to Dec. 31, 1936	4*s*. (4*s*. 4*d*.)	1939–48	3*s*. (3*s*. 2*d*.)

Index to all Reports and Memoranda published in the Annual Technical Reports, and separately—

April, 1950 - - - - R. & M. No. 2600 2*s*. 6*d*. (2*s*. 7½*d*.)

Author Index to all Reports and Memoranda of the Aeronautical Research Council—

1909–January, 1954. R. & M. No. 2570 15*s*. (15*s*. 4*d*.)

Indexes to the Technical Reports of the Aeronautical Research Council—

December 1, 1936 — June 30, 1939	R. & M. No. 1850	1*s*. 3*d*. (1*s*. 4½*d*.)
July 1, 1939 — June 30, 1945	R. & M. No. 1950	1*s*. (1*s*. 1½*d*.)
July 1, 1945 — June 30, 1946	R. & M. No. 2050	1*s*. (1*s*. 1½*d*.)
July 1, 1946 — December 31, 1946	R. & M. No. 2150	1*s*. 3*d*. (1*s*. 4½*d*.)
January 1, 1947 — June 30, 1947	R. & M. No. 2250	1*s*. 3*d*. (1*s*. 4½*d*.)

Published Reports and Memoranda of the Aeronautical Research Council—

Between Nos. 2251–2349	R. & M. No. 2350	1*s*. 9*d*. (1*s*. 10½*d*.)
Between Nos. 2351–2449	R. & M. No. 2450	2*s*. (2*s*. 1½*d*.)
Between Nos. 2451–2549	R. & M. No. 2550	2*s*. 6*d*. (2*s*. 7½*d*.)
Between Nos. 2551–2649	R. & M. No. 2650	2*s*. 6*d*. (2*s*. 7½*d*.)

Prices in brackets include postage

HER MAJESTY'S STATIONERY OFFICE

York House, Kingsway, London W.C.2; 423 Oxford Street, London W.1 (Post Orders: P.O. Box 569, London S.E.1), 13a Castle Street, Edinburgh 2; 39 King Street, Manchester 2; 2 Edmund Street, Birmingham 3; 109 St. Mary Street, Cardiff; Tower Lane, Bristol, 1; 80 Chichester Street, Belfast. *or through any bookseller*

S.O. Code No. 23–2908